GRAIN REFINEMENT OF MAGNESIUM AND AZ91E MAGNESIUM ALLOY BY ADDITION OF MgB_2 INOCULANT

by

Payam Emadi,
B.Eng, Ryerson University, 2014

A thesis
presented to Ryerson University

in partial fulfillment of the
requirements for the degree of
Master of Applied Science
in the program of
Mechanical and Industrial Engineering

Toronto, Ontario, Canada, 2018

AUTHOR'S DECLARATION

I hereby declare that I am the sole author of this thesis. This is a true copy of the thesis, including any required final revisions, as accepted by my examiners.

I authorize Ryerson University to lend this thesis to other institutions or individuals for the purpose of scholarly research.

I further authorize Ryerson University to reproduce this thesis by photocopying or by other means, in total or in part, at the request of other institutions or individuals for the purpose of scholarly research.

I understand that my thesis may be made electronically available to the public.

ABSTRACT

GRAIN REFINEMENT OF MAGNESIUM AND AZ91E MAGNESIUM ALLOY BY ADDITION OF MgB_2 INOCULANT

Master of Applied Science, 2018

Payam Emadi

Mechanical and Industrial Engineering

Ryerson University

The increased use of magnesium alloys with improved mechanical properties is a prominent strategy towards increasing fuel efficiency of vehicles and decreasing emissions. This study investigates the grain refining efficiency and fading of MgB_2 micro- and nano-particle added Pure Mg and AZ91E. Addition of micro and nano-sized MgB_2 provided a reduction in grain size for Pure Mg and AZ91E. Enhanced heterogeneous nucleation and grain growth restriction was believed to be the source of refinement. Fading was observed for both Pure Mg and AZ91E, with the nano-particle added castings showing an increased resistance. The elongation of the Pure Mg samples showed improvements, whereas no improvements for UTS and YS was seen. The improved ductility was believed to be due to the grain refinement and coefficient of thermal expansion mismatch. The AZ91E samples did not show improvements in mechanical properties. This was believed to be due to stress concentration from Al-Mn intermetallics.

ACKNOWLEDGMENTS

I would like to express my most sincere gratitude to my supervisor, Dr. Ravindran. Thank you for your kindness, guidance, and support during my graduate studies.

I would also like to thank my dear friends at the Centre for Near-Net-Shape Processing of Materials, Mr. Eli Vandersluis, Dr. Anthony Lombardi and Mr. Bernoulli Andilab for their kind help during this process.

I am especially thankful to Mr. Alan Machin for his friendship, technical support, and valuable input.

I am also grateful to Horace Chan, Nicholas Prabaharan and Michael Rinaldi for their hard work and dedication as undergraduate research assistants.

Finally, I would like to thank my family, friends and wonderful girlfriend Kiara for their constant support and motivation.

Table of Contents

List of Tables

List of Figures

Nomenclature

Symbol	Description	Units
Greek		
γ	Interfacial free energy	J/m^2
γ_{sl}	Interfacial energy of solid-liquid interface	J/m^2
γ_{ml}	Interfacial energy of the mould-liquid interface	J/m^2
γ_{sm}	Interfacial energy of the solid-mould interface	J/m^2
δ	Lattice disregistry	%
θ	Contact angle	Degrees
σ_y	Yield strength	MPa
σ_o	Stress to initiate dislocation motion	MPa
σ_{SL}	Solid liquid interfacial energy	MPa
English		
a	Lattice parameter	nm
C_0	Initial concentration of the solute in the melt	wt.%
d	Average grain diameter	m
r	Radius of nucleus	m
f_r	Interatomic misfit	%
G*	Critical free energy	J
ΔG	Gibbs free energy	kJ/mol
G_v	Free energy of the liquid per unit volume	J/m^3
k	Equilibrium partition coefficient	wt.%/wt.%
m	Slope of liquidus line	K/wt.%
Q	Growth restriction factor	K
r*	Critical radius of nucleus	μm
S	Entropy	J/K
S_d	Average particle spacing	μm
t	Time	sec
ΔT	Undercooling	°C

T_m	Melting point of the liquid	°C
X_{cs}	Size of a previously nucleated grain	µm
X_{nfz}	End of nucleation free zone	µm
X'_{dl}	Distance from the liquid/solid interface	µm
X_{sd}	Distance from the nucleation free zone	µm
z	Fraction of undercooling required to activate the next nucleant	

Abbreviations

CS	Constitutional subcooling
CFF	Ceramic foam filter
EDS	Energy dispersive X-ray spectroscopy
HCP	Hexagonal close-packed
UTS	Ultimate tensile strength
RE	Rare earth
SEM	Scanning electron microscope
YS	Yield strength

Elements

Ag	Silver
Al	Aluminum
Ar	Argon
B	Boron
Be	Beryllium
Bi	Bismuth
C	Carbon
Ca	Calcium
Cd	Cadmium
Cl	Chlorine
Co	Cobalt
Eu	Europium
Fe	Iron
Hg	Mercury

La	Lanthanum
Li	Lithium
Mg	Magnesium
Mn	Manganese
Na	Sodium
Ni	Nickel
O	Oxygen
Pr	Praseodymium
Si	Silicon
Sm	Samarium
Sn	Tin
Tb	Terbium
Ti	Titanium
W	Tungsten
Yb	Ytterbium
Zn	Zinc
Zr	Zirconium

1. Introduction

Magnesium (Mg) is the lightest metallic structural material available [1]. Its excellent specific strength, good castability, and abundance factor into Mg alloys becoming increasingly popular engineering materials, particularly in the automotive industry. Light-weighting automobiles is a very prominent strategy towards increasing fuel efficiency and decreasing harmful emissions. For instance, a 10 % reduction in vehicle weight can result in a 3 % reduction in CO_2 emissions, given that no other changes are made to the vehicle (only mass is removed and as a result, the power to mass ratio increases) [2, 3]. To reduce vehicle weight, Mg alloys must become competitive with aluminum (Al) alloys. This can be achieved by developing Mg alloys with improved mechanical properties such as strength and ductility.

A drawback of Mg alloys is their limited mechanical properties, especially at elevated temperatures. Magnesium alloys possess relatively low strength, low ductility, low creep resistance, and poor workability due to their hexagonal close-packed (HCP) crystal structure. One of the most effective methods of improving the mechanical properties of Mg alloys is grain refinement. A finer grain size can simultaneously improve the strength and ductility of cast alloys [4]. The grain size can be influenced by casting parameters (e.g., cooling rates) and the addition of potent nucleants.

The focus of this research study is to develop an efficient and commercially viable grain refiner for Mg-Al alloys. Grain refinement can help to improve mechanical properties, for example, Ultimate Tensile Strength (UTS), Yield Strength (YS), and % Elongation. Furthermore, grain refinement aids in reducing defects that arise from casting such as porosity and segregation. Therefore, Mg castings improved through grain refinement may be effectively utilized in industry to manufacture light, environmentally-friendly, and cost-effective components.

1.1. Objective

The purpose of this research was to examine the effect of MgB_2 micro- and nano-powder on the grain size and mechanical properties of Pure Mg and AZ91E magnesium alloy. Various addition levels and particle sizes were investigated to optimize the casting parameters.

1.2. Outline of Thesis

An overview of this thesis is provided in Figure 1-1 below:

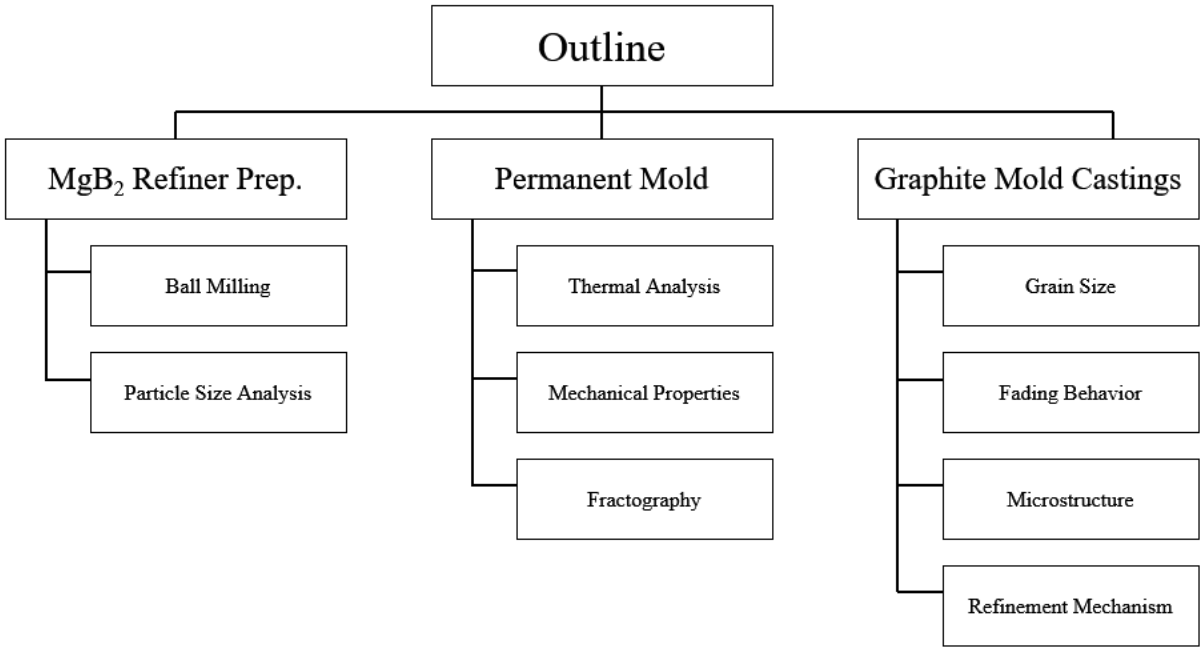

Figure 1-1: Outline of thesis

2. Literature Review

The continually increasing interest in Mg alloys for automotive applications is based on the combination of high strength and low density. Magnesium is the lightest of all engineering structural metals with a density of 1.74 g/cm^3 [1]. Magnesium is approximately 35 % lighter than Al (2.74 g/cm^3 [5]) and over four times lighter than steel (8.05 g/cm^3 [6]). For this reason, Mg alloys are desirable as structural materials in all applications where weight savings are critical. Magnesium has a very high strength-to-weight ratio compared to most commonly used metals such as steel and Al. Other advantages include excellent machinability, high die casting rates, good castability, and dimensional accuracy which promote the increased utilization of this metal in the automotive industry [7, 8].

Magnesium is rarely used for engineering applications without being alloyed with other metals since Pure Mg has low mechanical properties. Some common alloying elements with Mg are Al, zinc (Zn), manganese (Mn) and zirconium (Zr). The effects of these elements are summarized in the following.

Aluminum: The maximum solubility of Al in a Mg matrix is 12.7 wt.% at the eutectic temperature (Appendix A) [9]. Aluminum aids to refine grain size, increase strength and increase hardness. Furthermore, Al widens the alloy's freezing range, which facilitates easier casting. Commercial alloys rarely exceed 10 wt.%, and 6 wt.% has been shown to achieve its optimum strength and ductility [10].

Zinc: Zinc is usually used in combination with Al to increase the room temperature strength of the alloy [10]. Furthermore, it is also used with rare earth (RE) elements such as Zr or Thorium (Th) to produce alloys which can be precipitation hardened. Zinc also aids to reduce the corrosive effects of Iron (Fe) and Nickel (Ni) impurities.

Manganese: Manganese improves the corrosion resistance of Mg alloys by eliminating Fe and other heavy metal elements. This is done by combining into compounds, which are comparatively harmless and settle to the bottom of the melt or float to the top and are skimmed away during the casting procedure [10].

Zirconium: Zirconium is a highly efficient grain refiner for Al-free Mg alloys. Zirconium present in solid solution provides a fine grain structure and as a result, increases the material's

strength [10]. Zirconium cannot be used with Mg-Al or Mn containing alloys as it forms stable intermetallics with these elements and is therefore removed from solution.

Currently, most Mg-based components used in the automobile industry including instrument panels, steering column supports, seats, valve covers, and transfer cases, are mainly manufactured by high pressure die casting processes with conventional Mg alloys. The details of these and other commonly used Mg alloys can be seen in Table 2-1 below:

Table 2-1: Common Mg alloys and their uses [6, 10, 11]

Alloy Designation	Alloying Additions	Uses	Basic Properties and applications
AZ91A, B, D-F	9.0 % Al, 0.7 % Zn, 0.13 % Mn	General casting alloy	Excellent castability and good strength at T<150C
AZ91 C, E-T6			General purpose alloy with moderate strength
AZ31	3 % Al, 1.0 % Zn, 0.2 % Mn	Wrought magnesium products	Good extrusion alloy
AM60A, B-F, AM50 A-F	Mg-Al system	High pressure die casting alloy	Excellent ductility and energy-absorbing properties greater toughness and ductility compared to AZ91, slightly lower strength preferred for automotive structural applications
AM20-F		Casting alloy	High ductility and impact strength, poor die castability
AS41A-F, AS21-F	Mg-Al-Si system	General casting alloy	Better creep resistance compared to AZ91 at elevated temperature but lower strength
AE42 -F, AE44-F	Mg-Al-RE system	General casting alloy	Low castability, excellent creep behavior
AJ62	Mg-Al-Sr system	High pressure die casting	Good thermal and mechanical strength Superior castability, corrosion resistance, and creep behavior
MRI 153M, MRI 230D	Mg-Al-Ca-Sr system	Casting alloy	Good strength and creep resistance For high-temperature applications
ZE41	4.2 % Zn, 1.2 % RE, 0.7 % Zr	Specialist casting alloy	RE addition improves creep strength at elevated temperatures

2.1. Grain Refinement of Magnesium Alloys

Material scientists have been seeking alternative methods of improving the properties of magnesium alloys for several years. As a result of extensive research, grain refinement has been identified as an effective technique. Grain refinement can improve strength without sacrificing ductility. Furthermore, it aids in reducing defects that arise from casting such as porosity and segregations. Lastly, grain refinement can also eliminate columnar structure, which in turn improves the formability of wrought alloys.

Grain refinement techniques for Mg alloys can be divided into two groups. First, is thermo-mechanical treatments on solid Mg alloys. These techniques refine grains by severe plastic deformation. The plastic deformation promotes grain refinement through the activities of dislocations, twinning and grain growth, which in turn leads to small equiaxed grains [12]. The second group of techniques used for grain refinement are methods that are implemented during the casting process either by using various stirring techniques such as ultrasonic stirring [13] or through melt treatment techniques such as inoculation, superheating [14]. Mechanical vibrations induced during solidification have also been shown to improve grain size [15, 16].

Inoculation is the process of adding grain refiners and or solute elements to achieve a finer grain size. These additions help to promote heterogeneous nucleation and restrict grain growth. To date, Zr has been reported to be one of the most successful grain refiners for cast Mg alloys. A grain size decrease of greater than 80 % by the addition of 0.15 wt.% Zr has been reported by researchers [17]. For Mg alloys containing Al, Si, or Mn, grain refinement with Zr is not possible. This is mainly because Zr forms intermetallic phases with the elements above which are detrimental to its material properties. Furthermore, Zr addition to Mg is also very costly. Since Mg-Al systems are the most commonly used cast Mg alloys in the industry, extensive research has been performed to identify a common grain refiner for both Mg-Al and Al-free Mg alloys.

2.2. Nucleation

The process of nucleation involves the appearance of microscopic particles or nuclei, which are capable of growing in the melt. During growth, the nuclei change in size which leads to the disappearance of the parent phase. The transformation is completed if the growth of the new phase

particles is allowed to continue until the equilibrium fraction is attained [18]. Nucleation can be divided into two different categories: 1) Homogeneous nucleation and, 2) Heterogeneous nucleation. The two types of nucleation will be expanded upon in the following sections.

2.2.1 Homogeneous Nucleation

Homogeneous nucleation refers to the process of formation of solids within the melt without any interference of foreign materials [18]. During the process of solidification, microscopic particles of crystalline solids called embryos are formed. If there is sufficient undercooling available, the embryo will survive and grow into a nucleus. Conversely, if the undercooling is not adequate, the embryo will re-melt. Because the nucleus has the same composition as the melt, this process is termed homogeneous nucleation.

Consider the formation of an embryo with a radius r. The formation of this embryo results in a free energy change in the system in two ways. The first change is a decrease in free energy as a consequence of a change in volume of radius r from the transformation of liquid to solid state. Second, there is an increase in free energy, which is a result of a newly created liquid-solid interface. The change in free energy can be described by Equation (1) below [18]:

$$\Delta G = \frac{4}{3}\pi r^3 \Delta G_v + 4\pi r^2 \gamma \quad (1)$$

Where,

ΔG_v is the free energy per unit volume and,

γ is the interfacial energy per unit area

Figure 2-1 (a) displays the free energy contributions mentioned above as a function of nucleus radius r. Figure 2-1 (b) shows the two contributions and a sum of both contributions as well. By examining the figure, it can be seen that the free energy change increases to a maximum and subsequently decreases. The maximum of the curve corresponds to a critical nucleus radius of r^*. During solidification, if an embryo reaches the critical radius r^*, its growth will continue and it will form a nucleus. A critical free energy, G^* occurs at the critical radius and, consequently, at the

maximum of the curve. This G* corresponds to an activation free energy, which is the free energy required for the formation of a stable nucleus [18].

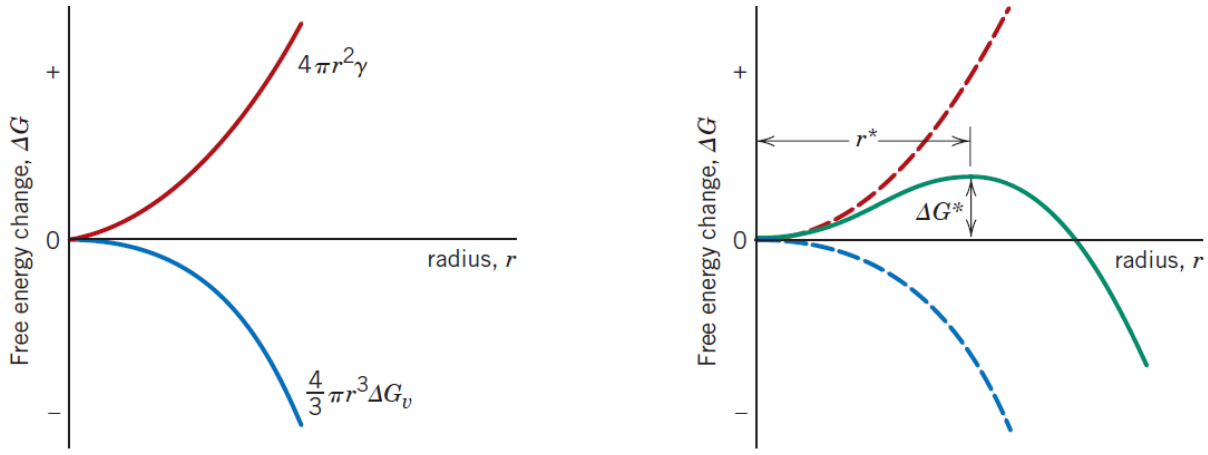

(a) **(b)**

Figure 2-1: (a) Plot of surface free energy and volume free energy as a function of radius r, (b) Plot of summation of volume and surface free energy [18]

Taking the first derivative of Equation (1) with respect to r we have [18]:

$$\frac{d(\Delta G)}{dr} = \frac{4}{3}\pi\Delta G_v(3r^2) + 4\pi\gamma(2r) = 0 \quad (2)$$

Solving Equation (2) for r we have [18]:

$$r^* = -\frac{2\gamma}{\Delta G_v} \quad (3)$$

Where r^* is the minimum solid particle radius required for an embryo to grow into a nucleus.

Substituting Equation (3) into Equation (1) we have [18]:

$$\Delta G^* = \frac{16\pi\gamma^3}{3(\Delta G_v)^2} \quad (4)$$

Where ΔG^* is the minimum activation free energy required to form a stable nucleus [18].

2.2.2 Heterogeneous Nucleation

Heterogeneous nucleation refers to the process of nuclei forming on inhomogeneities in the melt [18]. Theses inhomogeneities include but are not limited to intermetallics, casting mould walls and impurities. Heterogeneous nucleation occurs more readily compared to homogeneous nucleation because of the lower free energy requirements resulting from nuclei forming on pre-existing surfaces [18].

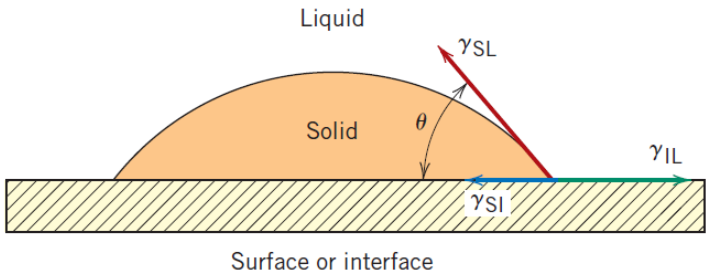

Figure 2-2: Heterogeneous nucleation of a solid from a liquid [18]

To further understand this method of nucleation, Figure 2-2 depicts heterogeneous nucleation from a surface or interface. This figure displays the interfacial energies as vectors that exist along the phase boundaries: γ_{SI} is the solid-surface, γ_{SL} represents the solid-liquid, and γ_{IL} represents the liquid-surface. Performing a force balance on the system we have [18]:

$$\gamma_{IL} = \gamma_{SI} + \gamma_{SL}\cos\theta \quad (5)$$

Where θ is the wetting angle.

Following this, by following a procedure similar to the procedure for homogeneous nucleation described above, we can determine r^* and ΔG^* [18]:

$$r^* = -\frac{2\gamma_{SL}}{\Delta G_v} \quad (6)$$

$$\Delta G^* = \left(\frac{16\pi\gamma_{SL}^3}{3\Delta G_v^2}\right) S(\theta) \quad (7)$$

Where $S(\theta)$ is a function of the wetting angle θ and is a value between 0 and 1.

By examining Equation (7) and comparing it Equation (4), it is evident that a lower activation energy is required to initiate heterogeneous nucleation in comparison to homogeneous nucleation (by a factor of $S(\theta)$). This conclusion is depicted in Figure 2-3 below:

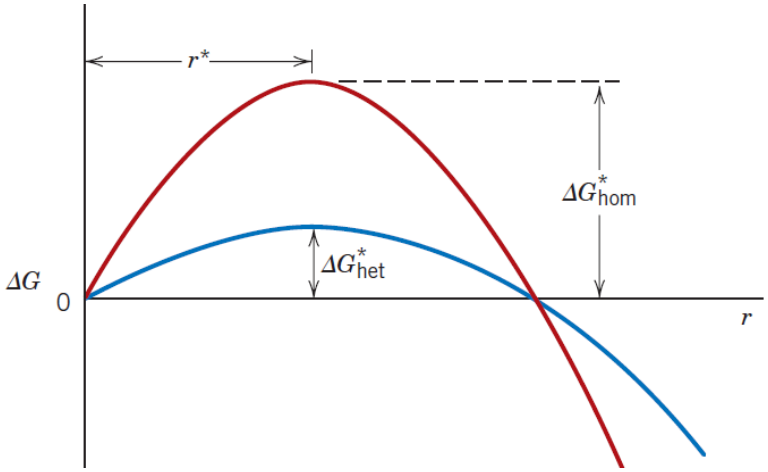

Figure 2-3: Free energy VS. embryo/nucleus radius for homogeneous and heterogeneous nucleation [18]

2.3. Grain Growth Restriction

The effects of solute elements on grain refinement are widely accepted and studied in literature. The fundamental basis is that for grain refinement to be effective, some amount of solute is essential in the melt to restrict the growth of the grains. This can be done by inducing constitution subcooling (CS) ΔT_c, ahead of the growing dendrite by solute element segregation, which in turn suppresses the growth of the dendrite through promoting further nucleation when $\Delta T_c > \Delta T_n$ in the CS zone [19]. In order to quantify the impact of CS on grain size, a Q value which is also termed the "growth restriction factor" (GRF) is used [20]. A high Q value corresponds to a high rate of CS zone establishment which consequently results in a finer grain size. The GRF can be express using Equation (8) below [19]:

$$Q = mC_0(k-1) \quad (8)$$

Where,

m is the slope of the liquidus line,

C_0 is the initial composition of the alloy, and

k is the equilibrium partition coefficient for the element which measures how a substance distributes or partitions itself between two immiscible solvents.

It should be noted that Equation (8) is only valid for a binary system. For alloys containing more than one alloying element, the Q value can be calculated using Equation (9) below [19]:

$$Q_{\sum bin} = Q_{\sum bin,i} = \sum m_{bin,i}\left(k_{bin,i} - 1\right)c_{0,i} \quad (9)$$

Equation (9) suggests the additive contribution of the multiple solutes. Moreover, the equation falls short because it does not consider the interaction of solutes with one another. Table 2-2 shows the Q values for some typical elements that may be used for grain refinement of Magnesium at $C_0 = 1.0$ wt. %:

Table 2-2: Growth restriction factors for common elements [17]

Element	m	K	Q = m(K − 1)
Na	−6.878	0	6.878
Pd	−4.07	0	4.07
Nd	−3.557	0	3.557
Co	−3.178	0	3.178
Sm	−3.4	0.135	2.943
Pr	−2.909	0	2.909
La	−2.895	0	2.895
Yb	−3.098	0.133	2.685
Ag	−4.217	0.366	2.675
Cd	−2.644	0	2.644
Hg	−3.15	0.174	2.602
Eu	−2.49	0	2.49
Tb	−2.99	0.306	2.073
Li	−7.52	0.73	2.034

2.4. Selection of Effective Nucleants and Predictive Models

For many years, heterogeneous nucleation had been believed to be the only cause of grain refinement. However, the theory failed to explain the grain refinement process for several alloy systems such as Al-Ti-B master alloy in Aluminum. This is because the theory failed to take into account the potency of nucleants. The potency of nucleants can be quantified by the amount of undercooling required to initiate nucleation. In other words, a potent nucleant requires a lower amount of undercooling to initiate nucleation .

Currently, the available theories to model the potency of nucleants can be divided into two major groups. The first group proposes that a potent nucleant should have good crystallographic matching with the host material in order to reduce the interfacial energy between the nucleant and the host matrix. The models representing this group are the Turnbull and Vonnegut model [21], the Bramfitt model [22] and the Edge-to-Edge matching model [23]. The second group of models focuses on inoculant particle size and are termed Free Growth models. The models are based on the theory that a potent nucleant should have a particle size larger than the critical radius for nucleation otherwise nucleation will not occur [24]. Also, the role of solute elements was also determined to be significant for grain refinement. The reasons for this are 1) Segregation of solutes restricts the growth of previously formed grains which leads to more time for new grains to form, 2) The segregation produces constitutional subcooling zone at the front of the solid-liquid interface which enhances the nucleants to nucleate new grains ahead of the growing interface and therefore inhibit the growth of existing grains, and 3) The new grains can also restrict the growth of grains formed earlier [25]. Details of the more commonly used models mentioned above will be provided in the following sections.

2.5. Turnbull/Vonnegut and Bramfitt Model

Turnbull and Vonnegut were the first to notice the role of crystallography in grain refinement and proposed an empirical parabolic dependence model relating the critical subcooling for nucleation (ΔT_n) and the lattice disregistry parameter (δ) [21]. ΔT_n can be determined using Equation (10) below [21]:

$$\Delta T_n = \left(\frac{c}{\Delta S_v}\right)\delta^2 \tag{10}$$

Where,

c is the concentration of the solute,

ΔS_v is the entropy difference per unit volume between the inoculant and the nucleus formed on it

δ is the lattice disregistry and can be calculated by using Equation (11) below [21]:

$$\delta = \frac{\Delta a}{a_0} \tag{11}$$

Where,

Δa is the difference in lattice parameters between the low index planes of the inoculant and the nucleus and,

a_0 is the lattice parameter in the low index plane of the nucleus

In this model, a potent nucleus should have a lattice disregistry factor of $\delta \leq 0.005 - 0.015$ [21]. The Turnbull and Vonnegut model is only limited to systems with nuclei and inoculants sharing the same atomic configuration on their low index planes. Therefore, a modified model was proposed by Bramfitt [22]. The modified model is commonly referred to as the Planar Disregistry model or the Plane to Plane Matching model (P2PM). In this model, the major change is the redefinition of δ from linear disregistry to planar disregistry which can be determined by Equation (12) below [22]:

$$\delta_{(hkl)_n}^{(hkl)_s} = \sum_{i=1}^{3} \frac{\frac{\left| d_{[uvw]_s^i} cos\theta - d_{[uvw]_n^i} \right|}{d_{[uvw]_n^i}}}{3} * 100 \tag{12}$$

Where, n and s denote the nucleus and the inoculant/substrate,

(hkl) is a low index plane,

$[uvw]$ is a low index direction on the (hkl) plane and,

θ is the angle between a pair of adjacent low index directions on the (hkl) plane [22].

Bramfitt [22] based on a series of experiments with iron and previously identified nucleants, determined a lattice disregistry criterion of 12 %, below which the inoculants are considered to be potent nucleants.

2.6. Edge to Edge Matching Model

Edge to Edge Matching (E2EM) is one of the more recent models that can successfully interpret the efficiency of grain refiners. The model was originally developed to predict and understand crystallographic features of diffusional phase transformations. Furthermore, it is known that the interfacial energy between the substrate and the solid is critical to the potency of a substrate. The energy on the newly formed interface must be lower than the surface energy of the same area of the interface if it formed directly in liquid metal [26]. In a coherent or partially coherent interface, strain energy is present if there is not exact matching between the substrate and the solid and to minimize this strain energy, maximum atom matching on the interface is required [26].

First, the close-packed or nearly close-packed directions must be identified by calculating the atomic linear density; these directions will be used as matching directions [26]. Second, the interatomic misfit f_r , between phases along the directions identified in step one are determined [26]. Figure 2-4 illustrates the atomic matching criteria.

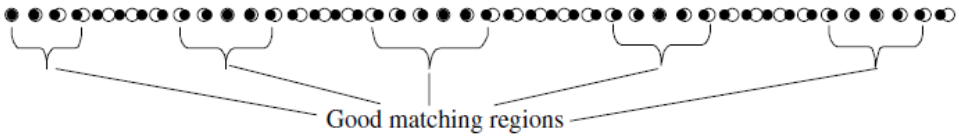

Schematic illustration of atom row matching with small misfit along the row direction.

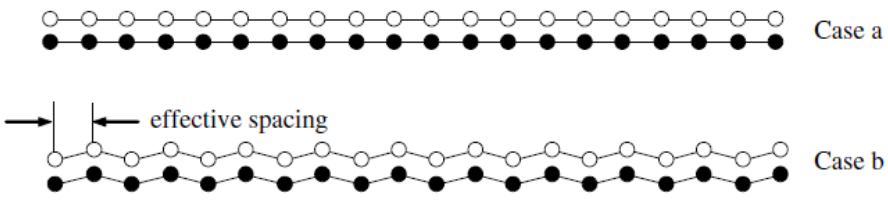

Schematic illustration two different types of atom row matching.

Figure 2-4: Interatomic mismatch and atomic matching criteria [27]

In order to maximize the probability of atom row matching, the planes that contain the atom rows should have equal or similar interplanar spacings and be arranged to meet edge to edge similar to Figure 2-5 below [27]. These planes can be identified by calculating planar atomic density or by using analytical geometry. Alternatively, a simple way to determine these planes is by using the International Powder Diffraction File or PDF. The planes with the highest diffraction intensity are generally the close-packed or nearly close-packed planes [27]. Also, the relative difference in d-values of any two close or nearly close-packed planes between two phases is termed as d-value mismatch [26]. Normally, when the d-value mismatch between the matching planes is equal to or less than 6 %, the matching planes are parallel or have small rotations about the matching direction which in turn means that the plane pair has potential to form a good match [26].

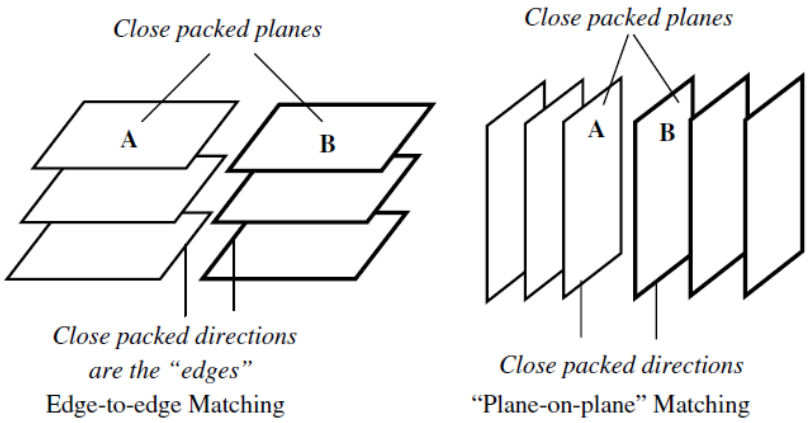

Figure 2-5: Illustration of edge to edge matching planes [26]

To conclude, the E2EM model and other models mentioned above may produce similar results for simple systems. However, for complex systems, the E2EM model is more accurate because in reality, it is the atoms that are matching rather than lattice points.

2.7. The Free Growth Model (Inoculant Particle Size Effect)

For grain refinement, in addition to the interfacial structure, the size of nucleants is also an important factor affecting the heterogeneous nucleation rate and therefore, the grain refining

efficiency. It has been determined that the critical condition for a particle in the liquid metal to promote heterogeneous nucleation is $d \geq 2r^*$, where d is the diameter of the nucleant and r^* is the critical radius of a nucleus beyond which the nucleation can occur [24]. Furthermore, this is known as the free growth model and it correlates the critical subcooling and the size of the nucleant with the Equation (13) below [24]:

$$\Delta T_n = \frac{4\sigma_{SL}}{\Delta S_v d_p} \tag{13}$$

Where,

σ_{SL} is the solid-liquid interface energy,

S_v is the entropy of fusion per unit volume and,

d_p is the diameter of the particle

2.8. The Interdependence Theory

The interdependence theory was proposed as an analytical model describing the effects of nucleants and solutes on grain formation and size [25]. The theory assumes that successive nucleation events depend on the growth of a previously nucleated grain. Furthermore, the theory is based on the dependence of the as-cast grain size on three major terms. These terms are as follows:

1. The size of a previously nucleated grain, X_{cs} is large enough to develop a sufficient constitutional subcooling zone for new nucleation to occur.
2. The distance, X'_{dl} from the liquid/solid interface to the point where the CS is sufficient to nucleate a new grain or the nucleation free zone.
3. The distance, X_{sd} from the nucleation free zone to the next most potent nucleating site where a new nucleation event can take place.

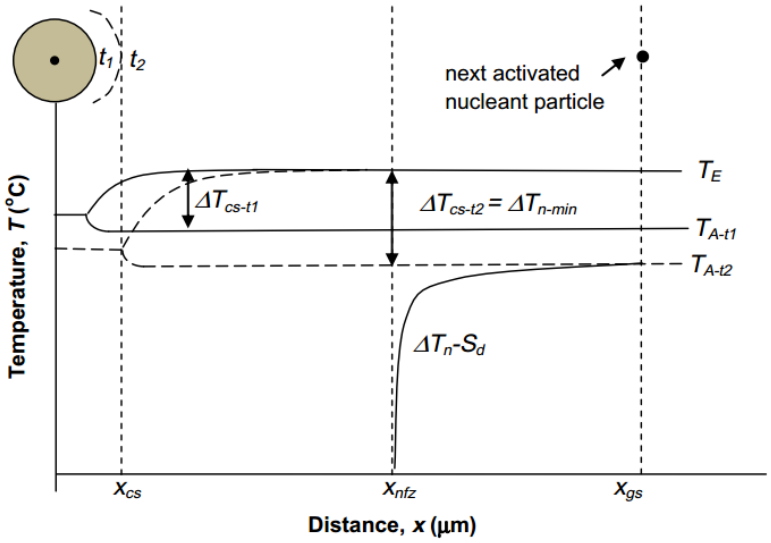

Figure 2-6: Nucleation process [25]

St. John et al. [25] theorized that a growing grain is represented by the circle on the top left of Figure 2-6 and a potential nucleant is displayed on the top right. Furthermore, according to the Free Growth Model (described above), the exponential curve represents the relationship between the subcooling required for nucleation, ΔT_n and the average particle spacing, S_d. The inverse relationship between $\Delta T_n$and S_d shows that it is more likely to find an effective nucleant at distances further away from a previously nucleated grain. X_{cs} is the minimum distance required for the previously nucleated grain to grow in order for it to create the minimum required constitutional subcooling zone, ΔT_{n-min}, to promote the nucleation of the nucleus on the right hand side of Figure 2-6. t_1 and t_2 represent time 1 and time 2, the solid lines correspond to t_1 and the dashed lines correspond to t_2. At time t_1, the growing grain is not large enough to produce the required amount of CS but, at time t_2, after the grain grows, the CS becomes sufficient enough for the nucleation of the nucleus on the right. This typically happens when the $\Delta T_{n\text{-min}}$ and $\Delta T_n - S_d$ curves overlap each other. X_{nfz} denotes the end of the nucleation free zone at which the CS reaches its maximum. Following this, it can be seen that no nucleation will occur between X_{cs} and X_{nfz} because the CS will always be lower than ΔT_{n-min} in this region.

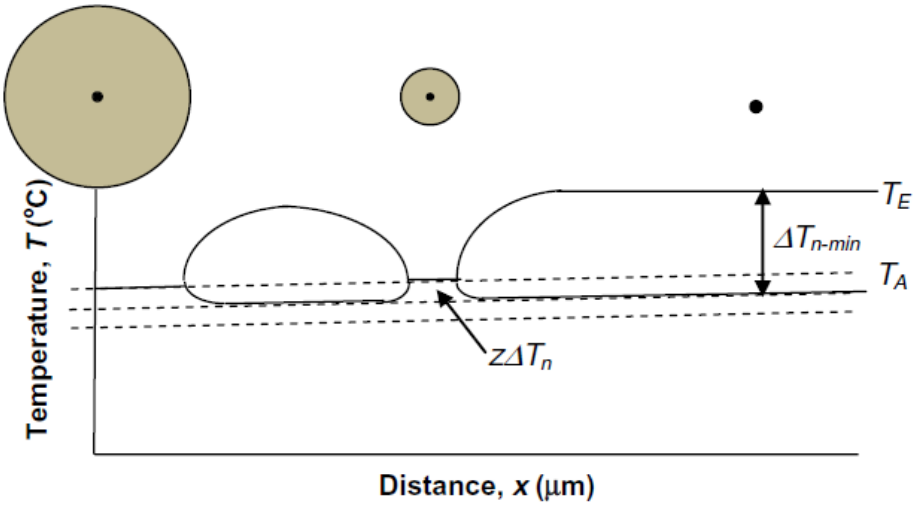

Figure 2-7: Repeating cycles of nucleation [25]

The cycle described above is repeating in nature and progresses toward the center of the melt. Figure 2-7 displays three repeating cycles of nucleation and grain growth. The dashed lines represent the relative amount of grain growth required in order to activate the next potent particle. The amount of undercooling needed to achieve this is denoted by $z\Delta T_n$, where z is the fraction of undercooling required to activate the next nucleant. This repetition is what leads to grain refinement. In simple terms, the diffusion field created by the newly formed grain progresses back toward the previous grain. Once the diffusion fields of both grains overlap, the amount of CS between the grains is reduced and therefore, inhibiting the further growth [25].

2.9. Grain Refinement of Aluminum-Free Magnesium Alloys

The grain refinement of aluminum free magnesium alloys is well established both scientifically and commercially. It has been shown that alloys containing little or no impurity levels of Fe, Al, Si, Mn, and Si are readily grain refined by Zr master alloys [9, 28]. Zirconium is, however, an expensive grain refiner and poses a major challenge to reduce the costs of the grain refinement process. Some examples of Al-free Mg alloys are ZK60, ZE41 WE43, ML10, and AM-SC1.

The maximum solubility of Zr in Pure Mg at 654 °C is 0.45 wt.% [29]. Initially, it was believed that adding Zr to the melt at the time of pouring was more effective and the undissolved Zr was

thought to be irrelevant to the grain refinement. Contrariwise, Tamura et al. [30] showed that undissolved Zr plays a major role in grain refinement. In the Mg melt, the two key factors that affect the soluble and insoluble Zr are the uptake of iron and the settling of Zr particles. Uptake of iron from a steel crucible can consume the soluble Zr content when the melt is held at temperatures above 750 °C. Qian et al. [31, 32] also found that either of these conditions can cause an increase in grain sizes in the alloy. The other factor was found by Hildebrand [33] who determined that the soluble Zr content in the magnesium alloy is affected by the alloy composition. He determined that the soluble Zr content is a function of Zn content in the alloy. Furthermore, he found that Zn and Zr form stable intermetallic compounds when the Zn content exceeds approximately 4 %.

In Mg alloys containing Al, a reaction between Zr and Al occurs inhibiting the nucleating potential of Zr [34]. The result is the formation of an Al_2Zr phase as observed by Kabirian et al. [35] with the addition of Zr to AZ91 Mg-Al alloy. The presence of the aforementioned particles leads to grain coarsening in the as-cast state but conserved grain sizes during aging because of the high thermal stability of Al_2Zr.

Since many commercial Mg alloy systems make use of Al, an alternative grain refiner for Mg-Al alloys is a necessity. The following sections describe some of the benefits and shortfalls of grain refiners for Mg-Al alloys.

2.10. Grain Refinement of Magnesium – Aluminum Alloys

Magnesium-Aluminum based alloys currently lack an effective, reliable and readily available grain refining system [36]. Accordingly, several potential grain refiners have been identified and developed for these alloys. The following sections describe some more effective techniques currently used for refinement.

2.10.1 Melt Superheating

The process of holding the melt temperature above the liquidus is known as superheating [37]. In foundry practices, the majority of metals and alloys should not be heated above their liquidus temperatures because elevated temperatures promote gas absorption, oxidation, and grain coarsening [38]. Conversely, superheating aluminum-based magnesium alloys has been shown to

have benefits regarding grain refinement. The grain refining effect of superheating is affected by a large number of factors such as the following:

Effect of Alloy Composition:

In superheating, Al is a key element for successful grain refinement. Magnesium alloys containing high aluminum contents are readily grain refined by superheating as opposed to low Al content alloys [9]. The iron and Mn content in Al-based Mg alloys have a significant contribution to the grain refinement. It has been found that alloys being treated for grain refinement using superheating should contain at least 10 ppm of Fe and Mn [39]. Silicon content in the alloy also helps in refinement but to a lesser degree compared to Fe and Mn. Moreover, the effects of Si disappear with high Fe content in the alloy [39]. Titanium, Be and Zr have been found to inhibit grain refinement by superheating [9].

Effect of process variables:

Tiner [40] determined that there is a specific temperature range for maximum grain-refining efficiency by superheating. Once a fine grain size is attained, increasing holding time at the superheat treatment temperature or repeating the process did not show any further refining effect [39]. Rapid cooling from superheating temperature to the pouring temperature is required for a successful process. The superheating effect disappears upon re-melting. There were four hypothesis for this process: 1) Al-Fe or Al-Mn-Fe intermetallics can precipitate from the melt as a result of Fe pickup and subsequently act as nucleation sites [9], 2) Temperature solubility theory dictates that particles that are too large in size at normal melt temperatures and are in few number for grain refinement dissolve into the melt and re-precipitate as a large number of fine nucleation sites upon cooling [41], 3) Nucleation on Al_4C_3 particles [9], which is based on the assumption that there is an absorption of carbon from the steel crucible walls at very high temperatures and, 4) Nucleation of magnesium oxide, aluminum oxides or similar non-metallic inclusions formed during the superheating process is the final hypothesis suggested [39, 40]. On the commercial scale, grain refinement by superheating is less practical for a large melts. It consumes excess time and fuel, and it reduces the life of the crucible.

2.10.2 Carbon Inoculation

Researchers have found that similar to superheating, carbon inoculation is effective for magnesium alloys that contain aluminum [14]. This involves introducing carbon into the molten alloy in the form of graphite, paraffin wax, lamp-black, organic compounds such as hexachloroethane (C_2Cl_6) and hexachlorobenzene (C_6Cl_6), carbides (Al_4C_3, SiC, CaC_2) and bubbling the melt with carbonaceous gases [9, 39].

Magnesium - Aluminum type alloys that can be effectively grain refined by carbon inoculation normally contain more than 2 % of Al. Al_4C_3 particles are considered effective nucleants for magnesium grains, as such there is a consensus about the mechanism of carbon inoculation [9, 14]. This is further supported by the recent development that the addition of an Al-Al_4C_3-SiC master alloy to AZ31 and AZ61 results in obvious grain refinement in both alloys [42]. Following the Al_4C_3 hypothesis, the master alloy was reportedly made by reacting SiC with molten aluminum. Carbon inoculation is an effective approach for grain refinement of Mg-Al alloys. The major challenge is how to consistently introduce carbon into molten magnesium while having no excess carbon left in the melt from a corrosion point of view [17].

2.10.3 The Elfinal Process

Grain refinement by adding $FeCl_3$ is known as The Elfinal process. The process was based on the hypothesis that the iron particles could act as nucleation sites for magnesium grains. It was first reported in a Belgian patent granted by Farbenindustrie in 1942 which claimed that Mg-Al-Zn alloys could be grain refined by the addition of 0.4 to 1 % of anhydrous $FeCl_3$ at temperatures between 750 °C and 780 °C [9]. Even though the approach worked well for grain refinement, the mechanism proposed for the process was highly disputed. Different mechanisms to explain the process have been proposed. Emley [9] proposed that hydrolysis of $FeCl_3$ in the magnesium melt gave rise to large amounts of hydrogen chloride (HCl) fumes, which subsequently attached to the steel crucibles and liberated carbon into the melt. The other mechanisms proposed by Emley was that magnesium grains nucleate on Fe-Mn-Al particles that have a good crystallographic match with magnesium [9]. Cao et al. [43] conducted experiments of melting Mg-Al alloys using carbon-free aluminum titanite crucibles and noticed grain refinement hence; he suggested that refinement has little to do with the Al_4C_3 particles proposed by Emley. Based on their observations, they suggested that magnesium grains nucleating on Fe-containing intermetallic particles gives rise to

grain refinement. The other observation found was that Fe is detrimental to the corrosion resistance of the magnesium alloys and in addition, the release of Cl and HCl makes the technique less attractive than the others.

2.10.4 Titanium Based Grain Refiners

It is well known that Titanium (Ti) is a significant grain refiner for aluminum alloys, however, the same statement cannot be made for magnesium alloys. This is mainly because of the limited solubility of Ti in Mg. Because of the uncertainty regarding the liquidus and solidus lines on the Mg-rich side of the Mg-Ti binary phase diagram, there is a significant amount of discrepancy in literature [44]. The high Q value of Ti (Table 2-2), leads to the expectation that it would be a very effective grain refiner but because of the solubility issues, experimental studies are very scarce and contradictive.

Work performed by Lee [45] reported grain coarsening as a result of adding Ti to AZ91. Conversely, Wang et al. [46] reported significant grain refinement by adding Ti to an AZ31 alloy coupled with varying cooling rates and Low-Frequency Electromagnetic Casting (LFEC). The major difference between the two studies was the amount of Ti added to the alloy. Additions of 0.01 wt. % effectively reduced grain size, but additions of 0.1 to 0.8 wt.% acted as grain coarseners. Furthermore, Wang et al. [46] reported that with fixed compositions, cooling rates from 3 K/s to 6 K/s resulted in finer grain size but cooling rates between 6 K/s and 10 K/s had the opposite effect. The grain refinement as a result of Ti addition was attributed to the peritectic reaction on the Mg-rich side of the Mg-Ti system binary phase diagram (similar to the addition of Zirconium to Mg) [46]:

$$L + \alpha(Ti) \leftrightarrow \alpha(Mg) \tag{14}$$

Furthermore, the grain refinement due to LFEC was a result of bringing a lower temperature melt to the center of the mould, leading to greater undercooling and enhanced nucleation in addition to breaking down dendritic arms. Figure 2-8 displays the mechanical properties of the alloys described above.

The mechanism of grain refinement was postulated to be Al combining with Ti elements to form $TiAl_3$. The $TiAl_3$ intermetallics distribute in the matrix and the second phase as seen in Figure 2-9 which impedes the growth of the $\alpha -$ Mg grains by concentration along the grain boundaries

[47]. Also, the Ti elements suppress Al from spreading in the melt which in turn prevents the β phases from forming and growing [47]. Lastly, if the Ti concentrations were raised to over 0.4 wt.%, excess Ti gathered at the grain boundaries which destroyed the connection between the matrix and other phases and lead to cracking [47]. This is detrimental to the mechanical properties and the effect can also be seen in Figure 2-9.

As stated previously, the research on the effect of Ti solute on grain refinement of Mg alloys is too inadequate to reach any conclusion. In theory, based on the Q value of Ti, it should have high potential to refine the grains of cast Mg alloys but, because the solid solubility of Ti in Mg is near zero, the actual Q value is assumed to be very low. Therefore, the effect of Ti as a solute on grain refinement of cast Mg alloys could be very marginal. However, with further research and investigation, if proper Ti-containing master alloys can be developed to provide sufficient and effective heterogeneous nucleation sites in Mg alloy melts, promising grain refining results could be obtained, particularly for Mg–Al-based alloys.

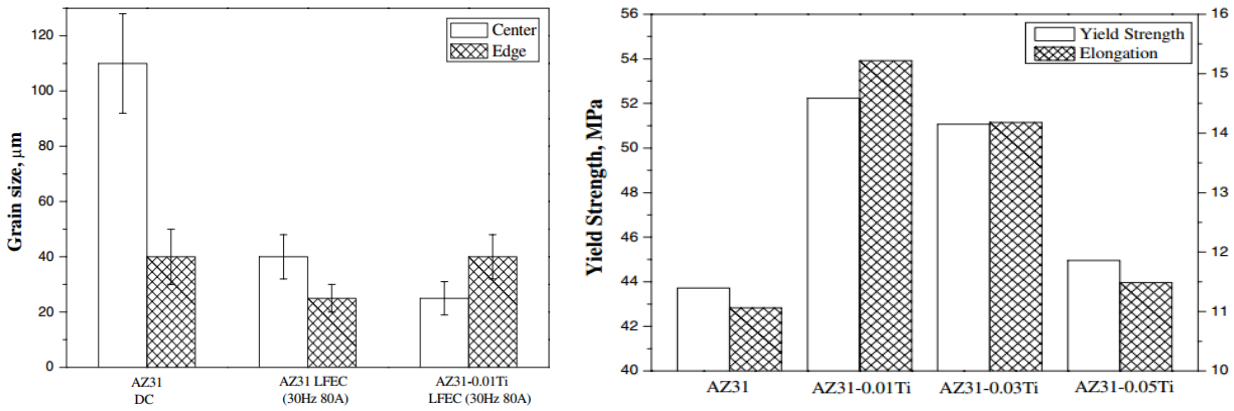

(a) **(b)**

Figure 2-8: (a) Grain size measurements for AZ31 and AZ31-0.01Ti alloys prepared by DC and LFEC processing, (b) Mechanical properties of the as-cast alloys solidified at a cooling rate of 6 K/s [47]

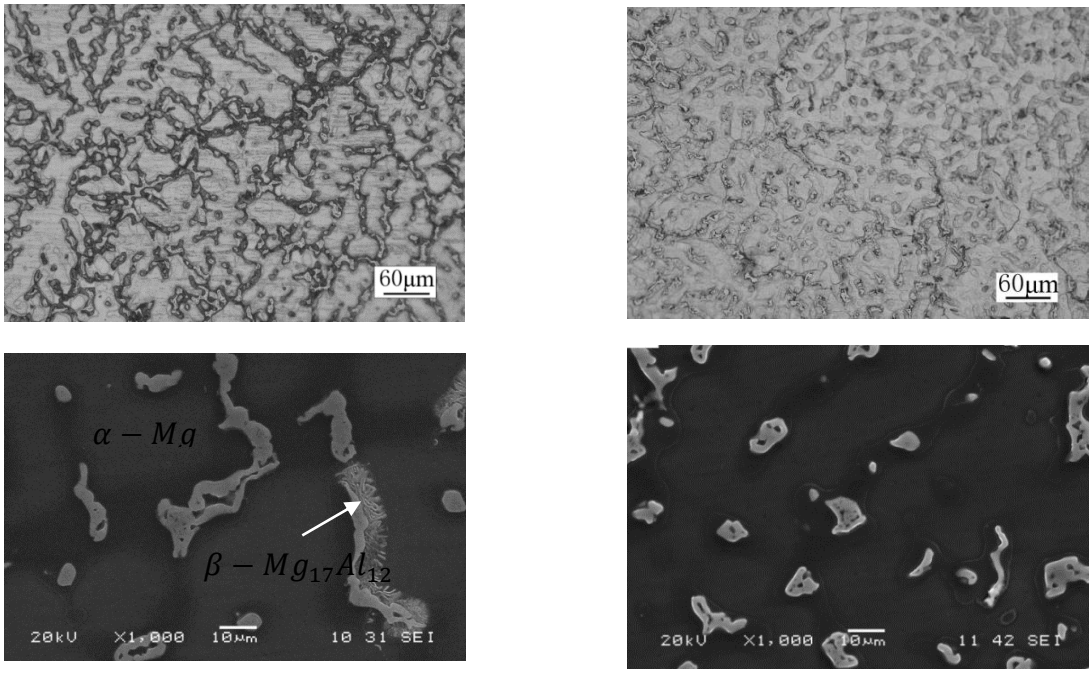

(a) (b)

Figure 2-9: (a) As-cast microstructures of alloy Base AZ91 and (b) AZ91+0.2Ti [47]

2.10.5 The Effect of Calcium as a Grain Refiner

Within the past several years, Calcium (Ca) has been studied extensively as a grain refiner for Mg alloys. Calcium is of particular interest because of its low cost relative to other grain refiners such as titanium or zirconium. Also, it has grain refining capabilities for both aluminum free and Mg-Al alloys which increases its appeal for the industry as a common refiner both systems is desirable. Lastly, Ca has a high Q-value of approximately 12 which indicates that it has good potential for grain refinement.

Data reported by Li et al. [48] based on Ca addition to AZ91D with a Mg-30 wt.% Ca master alloy reported significant grain size reduction with Ca contents of up to 1 wt.%. Figure 2-10 displays the grain size of the AZ91D alloy with varying amounts of calcium. It was determined that Ca addition promotes nucleation in the melt, elevates the formation temperature of Al_2Ca phase, and increases the impediment effect of constitutional undercooling in a diffusion layer ahead of the advancing solid/liquid interface and lowers the extent of the eutectoid reaction [48].

Figure 2-11 displays cooling curves for various Ca additions of this alloy. By examining the figure, it can be seen that by adding more Ca to the melt, the formation temperature of Al_2Ca increases which results in finer grains as the effect of CS is increased. Furthermore, the added Ca tends to form Al_2Ca rather than Mg_2Ca which therefore reduces the amount of Al present to participate in the eutectic reaction as evidenced by Figure 2-12 [48]. The decreased amount of Al available for the eutectic reaction assists in the refinement of the eutectic phase on the grain boundaries [48].

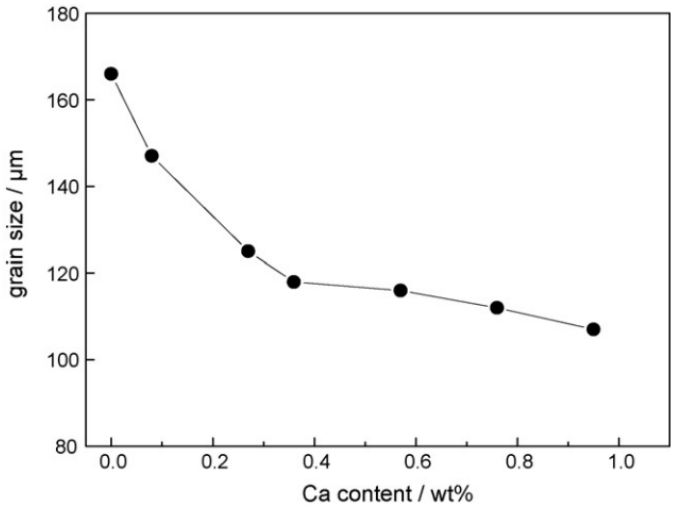

Figure 2-10: The effect of Ca on grain size of AZ91D alloy [48]

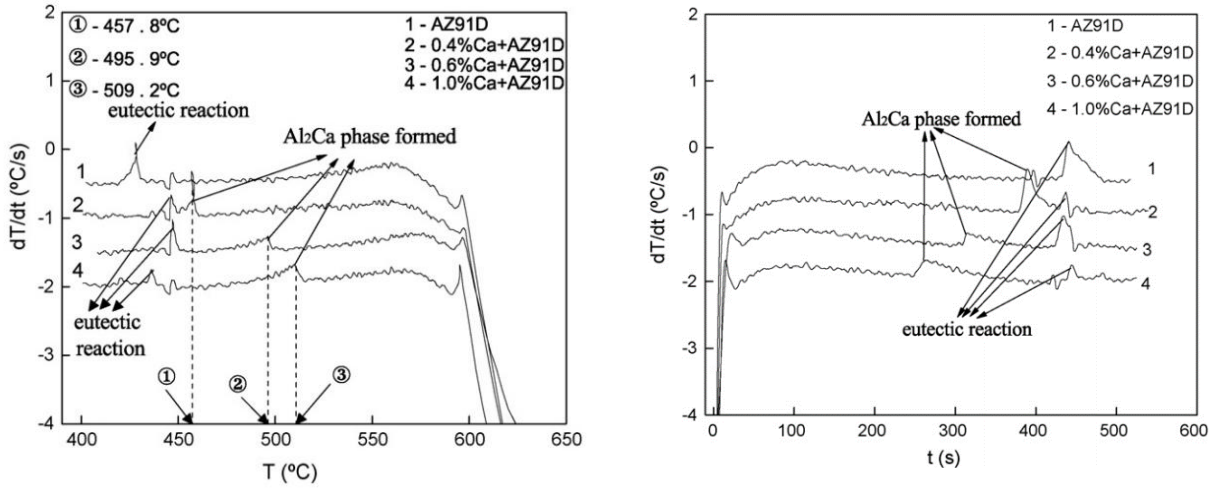

(a) (b)

Figure 2-11: (a) Effect of Ca on the formation temperature of Al_2Ca phase, (b) Effect of Ca on the eutectic reaction [48]

A similar study performed by Hirai et al. [49] confirmed the findings of Li et al. and also observed that Ca addition above 1 wt.% resulted in the formation of brittle eutectic compounds which led to decreased material properties such as strength and elongation as seen in Figure 2-12.

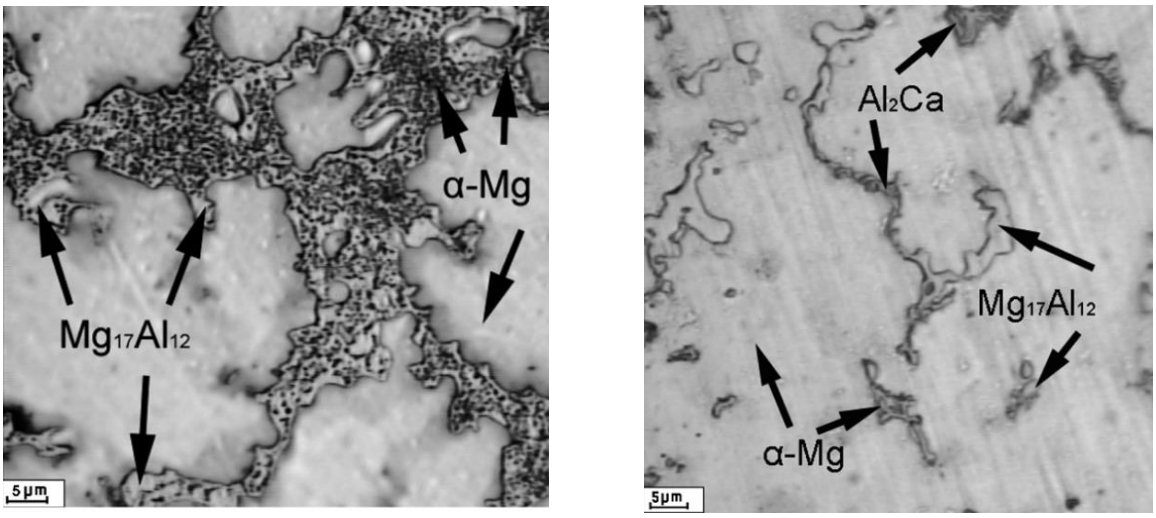

(a) (b)

Figure 2-12: Effect of Ca on eutectic structure morphology of AZ91D: (a) 0 wt.% Ca; (b) 1.0 wt.% Ca [48]

Based on current literature, it is considered that calcium inoculation is a promising approach to grain refinement in cast Mg alloys, particularly in Mg–Al-based alloys provided the actual effect of Ca addition on grain refinement is comprehensively known, and the mechanism is fully understood. Effective and low-cost master alloys of Ca will be beneficial to Mg manufacturers due to its good compatibility with both Mg-Al and Al-free Mg alloys. Comprehensive research work needs to be done to evaluate the effect of the solute together with the effect of potent nucleates.

2.10.6 The Effect of Silicon as a Grain Refiner

According to Table 2-2, the growth restriction factor of Silicon (Si) is approximately 9.25. This means that Si has strong potential for grain refinement. Studies performed by Srinivasan et al. [50, 51] confirmed the grain refining effects of Si, but also noticed negative side effects such as reduction in tensile properties and reduced mechanical properties at high temperature compared to the base alloy. Moreover, it was also noticed that adding other alloying elements such as Antimony

(Sb) and Strontium (Sr) strengthen the grain refining effects of Si and also improved the material properties.

The study involved the addition of Si and Pb to AZ91 alloy which led to grain size reduction of 80 to 60 μm on average. Srinivasan et al. [50] observed that when Si was added to the alloy, a new Chinese script type Mg_2Si phase was formed which assisted with grain refinement but, reduced the mechanical properties of the alloy due to their course nature and low melting point (~437 ℃). Figure 2-13 (a) displays the typical microstructure of an AZ91 alloy with no Si added and Figure 2-13 (b) displays the microstructure with 0.5 wt.% Si. The figure shows the Mg_2Si phase and its Chinese script type morphology. Subsequently, Srinivasan [50] added varying amounts of Sb and Si to the melt and determined that the additions altered the morphology of the Mg_2Si phase such that they transformed from the Chinese script type shape to a pentagon shape (Figure 2-14)

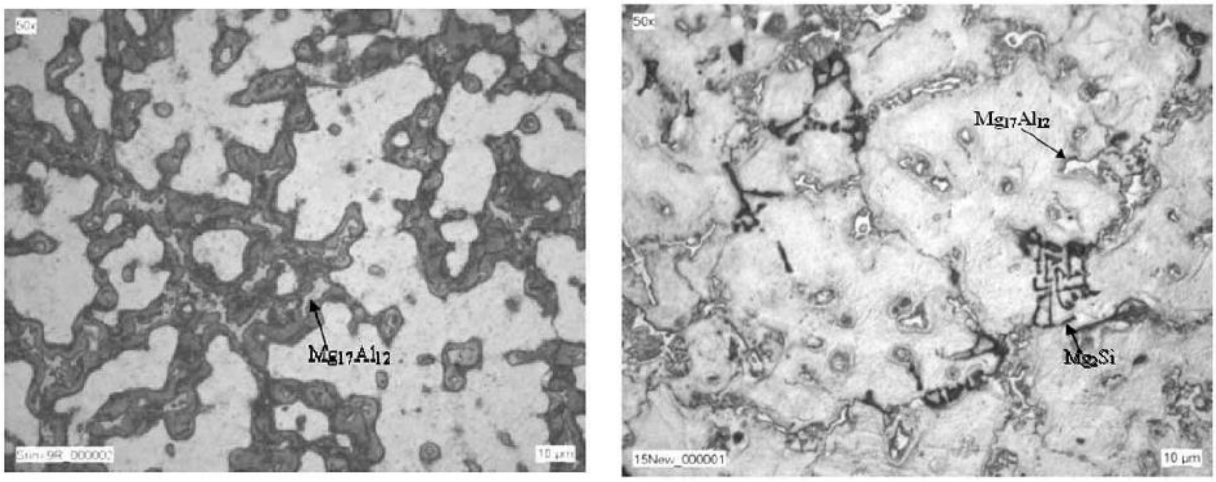

(a) (b)

Figure 2-13: (a) Microstructure of AZ91 magnesium alloy containing 0 wt.% Si, (b) Microstructure of AZ91 magnesium alloy containing 0.2 wt.% Si [50]

The new morphology and uniform distribution of the Mg_2Si phase improved the strength, ductility, and further reduced the grain size of the alloy as compared to the base AZ91 alloy, which can be seen by the values reported in Figure 2-15 [50].

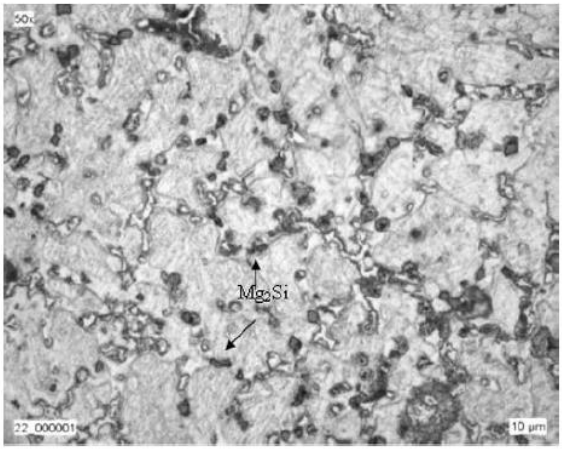

Figure 2-14: Microstructure of AZ91 alloy with 0.2 wt.% Si and 0.5 wt.% Sb showing the refined Mg_2Si particles [50]

Alloy	Al	Zn	Mn	Si	Sb
A1	9	1	0.2	—	—
A2	9	1	0.2	0.2	—
A3	9	1	0.2	0.5	—
A4	9	1	0.2	0.2	0.2
A5	9	1	0.2	0.5	0.2

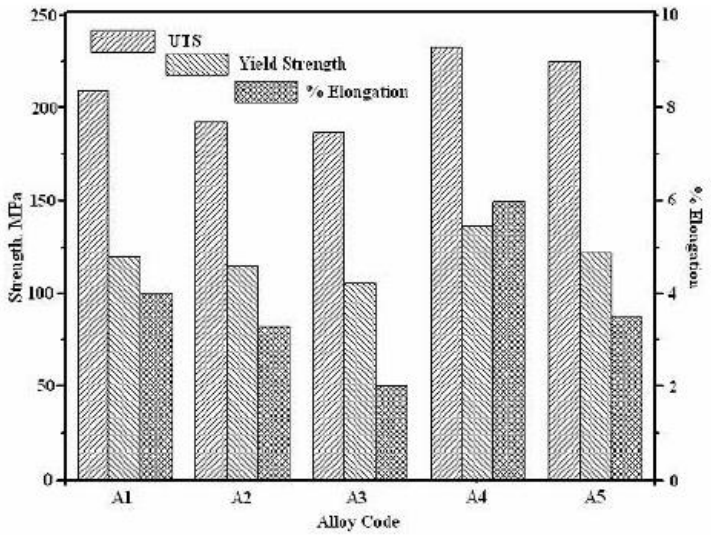

Figure 2-15: Tensile properties of the alloys tested at room temperature [30]

Other additions such as calcium (Ca), phosphorus (P) and strontium (Sr) are also commonly added to improve the effects of Si. Calcium addition was found to produce $CaSi_2$ which was believed to

act as heterogeneous nucleation sites, P addition resulted in the formation of $Mg_3(PO_4)_2$ which was also determined to be a strong nucleation site and Sr addition resulted in Sr becoming incorporated in the Mg_2Si phase which lead to altered morphology similar to Pb addition described above [52].

To completely exploit the grain refining potency of Si in Mg alloys, the growth restriction factor (Q-value) of Si should be calculated in different systems such as ternary or quaternary. Comprehensive understanding of the grain refining mechanisms of Si may lead to the development of new and more effective grain refiner for Mg alloys.

2.10.7 The Effect of Tin as a Grain Refiner

The effect of Tin (Sn) on the grain refinement of Mg alloys has not been thoroughly investigated. The effects of Sn addition on mechanical properties, however, has been widely studied. Therefore, this section will discuss the effect of Sn on microstructure and mechanical properties but have little emphasis on the grain refinement aspect.

Turen [53] investigated the effects of adding varying amounts of Sn to AZ91 Mg alloy. The study concluded that the UTS, YS, % EL, and resistance to hot tearing were significantly increased as a result of the addition of up 0.5 wt.% Sn and decreased with additions between 0.5 wt.% and 2 wt.%. [53]. Figure 2-16 displays the change in mechanical properties of the alloy with varying Sn.

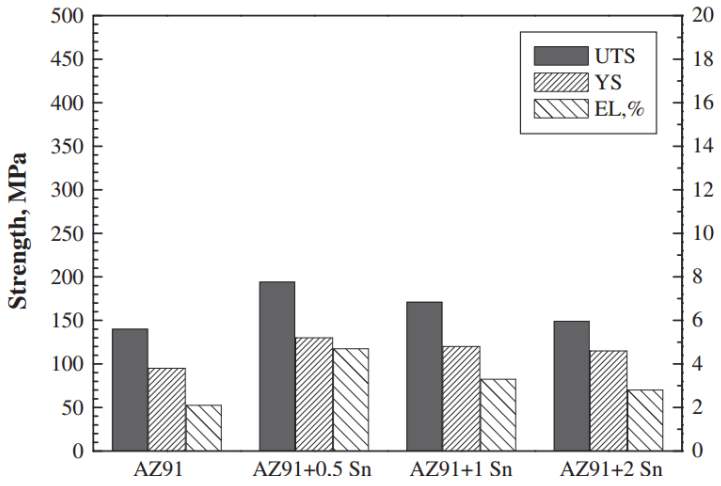

Figure 2-16: Ultimate tensile strength (UTS) and yield strength (YS) of AZ91 alloy as a function of Sn content [53]

The increases in mechanical properties were mainly attributed to two mechanisms, 1) Transformation of lamellar eutectics into fully divorced eutectics with smaller surface areas

(Figure 2-17 – c), thus fewer crack sites and 2) The formation of Mg_2Sn within the eutectic regions in the form of evenly distributed fine precipitates (Figure 2-17 – d) [53]. Conversely, as the percentages of Sn increased beyond 0.5 wt.%, coarsening of the Mg_2Sn phases was initiated and subsequently lead to decreased mechanical properties and increased susceptibility to hot tearing [53].

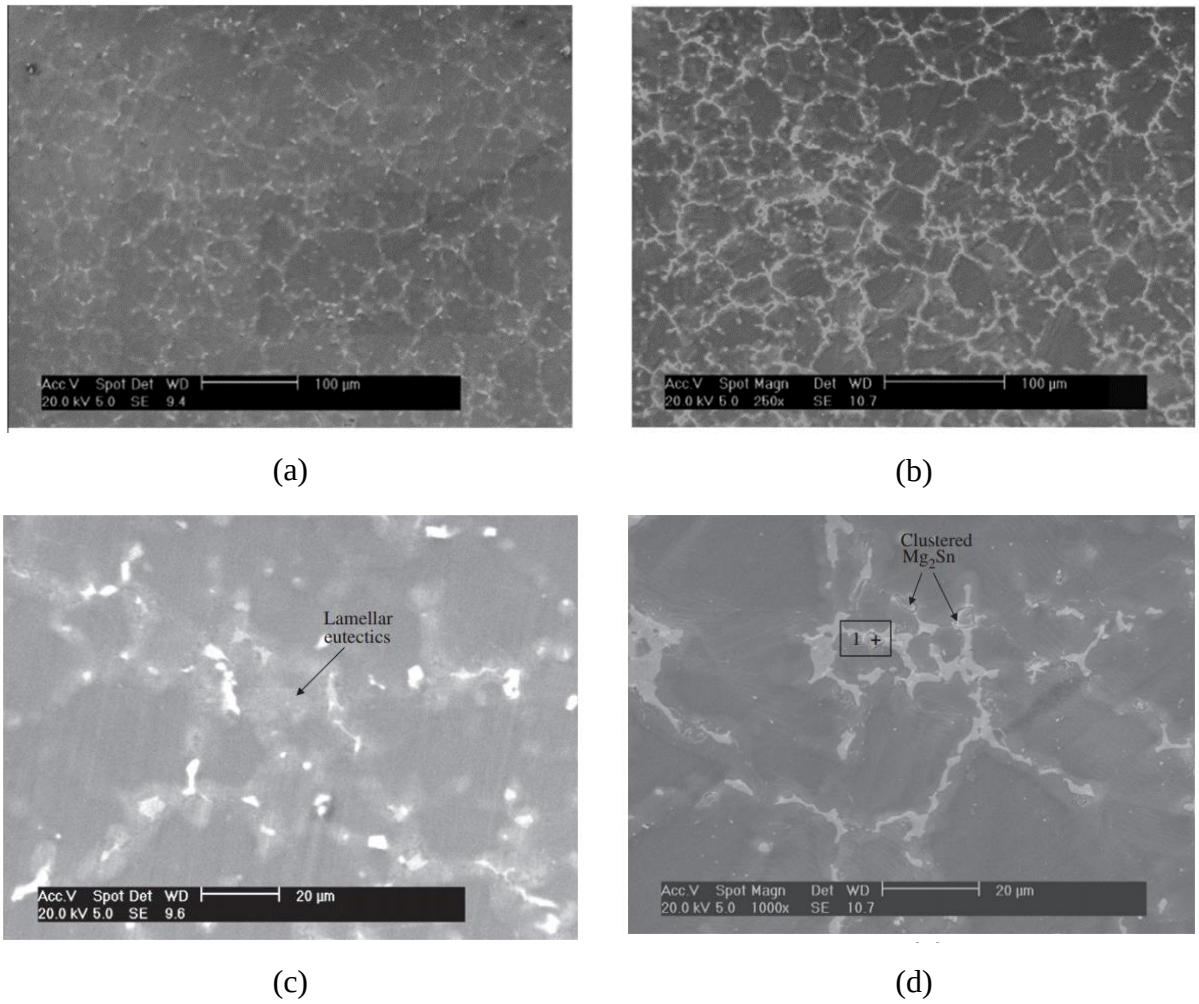

Figure 2-17: (a) microstructure AZ91 base alloy (b) microstructure of AZ91 + 2 wt.% Sn, (c) SEM micrograph of base AZ91 alloy (d) SEM micrograph of AZ91 + 2 wt.% Sn [53]

Figure 2-17 a) displays the microstructure of the as-cast AZ91 alloy, Figure 2-17 b) shows the microstructure after addition of 0.5 wt.% Sn. By examining these figures, clear grain refinement

can be seen. Unfortunately, the relative sizes of the grains were not investigated by [53]. It is clear that Sn proves to be an efficient alloying element concerning mechanical properties but its effects on grain structure of magnesium alloys requires further investigation.

2.10.8 The Effect of SiC Additions

Based on the lattice disregistry parameter, Silicon Carbide (SiC) has been identified as an effective grain refiner for Mg alloys (disregistry < 4 %). Furthermore, its low cost, relative to other alloying elements makes it very attractive to the industry. Silicon Carbide is abundant in nature and environmentally friendly which further promotes its desirability. Conversely, care must be taken during the preparation of carbon-based grain refiners because of the poor wettability between Mg and C. Additionally, excess additions can be detrimental to the mechanical properties of the alloy mainly because carbon is considered as an inclusion.

Based on studies performed to date, the grain refining mechanisms of adding SiC to Mg have not been clearly identified. One hypothesis is that SiC is a good grain refiner for Mg alloys with low Al content only. Such alloys lack effective nucleants therefore, additions of SiC can make an apparent contribution to their grain size by decreasing the amount of undercooling required for nucleation to occur.

A recent study performed by Elsayed [11] examined the effects of SiC addition on AZ91E alloy. Refiner addition was coupled with Ar bubbling to replace the degassing and inclusion removal effects of C_2Cl_6. The resulting microstructure which can be seen in Figure 2-18 consisted of mainly blocky Mn-Al particles that were in the center of grains alongside agglomerated Al-Mg-C-O (most likely Al_2MgC_2) particles. Upon further inspection, Elsayed determined that the blocky Mn-Al or (Mn-Al-Fe) particles contained concentrations of Si. The presence of Si indicates that the nucleant resulted from the addition of the Al-SiC and may be the result of the reaction product of the transformation of SiC to Al_2MgC_2. The agglomerated Al-Mg-C-O particles were assumed to be oxides or excess nucleants that were unable to position themselves to act as grain refiners. Therefore, a duplex nucleation mechanism of Mn-Al with Al-Mg-C-O nucleants was determined to be the principal mechanism of grain refinement which likely exists because the investigated alloy contained large percentages of Mn and Fe that also could be suitable nucleants when no other more appropriate phases are present [11].

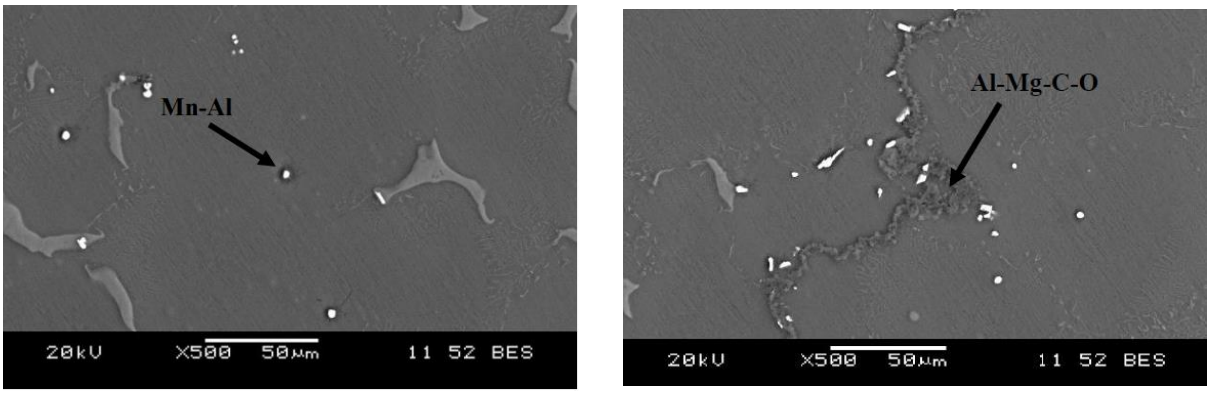

(a) (b)

Figure 2-18: (a) SEM Image of AZ91E with 0.50 wt.% Si-C, (b) SEM image showing Al-Mg-C-O agglomerated particles [11]

One of the main reasons for investigating SiC as a grain refiner was to replace C_2Cl_6. Therefore, in addition to microstructure, the mechanical properties of the alloys were also determined. Figure 2-19 and Figure 2-20 summarize the data gathered by Elsayed which is also a comparison with the efficiency of C_2Cl_6 additions. Elsayed [11] determined that addition of 0.50 wt.% Al-SiC to AZ91E alloys resulted in a significant decrease in average grain size (23 %), and increase in average YS (25%), UTS (10 %) and % Elongation (15 %) respectively as compared to the base AZ91E alloy.

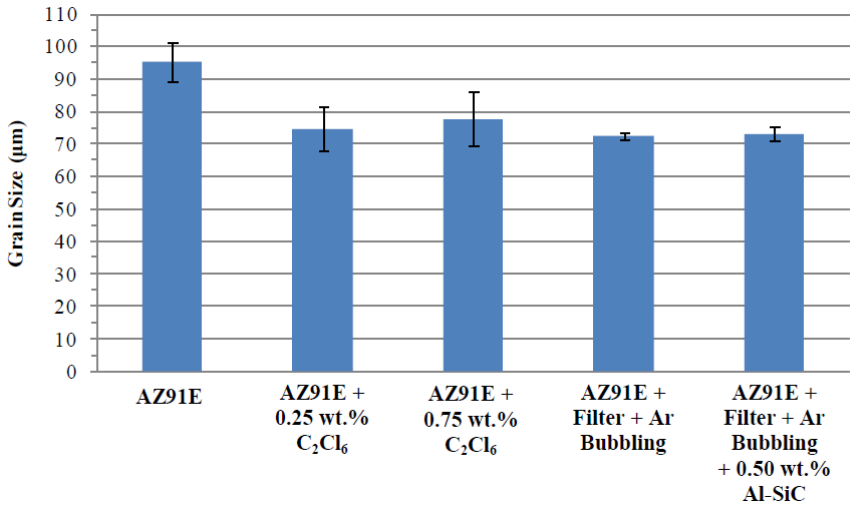

Figure 2-19: Effect of Al-SiC addition on grain size of AZ91E [11]

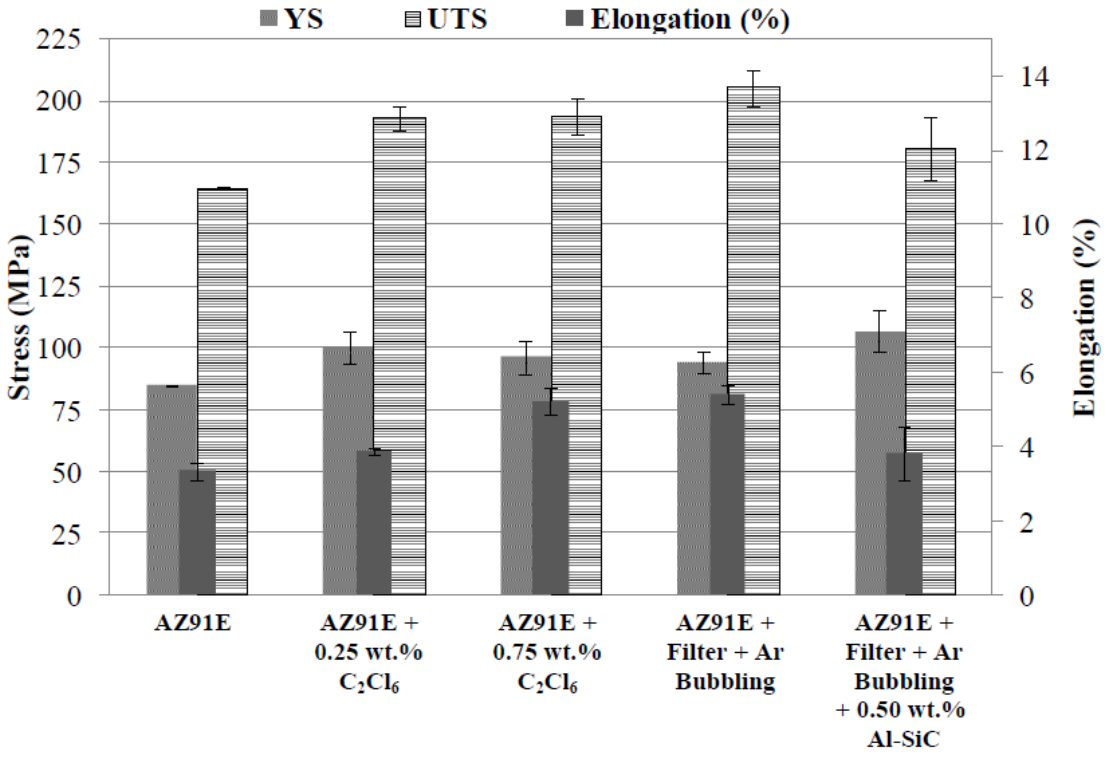

Figure 2-20: Effect of C_2Cl_6 addition and Al-SiC refiner addition on mechanical properties of AZ91E [11]

2.10.9 Aluminum-Carbon Based Grain Refiners

Similar to SiC, this grain refiner was developed to be an environmentally friendly alternative to C_2Cl_6. Aluminum - Carbon based grain refiners improve grain refinement by enabling easier C addition to Mg alloys. To avoid wettability issues, the Al-C additions were prepared by ball milling, compacting and sintering.

Elsayed [11] prepared in-situ grain refiners by ball milling powders of Al and graphite and subsequently consolidating the powders using Spark Plasma Sintering (SPS). The sintered particles were then added to an AZ91E alloy with varying compositions. The grain refinement mechanism using Al-C is thought to be similar to SiC additions. Figure 2-21 shows SEM images of the prepared alloys. The bright particles were Mn-Al or Mn-Al-Fe based and appear alongside dark Mg-Al-C-O.

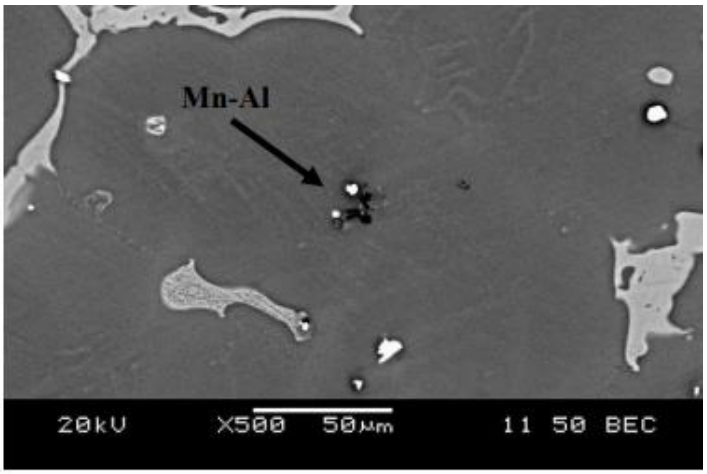

(a)

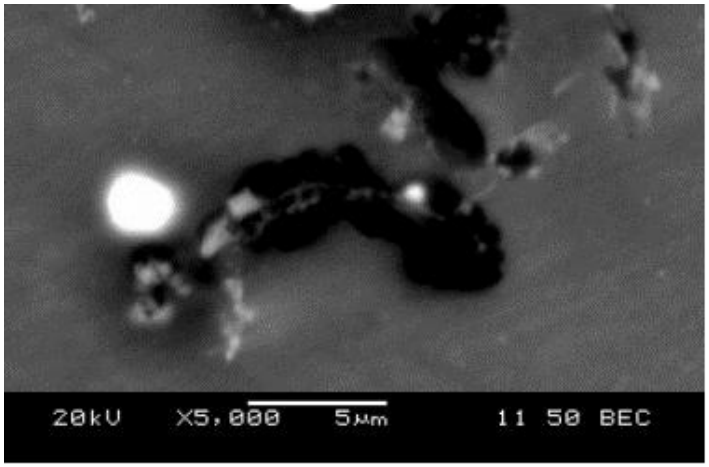

(b)

Figure 2-21: (a) SEM image of AZ91E + 0.50 wt.% Al-C, (b) Mn-Al-Fe based intermetallic alongside Al-Mg-C-O phase [11]

Similar to Si-C refiner addition, the addition of Al-C showed signs of duplex nucleation with Mn-Al or Mn-Al-Fe particles and Al-Mg-C-O or Al-C-O particles. The addition of the Al-C refiner did not show any other phases within its microstructure, unlike the Al-SiC refiner that contained agglomerated particles.

The grain refining effect and the resulting mechanical properties of the Al-C additions can be seen in Figure 2-22. The alloys with 0.50 wt.% Al-C addition showed a significant decrease in average grain size (21 %), and increase in average YS (18 %), UTS (24 %) and % Elongation (60 %) respectively as compared to the AZ91E castings. Elsayed [11] also noticed that because of the

mechanism of Al-C refiner addition to the melt (mechanical stirring), additional oxides were introduced into the castings as a result of agitation of the melt surface.

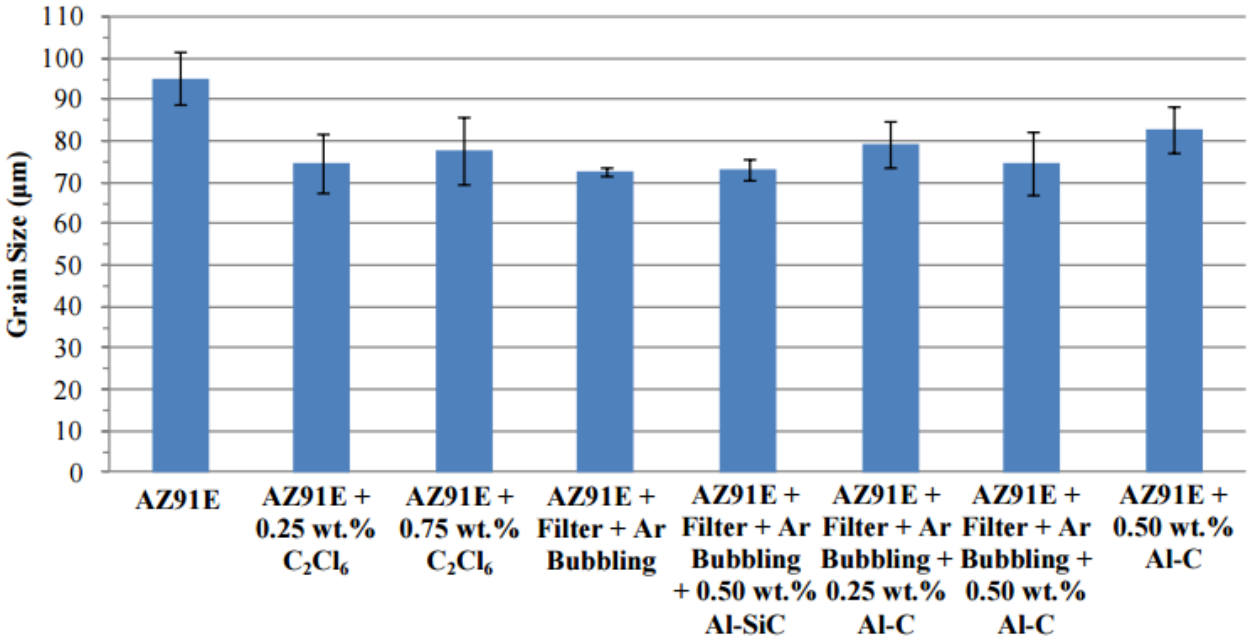

Figure 2-22: Effect of Al-C addition on grain size of AZ91E [11]

2.10.10 Aluminum-Boron Grain Refiner

Grain refiners utilizing KBF_4 salts have been developed to determine if an Al-B based grain refiner, containing AlB2 particles were capable of acting as sites for nucleation in Mg-Al alloys. One study by Suresh et al. [54] consisted of adding an Al-4B grain refiner to AZ91 Mg alloy to observe any reduction in grain size or any increases in ductility and strength. The procedure consisted of adding the Al-4B grain refiner to AZ91 at 740 °C and stirring the melt for 10 minutes to allow for reaction of the Mg alloy and the added grain refiner [54]. The melt was then poured into cast iron moulds preheated to 300 °C. The major results concerning grain size and mechanical properties are shown in Table 2-3. With increasing additions of Al-4B grain refiner, the grain size decreased. The optimal addition level to minimize grain size was 0.032 wt.% boron (B) with a grain size decrease from 100 µm to 30 µm (70 % decrease). At the optimal addition level (0.032 wt.% B), the Y.S. increased from 95 to 110 MPa, the UTS improved from 180 to 226 MPa, and the ductility increased from 3.3 to 4.8 % as compared to the base alloy.

Table 2-3: Grain Size and mechanical properties with the addition of Al-4B to AZ91 [54]

Alloy	Grain Size (µm)	Yield Strength (MPa)	Tensile Strength (MPa)	Ductility (% Elongation)
AZ91	100	95	180	3.3
AZ91 + 0.008 wt.% B	70	102	197	3.9
AZ91 + 0.02 wt.% B	45	107	211	4.4
AZ91 + 0.032 wt.% B	30	110	226	4.8
AZ91 + 0.04 wt.% B	30	113	229	4.9

The AlB_2 particles appeared as blocky structures approximately 4-8 µm in size. As seen in Figure 2-23, these particles were found in the center of grains which demonstrated their capacity to act as heterogeneous nucleation sites.

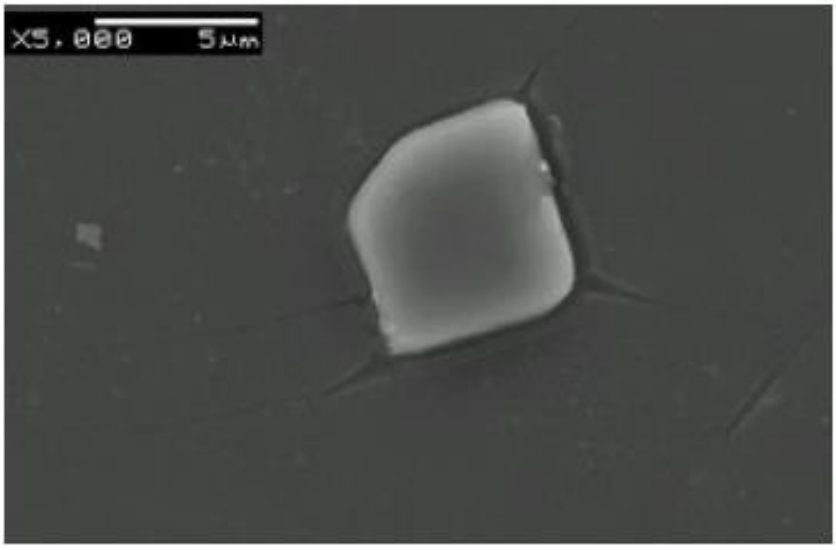

Figure 2-23: AlB_2 particle in AZ91 casting (0.032 wt.% B) [54]

The AlB_2 particles also met the requirements to act as good nucleating particles such as [14, 55]:

1. Similarity between the crystal structures of the base material and grain refiner. The lattice parameters of Pure Mg are a = 0.320 nm and c = 0.520 nm, while those of AlB2 are a = 0.301 nm and c = 0.325 nm.

2. Non-dissolution of the grain refining particle in the liquid base material.

3. Resistance to fading (melting point of AlB2 is 892 °C, well beyond the typical holding temperatures of Mg alloys (650 to 750 °C)) [27].

As the literature suggests, there is a continued quest to find suitable grain refiners for Mg-Al alloys for application in the industry. The two general directions of solving the grain refinement problem of Mg-Al alloys are to find a new additive that will perform the task efficiently or to significantly improve the efficiency of an existing method. Either way, the process requires a better understanding of what controls the formation of potent nucleanting particles in Mg-Al based alloys.

3 Experimental Procedure

3.1 Materials

This section describes the materials used in this study and outlines the processes required to perform the experiments. The compositions of the materials used are presented first followed by a detailed description of procedures and equipment utilized to prepare the castings.

3.1.1. Pure Mg

Commercial purity Mg (99.8 wt.%) obtained from Meridian Technologies Inc., Strathroy, ON Canada.

3.1.2. AZ91E Alloy

Virgin ingots of AZ91E Mg alloy (Meridian Technologies Inc., Strathroy, ON Canada) were one of the base materials used in this study. The chemical composition of the AZ91E alloy (batch analysis from the supplier) is presented in Table 3-1.

Table 3-1: Composition of AZ91E alloy (wt.%)

Mg	Al	Zn	Mn	Si	Fe	Be	Others
Balance	8.7	0.53	0.23	0.05	0.003	0.0012	0.3

3.1.3. MgB_2 Refiner

High purity 99 % (metal basis) magnesium boride MgB_2 was received in powder form (Alfa Aesar, Ward Hill, MA United States). The as-received particle size of the refiner was 100 mesh (<149 μm).

3.1.4. Graphite Mould

The graphite moulds were machined from 2.50 in (63.5 mm) diameter graphite rods (Graphitestore Northbrook, IL United States). The mould cavity was machined to produce castings with hemispherical bottoms 2.00 in (50.8mm) tall and 1.50 in (38.1 mm) in diameter. Figure 3-1

displays images of the dimensions of the graphite mould as well as the entire assembly used during casting. To obtain thermal data of the solidifying castings, K-type thermocouples with ceramic sleeves (Omega Engineering Inc., Laval, QC Canada) were inserted into the solidifying melt immediately after pouring. Low carbon steel thermocouple holders (Figure 3-1 – b) were used to ensure that the thermocouples were properly located during thermal data acquisition. The thermocouples were fixed in place using a set screw. The steel fixture/thermocouple assembly was fixed over a 1/8 in (3mm) thick steel plate that covered the melt to prevent oxidation.

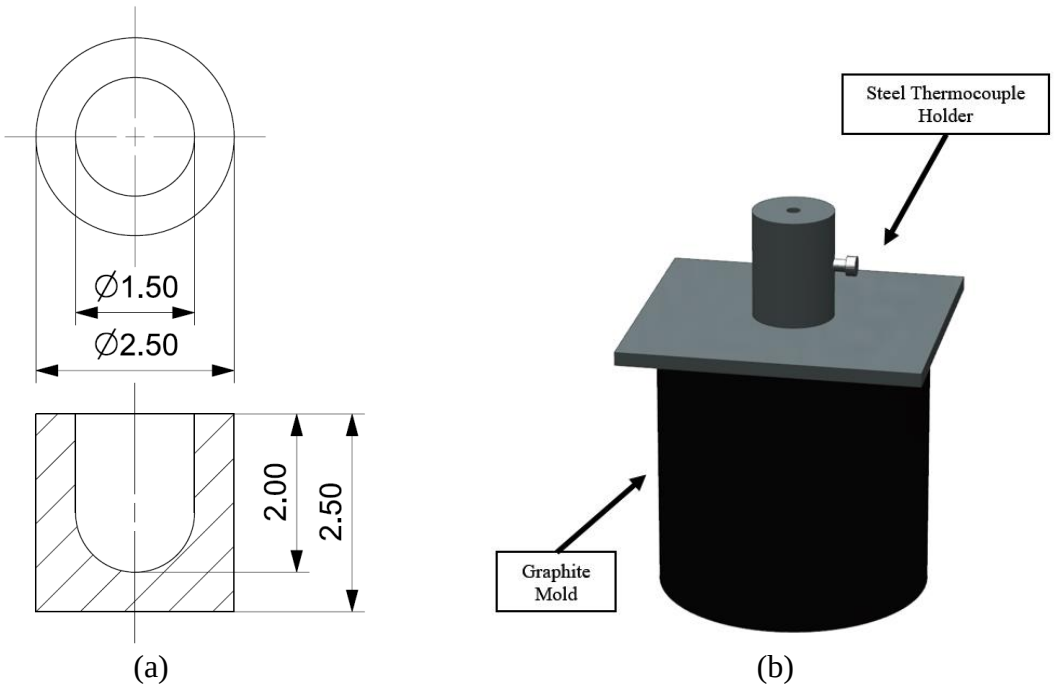

Figure 3-1: (a) Graphite mould dimensions (all dimensions are in inches) and (b) Graphite mould final assembly

3.1.5. Permanent Tensile Mould

An ASTM standard (B108-06) permanent mould as seen in Figure 3-2 was used to produce the Pure Mg and AZ91E Mg alloy tensile castings. The resultant castings were standard round tensile specimens with a gauge diameter of 0.50 in (12.7 mm) and a gauge length of 2.00 in (50.8 mm). A minimum of four tensile specimens were produced to represent each casting condition, for repeatability.

SFP MICAWASH NO. 15 a water-based refractory coating (SMELKO Foundry Products LTD., Milton, ON Canada) was applied to the permanent mould to reduce wear and ease casting removal and prevent contamination. The mould was cleaned by hand using a steel brush, then heated to 250°C, and cooled in air to 200°C before coating. A compressed air gun at a pressure between 30 - 40 kPa at a distance approximately 30 cm from the mould surface was used to apply the coating.

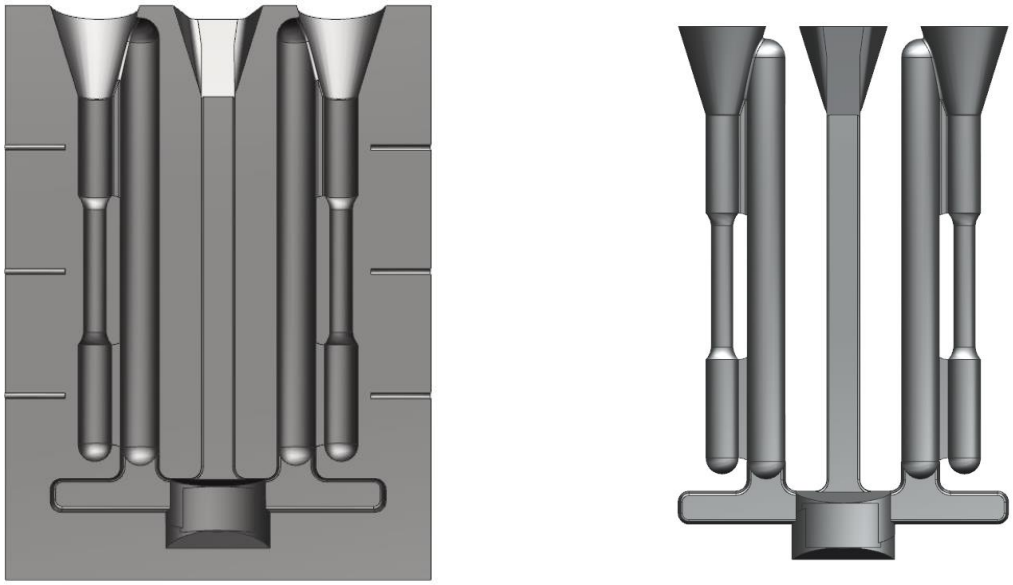

(a) (b)

Figure 3-2: (a) ASTM standard (B108-06) permanent tensile mould (b) resultant casting

Six K-type thermocouples (Omega Engineering Inc., Laval, QC Canada) with ceramic sleeves were inserted into slots machined into the tensile mould to measure the mould temperature during the casting experiments. The slots (Figure 3-3) extended approximately 34 mm into the mould wall at the parting line. Two of the three castings per addition trial utilized a thermocouple extending from the top of the mould to the center of the gauge of one of the tensile bar cavities in order to obtain thermal data of the solidifying castings. The thermocouples were connected to a data acquisition system for temperature monitoring.

The tensile mould was preheated using a natural gas furnace in two steps to ensure a homogeneous temperature distribution. First, the mould was placed in the furnace with the pouring cup facing down for 16 minutes. Subsequently, the mould was turned over with pouring cup facing up and

reheated for an additional 14 minutes. A typical heating cycle lasted 30 minutes and resulted in a mould temperature approximately 200 °C above the desired temperature. The mould was then allowed to cool in still air and homogenize in temperature before pouring. This mould heating method resulted in a temperature difference of approximately 5-10 °C between thermocouples located at the center of each tensile sample gauge.

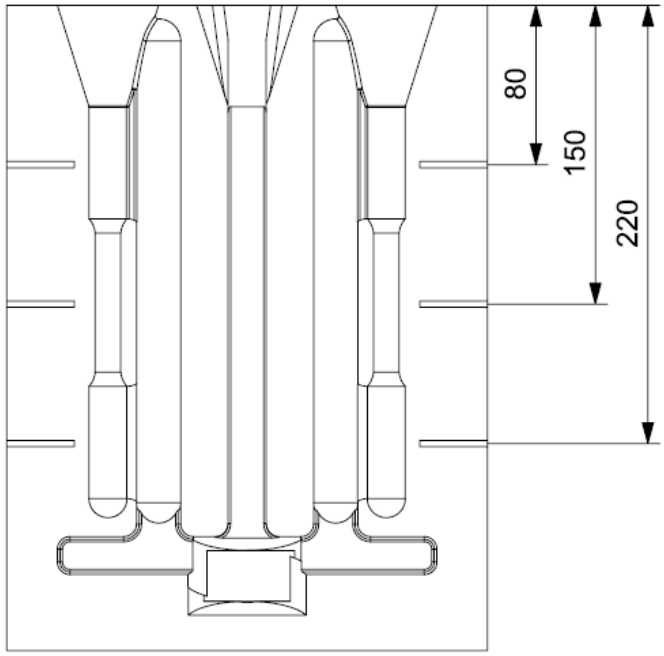

Figure 3-3: Thermocouple placement in permanent tensile mould

3.2 Ball Milling Procedure

The ball mill used was a Retsch PM 100 Planetary Ball Mill (Figure 3-4 – a). Tungsten carbide milling balls with a 3 mm diameter were used during the milling process. The WC-based grinding jar was 50 ml in size (Figure 3-4 – b). Approximately 60 % of the jar volume was filled with grinding balls to increase the friction surface required for producing very fine particles. Subsequently, 30 % of the grinding jar volume was filled with sample material, and the remaining 10 % was left empty. Since the target particle size was in the nano range, a colloidal grinding procedure was utilized. Isopropyl alcohol with 99.99 % purity was used as a dispersing agent. The alcohol was added to the sample until the mixture displayed a consistency like engine oil.

Figure 3-4: (a) PM100 planetary ball mill and (b) WC grinding jar

The ideal milling speed to avoid spillage and excess turbulence was determined to be 300 RPM which was determined by gradually increasing the speed of the ball mill until leaking from the grinding jar was observed. Following this, the highest speed without leakage was chosen as the ideal RPM. A grinding interval was also utilized during the milling process. The samples underwent grinding for 10 minutes. Subsequently, the jar was left to cool for 10 minutes and restarted in the opposite direction for an additional 10 minutes for a total of 30 minutes, which constituted one cycle of milling. Once the milling run was complete, 1 to 2 hours was added to the time to allow the powder to sufficiently cool.

The powder was collected by pouring the contents of the jar over a test sieve (with aperture sizes 20 to 50 % smaller than the balls) with a collecting pan. The sieve and pan were then placed on a sieve shaker. The vibratory movement of the sieve shaker helped to separate the sample material from the balls. The grinding balls were also flushed with alcohol to remove the trapped powder. Once the powder was collected, the jar and media were cleaned with ethanol, and the media underwent sonication to ensure no powder particles contaminated the media's surfaces.

3.3 Melting and Addition Procedure

Two melting procedures were required for this study. The first procedure was used for experiments examining grain refinement and fading of Pure Mg and AZ91E Mg alloy using MgB_2 as a grain

refiner with graphite moulds. The second portion of this study focused on the effect of grain refinement on the mechanical properties of permanent mould cast Pure Mg and AZ91E Mg alloy. Both procedures are described in the following sections.

3.3.1 Grain Refinement and Fading Experiments for Pure Mg and AZ91E Mg Alloy

Approximately 1 kg of Pure Mg or AZ91E Mg alloy was preheated for at least 30 minutes in a furnace at 250 °C. The ingots were then added to a low carbon steel crucible and placed into a custom designed electric resistance melting furnace (PSH Kilns, 5 kW, Oakville, ON Canada) set to a temperature of 775 °C. A cover gas consisting of 4.7 L/min of CO_2 + 0.5 vol.% SF_6 was used to prevent oxidation of the melt.

Three graphite moulds were then preheated to 750 °C. The required amount of grain refiner as required per trial was measured using a digital balance (Scientech-SP350). The grain refiner was poured into a steel scoop and placed in the preheating furnace to remove moisture. The melt temperature was checked periodically using a K-type thermocouple. Once the melt temperature was >760 °C, the oxides present on the surface were skimmed. The grain refiner was added to the melt and the mixture was stirred for 3 minutes at 300 RPM, using a preheated low carbon steel impeller.

To produce a casting with five minutes of holding, a timer was used to measure the time elapsed after grain refiner addition immediately after stirring ended. After five minutes of holding the melt in the melting furnace, one graphite mould was removed from the heating furnace and placed on a firebrick. A preheated ladle was then used to pour a portion of the melt into the mould at a pouring temperature of 720 °C (casting to represent 5 minutes of holding).

After pouring, the graphite moulds were covered with a steel plate, according to the assembly in Figure 3-1. The melting furnace temperature was lowered to 750 °C to maintain the melt temperature. After an additional 5 minutes of holding (total 10 minutes), the ladle was used to produce a second graphite mould casting (casting representing 10 minutes of holding). The same procedure was repeated once more for the final graphite mould to represent a holding time of 20 minutes. Any remaining melt was poured into a pig mould and not reused. A summary of the pouring procedure is outlined in Table 3-2.

Table 3-2: Experimental procedure for grain refinement and fading experiments with graphite moulds

Process	Important Parameters
	Raw Material Preparation
I	○ 1 kg of Pure Mg or AZ91E alloy was measured ○ MgB_2 powder (as required based on addition level)
II	○ Pre-heated ingots and refiner at 250 °C for 30 minutes
III	○ Pre-heated graphite moulds to 750 °C (Figure 3-1)
	Melting of Metal and Addition of Refiner
I	○ Placed ingots in melting furnace set at 775 °C ○ Cover gas: CO_2 + 0.5 vol.% SF_6 at 4.7 L/min
II	○ Checked melt temperature with K-type thermocouple (>760 °C)
III	○ MgB_2 powder was added to melt
VI	○ Melt was stirred at 300 RPM for 3 minutes ○ Timer for melt holding time was started
	Pouring
I	○ Thermal data acquisition system was started ○ Graphite mould was removed from furnace
II	○ Melt was ladle poured at 720 °C into graphite mould ○ Mould was covered with steel plate (Figure 3-1) ○ Melting furnace temperature set to 750 °C
III	○ Repeated steps I and II for 10 min and 20 min holding times

Table 3-3: Important casting parameters for grain refinement and fading experiments with graphite moulds

Pouring Temp. (°C)	Mould Temp (°C)	Holding Time (min)	MgB_2 Addition Level (wt.%)
720	750	5, 10, 20	0.0125
			0.02
			0.025
			0.03
			0.05
			0.1

The pouring temperature of 720 °C was used to match industry practices which maintain temperatures between 680 and 740 °C for permanent mould cast Mg alloys. The high mould temperature was to ensure that the mould walls did not act as a site for nucleation of grains. Also, it promoted a low cooling rate which translated in a large number of temperature measurements recorded by the data acquisition system during solidification. Holding times of 5, 10 and 20 minutes were used during this study to ensure appreciable fading. The addition levels of 0.1, 0.05, 0.025 and 0.0125 wt.% were chosen to be similar to research conducted by Suresh et al. [54] which examined grain refinement and fading of boron added AZ91 Mg alloy.

3.3.2 Permanent Mould Experiments (Tensile Castings)

Approximately 1 kg of AZ91E Mg alloy was preheated for a minimum of 30 minutes before melting. The ingots were melted in a low C steel crucible and placed into a custom designed electric resistance melting furnace (PSH Kilns, 5 kW, Oakville, ON Canada) set to a temperature of 775 °C. A cover gas consisting of 4.7 L/min of CO_2 + 0.5 vol.% SF_6 cover was used to prevent oxidation of the melt.

The melt temperature was checked using a K-type thermocouple. Once the melt temperature reached 760 °C, the tensile mould was preheated, removed from the gas furnace and left to cool on a refractory brick. The required amount of grain refiner was prepared and added to the melt using the same procedure as the graphite mould castings. Once the mould was sufficiently cooled, the melt was removed from the electric resistance furnace, skimmed of any oxides using a low carbon steel spoon and poured at 720 °C into the tensile mould. The corresponding mould temperature was 540 °C at the tensile gauge section. Any remaining melt was poured into a pig and not reused for subsequent experiments.

The melt was protected with the cover gas during pouring and for an additional 5 minutes as the casting solidified and cooled. The casting was then removed from the tensile mould and cooled to room temperature without the protection of the cover gas. A summary of the casting procedure is outlined in Table 3-4.

Table 3-4: Experimental procedure for permanent mould experiments

Process	Important Parameters
	Raw Material Preparation
I	o 1 kg of Pure Mg or AZ91E alloy was measured o MgB_2 powder (as required based on 0.025 wt.% addition level)
II	o Pre-heated ingots and refiner at 250 °C for 30 minutes
	Melting of Metal and Addition of Refiner
I	o Placed ingots in melting furnace at 775 °C o Cover gas: CO_2 + 0.5 vol.% SF_6 at 4.7 L/min
II	o Checked melt temperature with K-type thermocouple (>760 °C)
III	o Pre-heated permanent tensile mould to 540 °C
IV	o MgB_2 powder was added to melt o Melt was stirred at 300 RPM for 3 minutes
V	o Melt held for 5 minutes
	Pouring
I	o Thermal data acquisition system was started
II	o Melt was skimmed o Melt was poured with crucible at 720 °C

Table 3-5: Important casting parameters for permanent mould experiments

Pouring Temp. (°C)	Mould Temp (°C)	Holding Time (min)	MgB_2 Addition Level (wt.%)
720	540	5	0.025

3.4 Microstructure Analysis

The following sections describe the methods and techniques used for microscopy, polishing and microstructural analysis.

3.4.1 Optical Microscopy

All polishing for microscopy was conducted by hand and varied depending on if the sample to be examined was Pure Mg or AZ91E Mg alloy. After sectioning a sample using a hacksaw or an abrasive wheel, the samples were prepared according to the procedures described in Table 3-6 and Table 3-7.

For both Pure Mg and AZ91E, grinding steps I - V, water was used as a lubricant with a wheel rotation rate of 300 RPM. After grinding step V and after each polishing step, the sample was sonicated in ethanol for 1 minute. Polishing steps I, II and III were conducted with a wheel rotation rate of 100 RPM and step IV was performed with a stationary wheel. Care was taken to not use any water after the grinding steps as Mg has a high affinity for oxygen. The final polishing step also acted as an etchant for Pure Mg. Therefore, no further etching was required to reveal the grains.

Table 3-6: Manual grinding and polishing procedure for Pure Mg

Process	Surface	RPM	Duration (min)
	Grinding		
I	60 Grit SiC – with water	300	Until Plane
II	180 Grit SiC – with water	300	0.5
III	320 Grit SiC – with water	300	0.5
IV	600 Grit SiC – with water	300	0.5
V	1200 Grit SiC – with water	300	0.5
	Polishing		
I	Leco LeCloth® with Ethanol + 50 vol.% 5 µm alumina suspension	100	6
II	Leco LeCloth® with Ethanol + 50 vol.% 3 µm alumina suspension	100	5
III	Leco LeCloth® with Ethanol + 50 vol.% 1 µm alumina suspension	100	4
IV	Buehler ChemoMet® Cloth with 0.05 µm alumina and silica blend suspension	0	1.5

Table 3-7: Grinding and polishing procedure for AZ91E Mg alloy

Process	Surface	RPM	Duration (min)
	Grinding		
I	60 Grit SiC – with water	300	Until Plane
II	180 Grit SiC – with water	300	0.5
III	320 Grit SiC – with water	300	0.5
IV	600 Grit SiC – with water	300	0.5
V	1200 Grit SiC – with water	300	0.5
	Polishing		
I	Leco LeCloth® with 9 µm diamond paste and glycol-based diamond extender	100	6
II	Leco LeCloth® with 3 µm diamond paste and glycol-based diamond extender	100	5
III	Leco LeCloth® with 1 µm diamond paste and glycol-based diamond extender	100	4
IV	Buehler ChemoMet® Cloth with 0.05 µm alumina and silica blend suspension	0	1.5

3.4.2 Etching

Only the AZ91E samples were etched for grain size measurement. The samples were first heat treated at 412 °C for 16 hours with a forced air quench to dissolve the eutectic phase. After polishing, the samples were etched in 95 ml distilled water and 5 g citric acid solution for 15-20 seconds with minor agitation. Since the alloys contained more than 5 wt.% Al, the etching was stopped with water followed by an ethanol rinse and a blast of compressed air.

3.4.3 Grain Size Measurement

The grain size was measured along the cross-section of the graphite mould castings 0.75 in (19.05 mm) from the bottom over 200 grains. The grain size measurements for AZ91E were conducted using an optical microscope at a magnification of 100X using the Linear Intercept Method described in ASTM E112-13. The grain size measurements for the Pure Mg samples were performed with no magnification and using the Circular Intercept Procedure (ASTM E112 -13) to compensate for departures from equiaxed grain shapes. Each measurement trial represented an average of at least two samples.

3.4.4 Scanning Electron Microscopy

Scanning electron microscopy analysis was performed using a JOEL-SEM using back-scatter electron (BSE) imaging at a working distance of 11 mm and a potential of 20 keV. Only unetched samples were examined using SEM.

3.5 Thermal Analysis

Thermal analysis of the solidifying castings was performed for the grain refinement and fading experiments as well as the tensile mould experiments. This section describes the procedure used to obtain thermal data for both portions of the study.

3.5.1 Grain Refinement and Fading Castings (Graphite Mould)

The data acquisition unit (Daytronic System 10, DataPAC) with an accuracy of ± 0.1 °C was set to make temperature measurements every 0.2 seconds for 10 minutes. The data acquisition system was calibrated periodically with a temperature calibrator (Fluke - 714). Two measurements were performed for each casting condition to ensure repeatability and obtain a cooling curve that ranged from above the liquidus temperature to the solidus temperature. The thermocouple was located in the center of the melt as shown in Figure 3-1.

3.5.2 Tensile Castings (Permanent Mould)

The temperature measurements were made in the same manner as in the grain refinement and fading experiments except they were made for five minutes prior to pouring in six different locations on the mould (Figure 3-3). Thermocouples would interfere with the metal flow during solidification; therefore, an independent set of castings was produced specifically for thermal analysis.

3.6 Tensile Testing

Uniaxial tensile tests were conducted on the tensile bar samples at ambient temperature to determine the YS, UTS and % Elongation of the Pure Mg and AZ91E tensile bars. A computer controlled universal testing machine (United, Model STM-50kN) was used at a nominal speed of 12.5 mm/min (0.5 in/sec). An extensometer was attached to the gauge section to measure the

tensile strain. Four samples of each alloy were tested to determine the average tensile properties of the samples. Fracture morphologies and microstructures of the fracture surface were observed along the tensile loading direction using SEM.

4 Results and Discussion

4.1 Lattice Disregistry and Theoretical Considerations

To date, no study has been performed to investigate the grain refining effects of MgB_2 on Pure Mg and AZ91 Mg alloy. In this research, the Bramfitt model (Equation 12) [22] was used to predict the effectiveness of MgB_2 particles as a nucleant for Mg grains. The model, also known as the plane-to-plane matching model, uses crystallography as a basis to determine the nucleating potential for a particle and matrix system. This is done by comparing the interatomic spacings and the close-packed directions of pairs of low index planes from the nucleating particles and the host metal.

$$\delta_{(hkl)_n}^{(hkl)_s} = \sum_{i=1}^{3} \frac{\frac{\left| d_{[uvw]_s^i} cos\theta - d_{[uvw]_n^i} \right|}{d_{[uvw]_n^i}}}{3} * 100 \qquad (12)$$

The closed packed planes shown in Figure 4-1 namely, the (0001) planes were chosen as a low index planes for the nucleating particles and the host metal. The lattice parameters of Pure Mg are a = 0.320 nm and c = 0.520 nm [10], while those of MgB_2 are a = 0.307 nm and c = 0.352 nm [56].

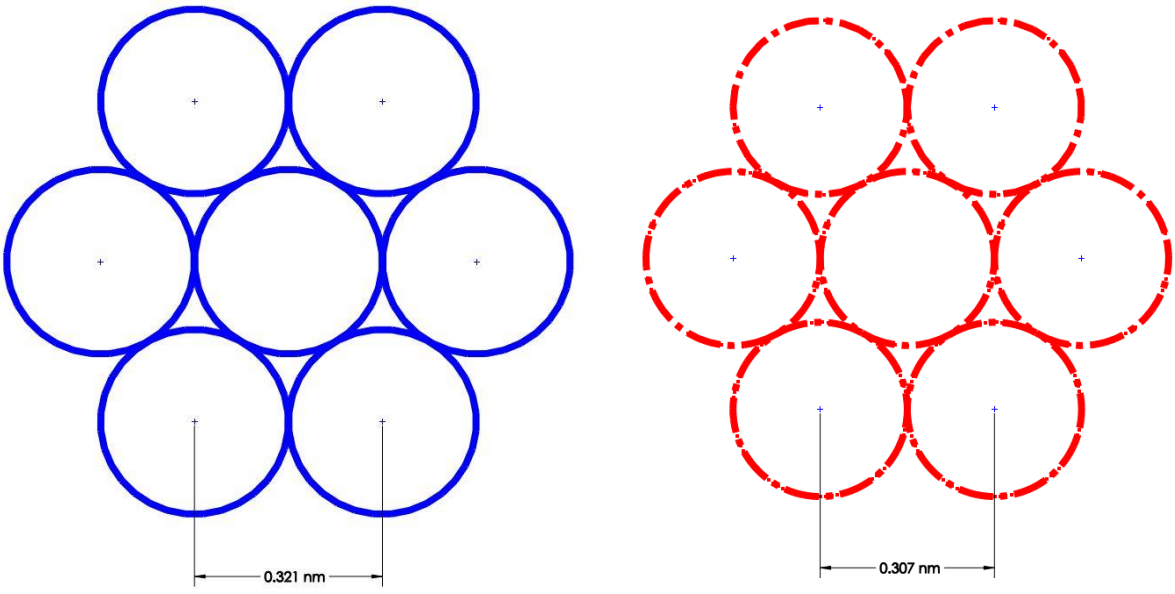

(a) (b)

Figure 4-1: Low index plane (0001) of a) Mg and b) MgB_2

To illustrate the similarity in crystal structure, Figure 4-2 displays a scaled version of the (0001) planes of Mg and MgB_2 superimposed on each other. By examining the figure, it is evident that the crystal structures have a high level of similarity. Following this, it can be expected that MgB_2 could act as an efficient refiner for Mg. Furthermore, the melting point of MgB_2 (830 °C [56]) is well beyond typical melting and holding temperatures for Mg alloys (650 to 750 °C). The density of MgB_2 is also higher compared to Pure Mg (2.57 g/cm^3 [56] compared to 1.74 g/cm^3 [10]). Therefore, it can be expected that it will also be resistant to fading effects.

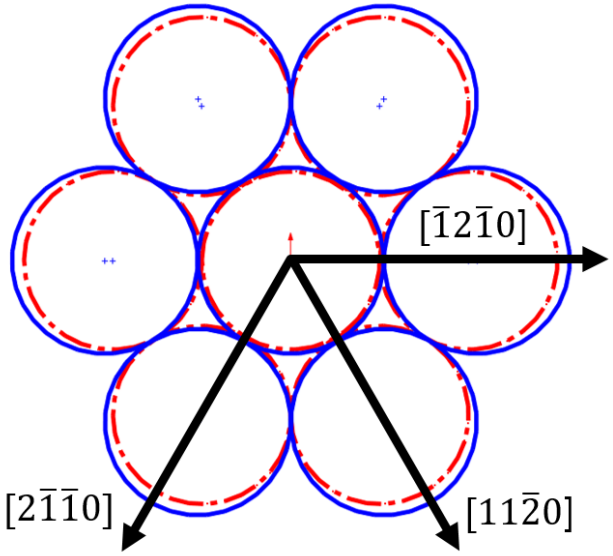

Figure 4-2: Superimposed (0001) planes of Mg (blue- solid) and MgB_2 (red - dashed) with closed packed directions

Table 4-1: Calculated values of planar disregistry between Mg and MgB_2 at ambient temperature for (0001) planes

	$[uvw]_s$	$[uvw]_{Mg}$	$d[uvw]_s$ (nm)	$d[uvw]_{Mg}$ (nm)	θ (deg)	$d[uvw]_s*\cos(\theta)$ (nm)	$\boldsymbol{\delta^{(hkl)_s}_{(hkl)_{Mg}}}$
$(0001)_{MgB2}$ ‖ $(0001)_{Mg}$	$2\bar{1}\bar{1}0$	$2\bar{1}\bar{1}0$	0.307	0.321	0	0.307	4.36 %
	$11\bar{2}0$	$11\bar{2}0$	0.307	0.321	0	0.307	
	$\bar{1}2\bar{1}0$	$\bar{1}2\bar{1}0$	0.307	0.321	0	0.307	

The planar disregistry value of the Mg – MgB_2 system at ambient temperature is summarized in Table 4-1. The minimum disregistry for the system was calculated to be 4.36 %. This value falls within the very effective range (<6 %) which suggests that it is possible for the Mg phase to nucleate on these particles on the basis of this orientation relationship [22]. Further, less effective orientation relationships can be seen in Appendix B.

Based on the results presented above, MgB_2 particles meet the requirements to act as efficient nucleating sites. Furthermore, as the melting point of MgB_2 is above typical holding temperatures for Mg alloys and its density is lower compared to Pure Mg, it can be assumed that it will also be resistant to fading.

4.2 Ball Milling and Particle Size Analysis

Planetary ball milling was performed to decrease the as-received MgB_2 particle size. In order to produce nano-particles, the MgB_2 powder was ball milled for a total of 480 minutes in 30-minute intervals as described in Section 3.2. The ball milling schedule used in this study is summarized in Table 4-2. Four samples of the ball milled powder was taken at 60, 240, 360 and 480 minutes of milling with the intention of assessing the size of the particles using scanning electron microscopy. This was done by diluting a sample of MgB_2 powder in ethanol and dropping a small amount on a polished brass rod.

Table 4-2: Summary of the ball milling schedule

RPM	Grinding Time (min)	Sample Name
0	0	t - 0
300	30	t - 30
300	30	t - 60
300	60	t - 120
300	60	t - 180
300	60	t - 240
300	60	t - 300
300	60	t - 360
300	60	t - 420
300	60	t- 480

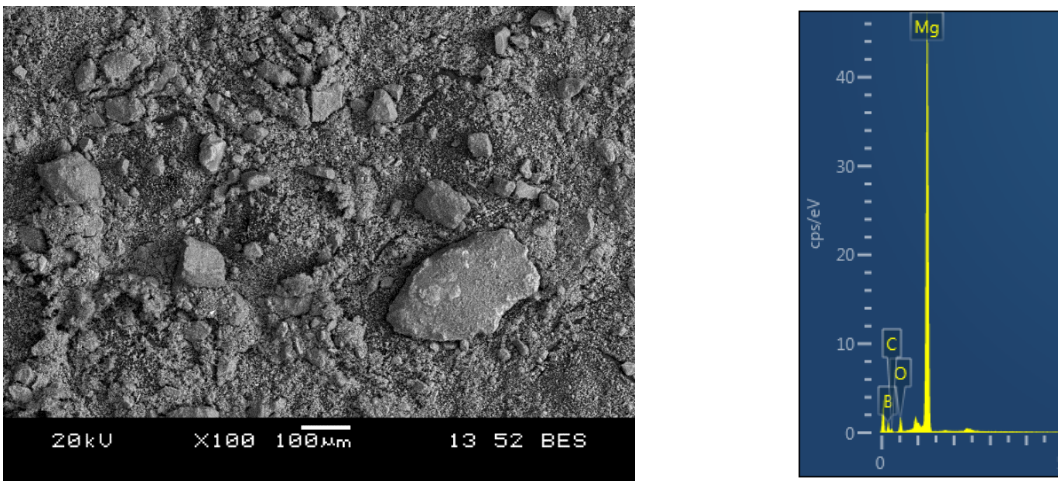

(a) (b)

Figure 4-3: (a) SEM image of the as received MgB_2 powder (b) EDS analysis of particles

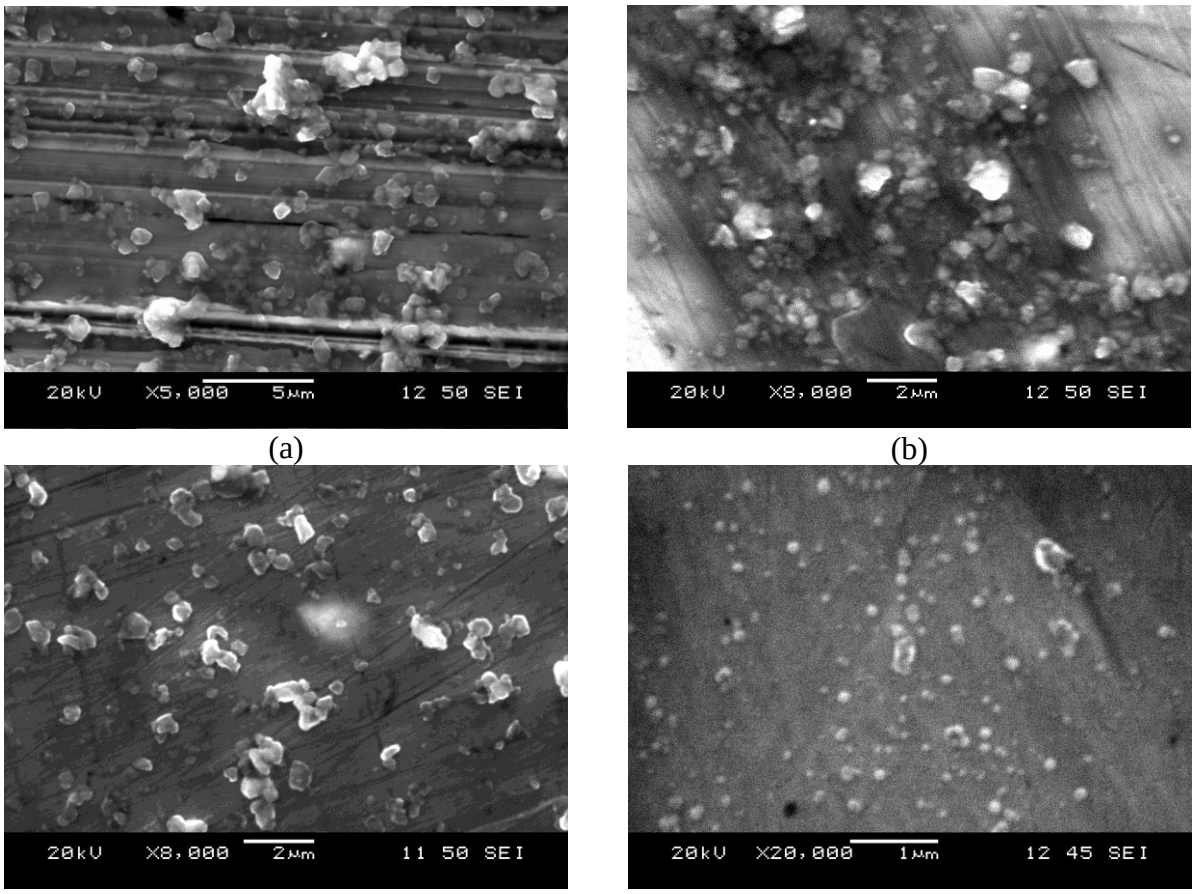

(a) (b)

(c) (d)

Figure 4-4: SEM images of the MgB_2 powder at (a) 60 minutes milling, (b) 240 minutes milling, (c) 360 minutes milling and (d) 480 minutes milling

Figure 4-3 displays an SEM image of the as-received MgB_2 powder. The corresponding EDS analysis clearly shows that the particles were indeed MgB_2 particles. Furthermore, a distribution of large (~150 µm) and small (~5 µm) can be observed, which is in line with the supplier specifications. The ball milled particles at 60, 240, 360 and 480 minutes of milling time can be seen in Figure 4-4. The figure indicates that as the milling time increased, the particle size decreased.

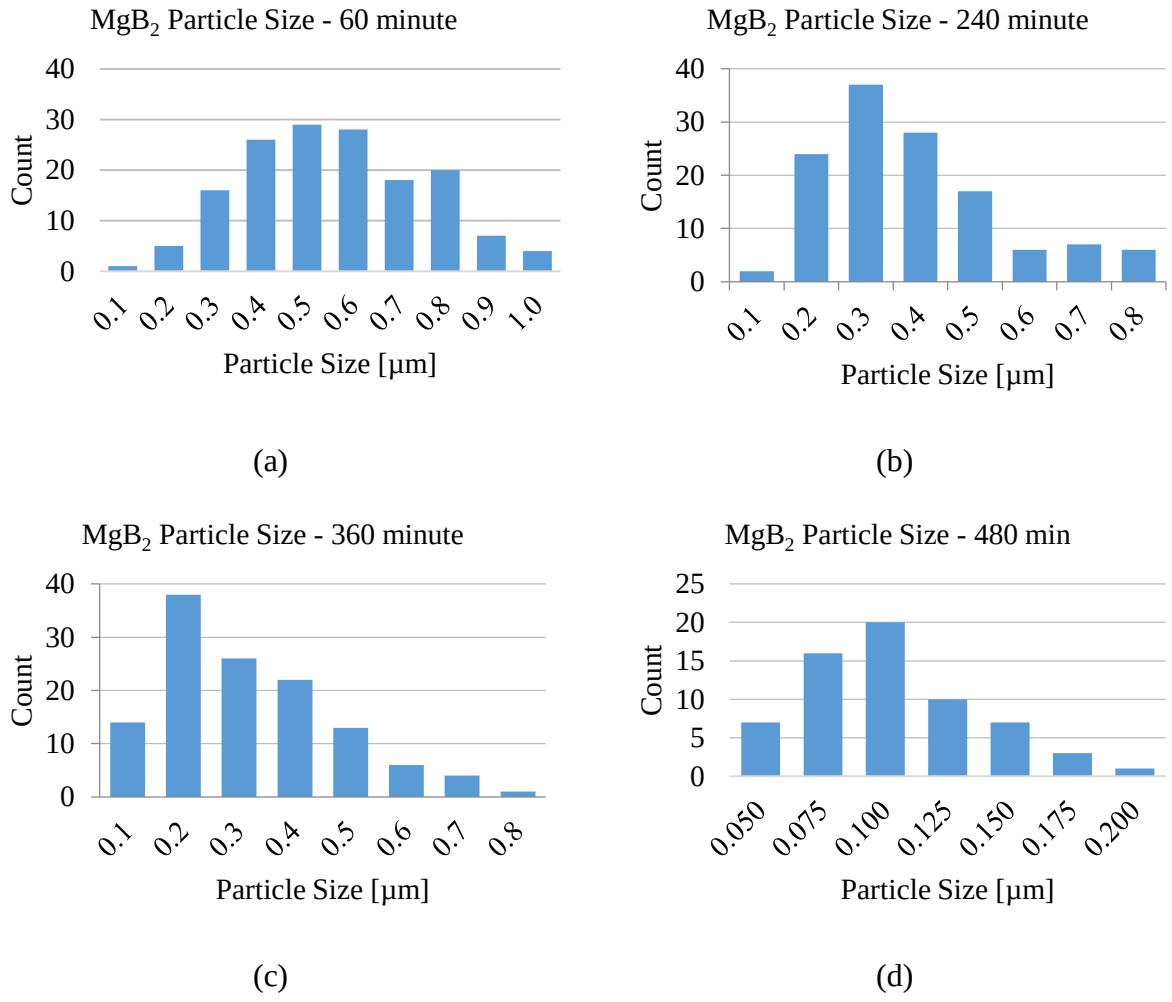

Figure 4-5: MgB_2 particle size distribution at a) 60 minutes milling, b) 240 minutes milling, c) 360 minutes milling and d) 480 minutes milling

For the purpose of this study, particles were assumed to be spherical. Using the SEM images, the area of each particle was measured using an image analysis software and a minimum of four samples. Following this, the effective diameter of each particle was calculated. With this analysis

technique, the particle size distribution for each milling sample was determined. The calculated particle size distributions for each sample can be seen in Figure 4-5. Results from the histograms indicated that at 480 minutes of milling the MgB_2 particles had been successfully reduced to an average diameter of 100 nm. It is interesting to note that there was a substantial reduction in particle size for the first 60 minutes of milling i.e., from 150 µm to 0.5 µm, but after that, the particle size decreased very slowly.

4.3 Grain Size Analysis

This section summarizes the effect of addition level and holding time on the grain size of Pure Mg and AZ91E with MgB_2 addition. The grain size measurements for the base samples are presented first followed by grain size measurements for the samples treated with inoculants.

4.3.1 Pure Mg

An optical macrograph of the as-cast base Pure Mg sample produced in a graphite mould is shown in Figure 4-6. The average grain size for the Pure Mg samples without grain refiner addition was 2466 µm. The microstructure consisted of an ingot type structure containing columnar grains around the edges and equiaxed grains in the center of the casting.

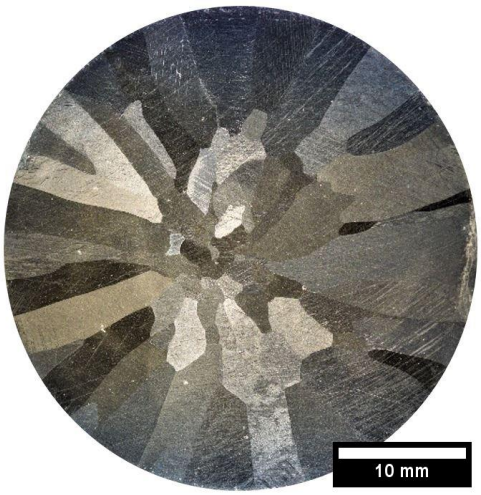

Figure 4-6: Optical macrograph of base Pure Mg

4.3.2 Pure Mg + MgB_2

Figure 4-7 displays optical macrographs of Pure Mg with varying MgB_2 additions and 5 minutes of holding time. All samples were cast in graphite moulds. When 0.0125 wt.% MgB_2 was added, the average grain size was reduced from 2466 to 1942 µm (Figure 4-7 – b). Further increase in MgB_2 addition to 0.02 wt.% led to an additional reduction in grain size to 1733 µm. At the 0.025 wt.% addition level, significant refinement in grain size was observed; an average grain size of 1577 µm was achieved (36 % reduction) (Figure 4-7 – c). However, with greater addition (0.05-0.1 wt.% MgB_2) no further refinement was seen (Figure 4-7 – d and e). The significance of the change in grain size was examined with an analysis of variance (ANOVA) in Appendix D.

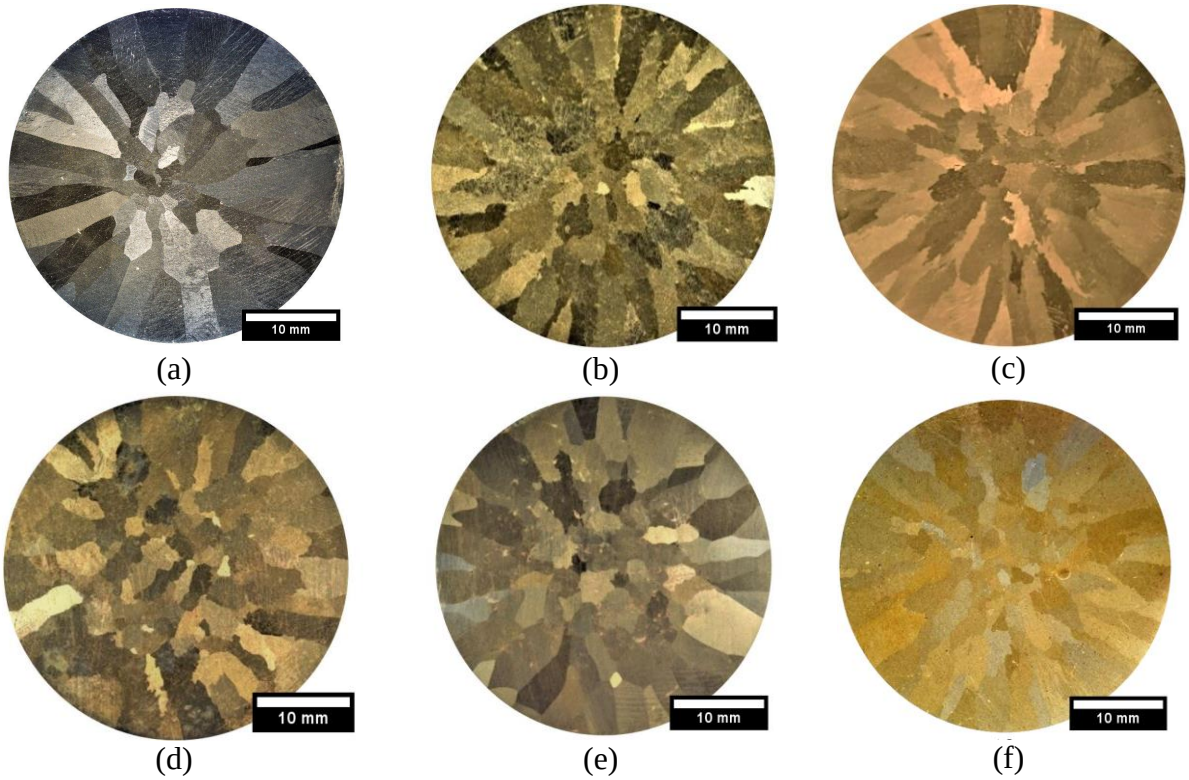

(a) (b) (c)

(d) (e) (f)

Figure 4-7: Optical macrographs of Mg at 5 minutes if holding time (a) Pure Mg (b) 0.0125 wt.% MgB_2, (c) 0.025 wt.% MgB_2, (d) 0.05 wt.% MgB_2, (e) 0.1 wt.% MgB_2 and (f) 0.025 wt.% MgB_2 nano powder

Figure 4-7 – f also displays an optical macrograph of Pure Mg + 0.025 wt.% MgB_2 nano-powder. The average grain size at this addition level was determined to be 1628 µm, which indicates a

34 % reduction in grain size compared to the base Pure Mg. It can also be observed that the grain size with micro-powder additions was finer as compared to the nano-powder additions (1577 µm in relation to 1628 µm).

The average grain sizes of the samples with varying levels of MgB_2 additions are summarized in Figure 4-8. Attributable to the low lattice disregistry calculated in section 4.1 (4.36 %), it is believed that the MgB_2 particles act as heterogeneous nucleation sites during solidification.

Grain coarsening was observed with additions greater than 0.025 wt.% MgB_2 which suggested that the nucleants became saturated in number. The higher addition levels may have led to agglomeration of the refiner particles which decreased the total number of available nucleating substrates.

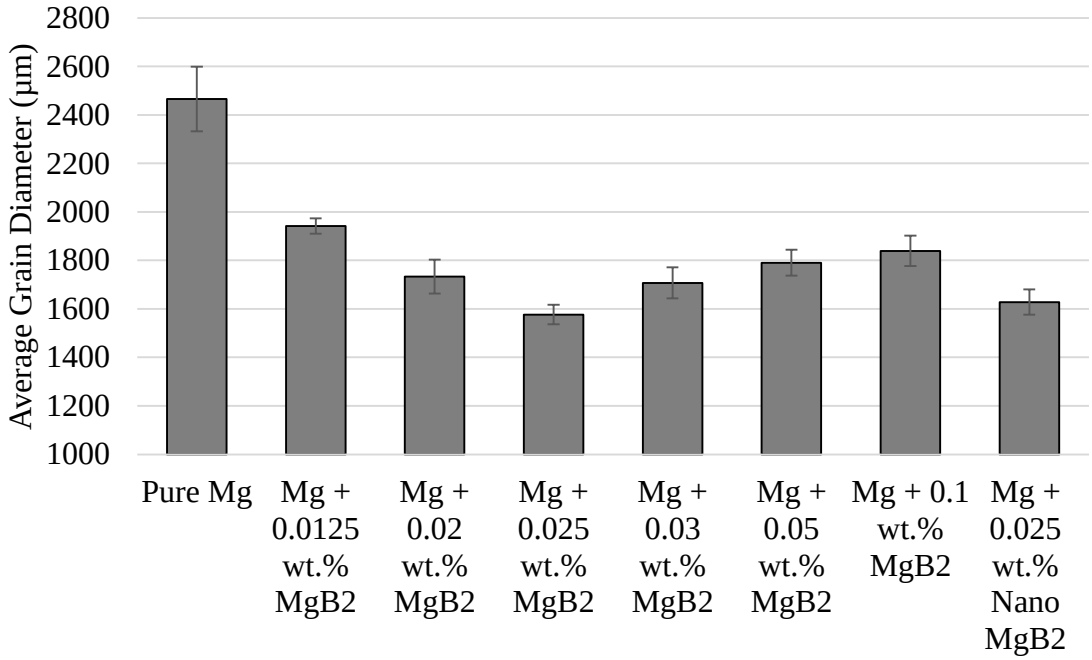

Figure 4-8: Effect of MgB_2 addition on the grain size of Pure Mg at 5 minutes holding time with error bars representing one standard deviation

It was also observed that with lower MgB_2 additions, the grain boundary shape changed from a smooth and laminar shape in the base metal to a serrated type shape. It is believed that this could have been a result of MgB_2 particles being rejected toward the grain boundaries during solidification. This will be further analyzed in the following sections.

During the experimental trials, the MgB_2 nano-powder showed signs of oxidation when it was added to the Pure Mg melt. However, this was not seen for micro-powder additions. The fine particle size of the nano-powder compared to the micro-powder made it more likely to oxidize when heated. Oxidation of the MgB_2 nano-powder was reduced by quickly plunging it under the melt surface, but the process might have introduced additional fine-sized oxides into the melt. Furthermore, as some of the particles oxidized, they may have lost their ability to act as nucleating substrates and therefore, resulted in a decreased level of refinement.

From these observations, it is evident that the addition of MgB_2 led to the grain refinement of Pure Mg. The micro-powder was determined to be a more potent refiner in comparison to the nano-powder. The ideal addition level for maximum refinement was found to be 0.025 wt.% (1577 µm – 36 % reduction). Therefore, it was decided to carry over the addition level for the AZ91E Mg alloy experiments.

4.3.3 AZ91E

Figure 4-9 displays an optical micrograph of the a solution heat-treated base AZ91E sample produced in a graphite mould. The microstructure of the samples consisted of an equiaxed type structure with no columnar grains around the edges. The average grain size for the AZ91E samples without grain refiner addition was 179 µm.

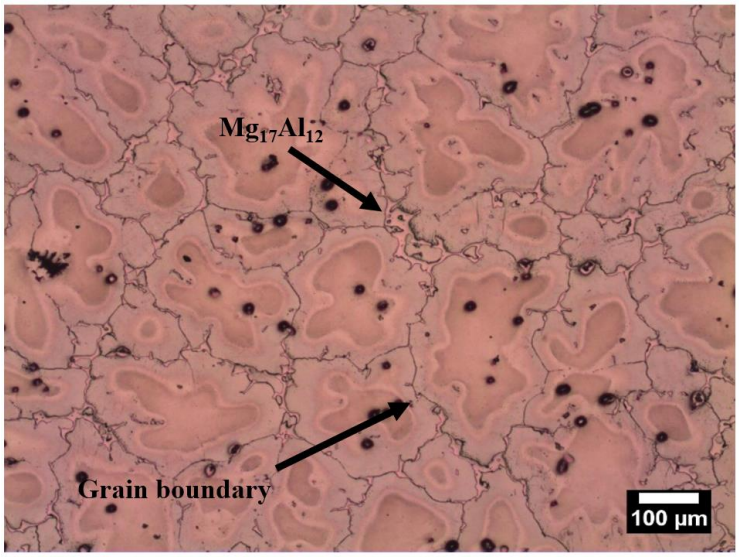

Figure 4-9: Optical micrograph of solution heat treated base AZ91E alloy

4.3.4 AZ91E + MgB_2

The microstructures of AZ91E with MgB_2 micro- and nano-powder additions and 5 minutes of holding time are presented in Figure 4-10. All samples were cast in graphite moulds, solutionized and etched prior to grain size measurement. Similar to the base AZ91E samples, the microstructure contained mainly equiaxed grains. The average grain size of the base AZ91E alloy was approximately 179 µm (Figure 4-10 – a). Upon adding 0.025 wt.% MgB_2 micro-powder, the average grain size decreased significantly to 100 µm (44 % reduction). For the MgB_2 nano-powder addition, however, the grain size only decreased to 117 µm (35 % reduction). The significance of the change in grain size was examined with an analysis of variance (ANOVA) in Appendix D.

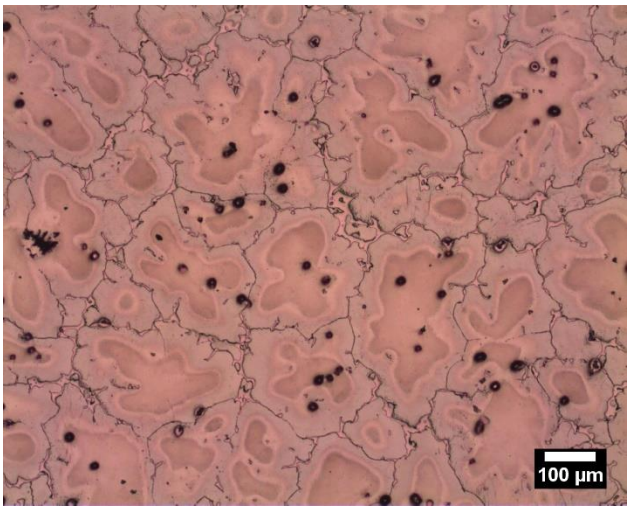

(a)

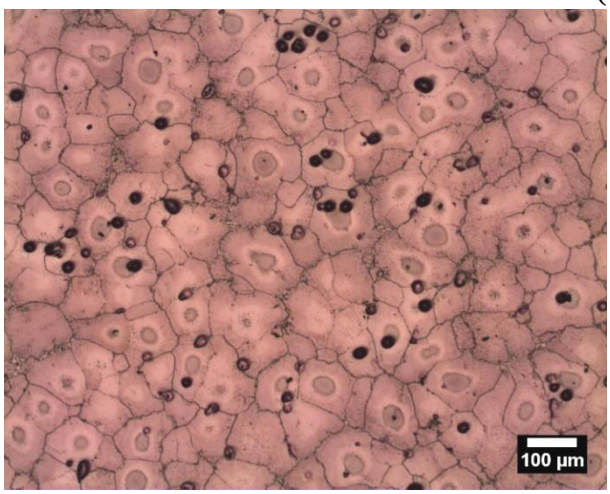

(b)

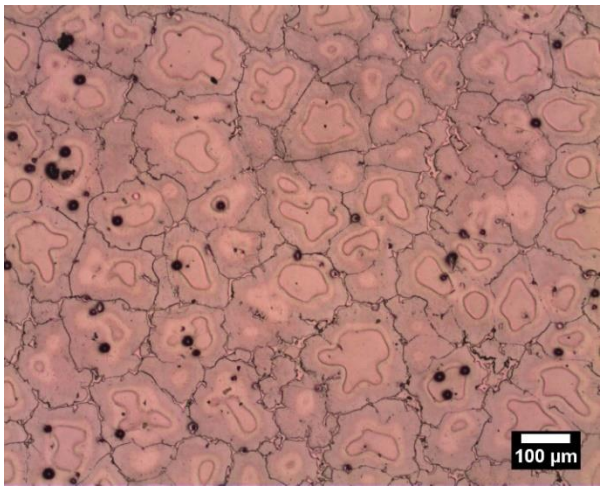

(c)

Figure 4-10: Optical micrographs of solution treated AZ91E with 5 minutes holding time (a) base AZ91E, (b) 0.025 wt.% MgB_2 micro-powder, (c) 0.025 wt.% MgB_2 nano-powder

The average grain sizes of the AZ91E samples with MgB_2 additions are summarized in Figure 4-11. The refinement in grain size was attributed to the high nucleating potential of the MgB_2 particles (4.36 % disregistry). Similar to the Pure Mg trials, the average grain size of the nano refined samples are larger than the micro refined (117 µm compared to 100 µm). The decreased potency of the nano refiners could have been a result of oxidation during the casting procedure.

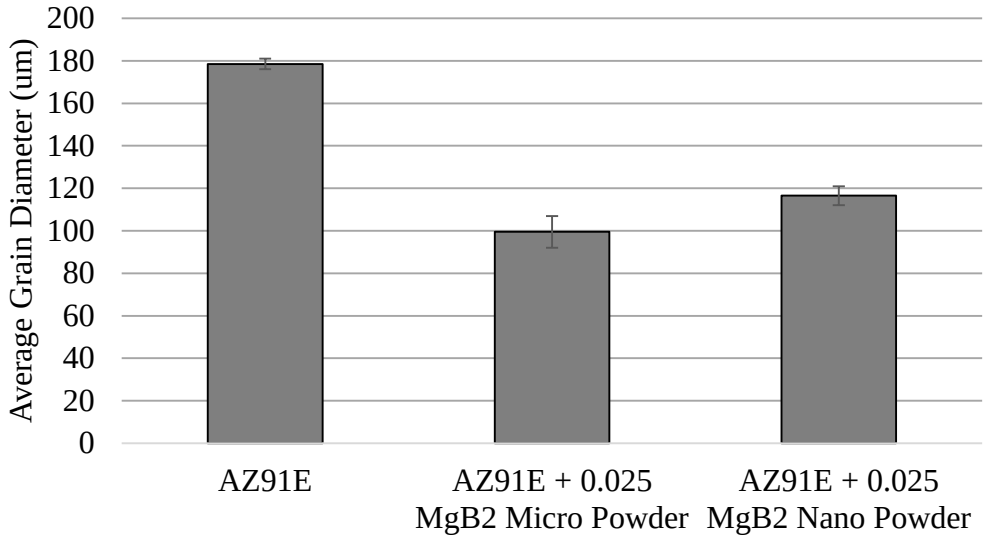

Figure 4-11: Effect of MgB_2 addition on the grain size of AZ91E at 5 minutes holding time with error bars representing one standard deviation

The grain size analysis indicated that the addition of MgB_2 resulted in the grain refinement of both Pure Mg and AZ91E Mg alloy. The addition level for efficient refinement was chosen to be 0.025 wt.% which led to a 44 % decrease in grain size for the micro additions and a 35 % decrease for the nano. It was also observed that the micro MgB_2 acted as a more efficient grain refiner compared to the nano-sized MgB_2 particles.

4.4 Thermal Analysis

Undercooling measurements were taken from cooling curves recorded from the tensile castings (Appendix C) using the thermocouple setup depicted in Figure 3-3. The measurements were used as an indicator of grain refinement. This was done by examining the temperature difference between the lowest point before the recalescence and the subsequent plateau temperature, as shown

in Figure 4-12. A casting with no undercooling or very little undercooling would be expected to indicate significant grain refinement, while a cooling curve showing undercooling similar to that of the base metals would indicate poor grain refinement [57].

Undercooling measurements of the Pure Mg castings without refiner additions is presented first followed by castings treated with MgB_2 powder. Of the grain refined castings, only the cooling curves corresponding to addition levels that provided the highest degree of grain refinement are presented in this section. It is worth noting that detecting the recalescence of Mg alloys is difficult due to the relatively low value of latent heat of fusion (8.48 kJ/mol) in comparison to iron alloys (13.81 kJ/mol) and aluminum alloys (10.71 kJ/mol) [18].

4.4.1 Pure Mg

Figure 4-12 shows a typical cooling curve for Pure Mg before inoculation. The average undercooling of the base metal was measured to be 2.0 °C. The cooling curve of Pure Mg + 0.025 wt.% MgB_2 with 5 minutes of holding time can be seen in Figure 4-13. From the curve it can be observed that additions of MgB_2 decreased the undercooling of the melt such that the measured average undercooling was 0.9 °C. Likewise, when 0.025 wt.% MgB_2 nano-powder was added (Figure 4-14), the undercooling decreased to 0.8 °C. Therefore, it is evident that MgB_2 can significantly reduce the required undercooling of Mg.

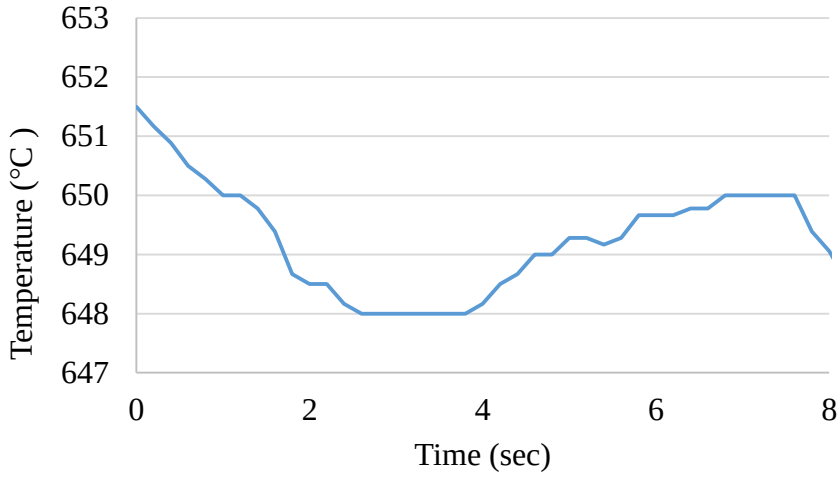

Figure 4-12: Typical cooling curve of Pure Mg

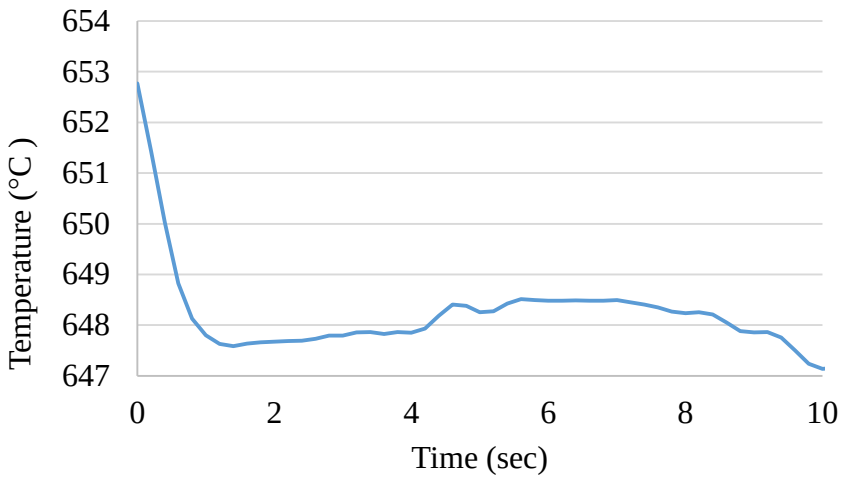

Figure 4-13: Typical cooling curve of Pure Mg + 0.025 wt.% MgB_2 micro-powder and 5 minutes holding time

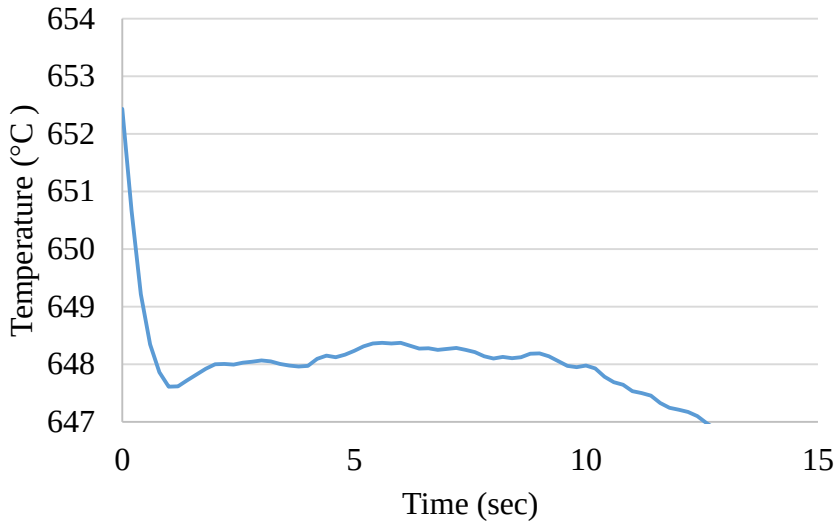

Figure 4-14: Typical cooling curve of Pure Mg + 0.025 wt.% MgB_2 nano-powder and 5 minutes holding time

Table 4-3 summarizes the measured average undercooling of Pure Mg with additions of MgB_2 micro- and nano-powder. When 0.025 wt.% MgB_2 was added to Pure Mg, the undercooling decreased from 2.0 °C to 0.9 °C for the micro-powder and 0.8 °C for the nano-powder. For Pure Mg, nucleation during solidification typically occurs in a homogenous manner, since no nucleating

elements exist in the melt, therefore, a certain degree of undercooling is needed before nucleation can begin. For the MgB_2 added Pure Mg samples, the decrease in undercooling indicates that the metal is well nucleated during solidification and that MgB_2 particles have effectively nucleated a great number of primary magnesium crystals [57]. The results obtained are in good agreement with the calculated lattice disregistry for the Mg-MgB_2 system (4.26 % - section 4.1) which suggested that MgB_2 would be an efficient refiner for Pure Mg.

Table 4-3: Average undercooling during solidification of Pure Mg at 5 minutes holding

Alloy	Average Undercooling (°C)
Base Pure Mg	2.0
Pure Mg + 0.025 wt.% MgB_2 micro-powder	0.9
Pure Mg + 0.025 wt.% MgB_2 nano-powder	0.8

From the results of the thermal analysis, it is clear that MgB_2 can act as a potent nucleant for Pure Mg. It was observed that with MgB_2 addition, the average undercooling of Pure Mg decreased significantly (2 °C for Pure Mg to 0.8 and 0.9 °C for Pure Mg + 0.025 wt.% micro and nano-powder respectively). The results indicated that the MgB_2 particles were responsible for the heterogeneous nucleation of primary magnesium, which can be attributed to the small lattice mismatch (4.36 %) between MgB_2 and Pure Mg.

4.4.2 AZ91E

The cooling curve of base AZ91E can be seen in Figure 4-15. From the curve, it can be seen that unlike Pure Mg, there is no apparent undercooling for the nucleation of primary Mg. The cooling curves of AZ91E with 0.025 wt.% MgB_2 are depicted in Figure 4-16 and Figure 4-17 respectively. Similar to the base alloy, no undercooling was observed for these cooling curves.

The nucleation temperature of base AZ91E was determined to be 596.8 °C. This temperature corresponds to a sudden change in slope of the cooling curve and marks the start of primary phase nucleation with the onset of latent heat release [58]. With the influence of MgB_2 particles, the nucleating temperature increased to 626.7 °C for the micro-powder and 612.1 °C for the nano-powder.

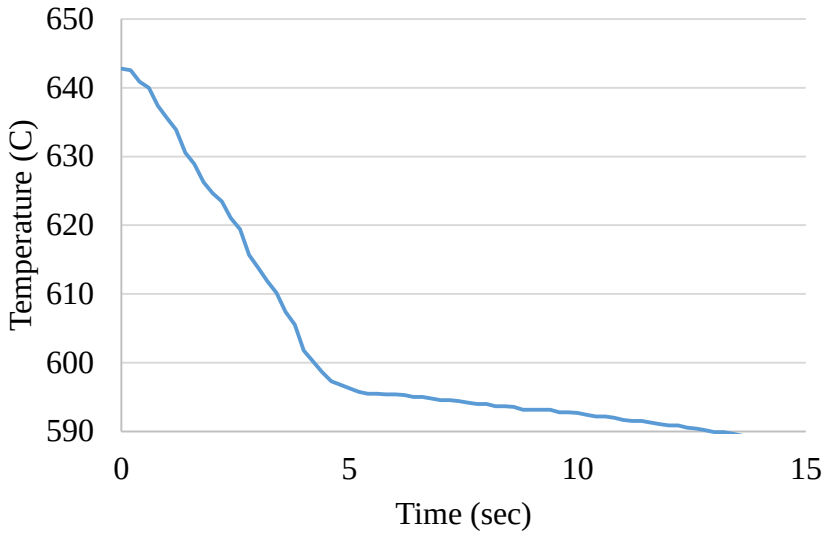

Figure 4-15: Typical cooling curve of Base AZ91E

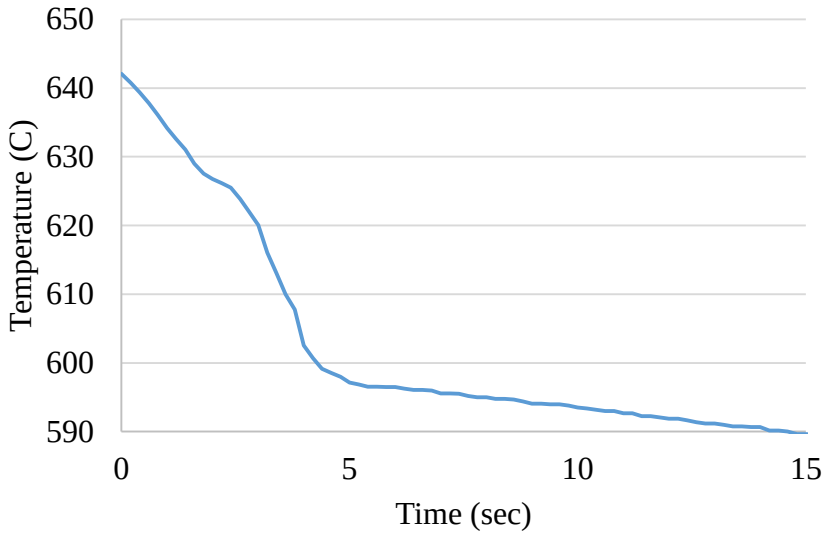

Figure 4-16: Typical cooling curve of AZ91E + 0.025 wt.% MgB_2 micro-powder and 5 minutes holding time

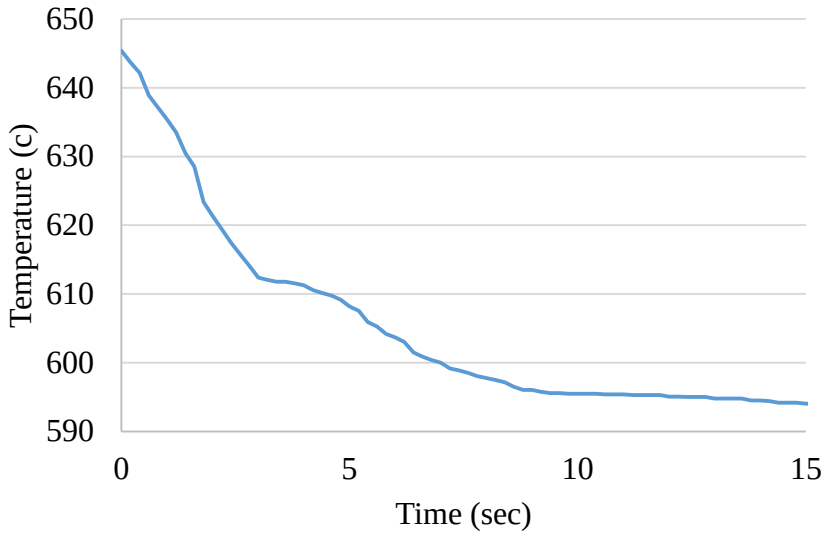

Figure 4-17: Typical cooling curve of AZ91E + 0.025 wt.% MgB_2 nano-powder and 5 minutes of holding time

A summary of the average nucleating temperature of AZ91E with various MgB_2 additions can be seen in Table 4-4. Upon adding MgB_2 micro- and nano-powder, the average nucleating temperature increased from 596.8°C to 626.7 °C and 612.1 °C respectively. The higher nucleation temperatures of the inoculated alloys suggest that the MgB_2 particles have effectively nucleated a significant number of primary magnesium crystals [59]. Furthermore, similar to Pure Mg, the low lattice disregistry between MgB_2 and Mg (4.36 %) also indicated that MgB_2 would be an efficient refiner for Mg.

Table 4-4: Average nucleating temperature during solidification of AZ91E at 5 minutes holding time

Alloy	Average Nucleating Temp. (°C)
Base AZ91E	596.8
AZ91E + 0.025 wt.% MgB_2 micro powder	626.7
AZ91E + 0.025 wt.% MgB_2 nano powder	612.1

From the results of the thermal analysis it is clear that MgB_2 can act as a potent nucleant for AZ91E. It was observed that with MgB_2 addition, the average nucleating temperature of the alloy increased. The higher nucleating temperature indicated that MgB_2 particles have effectively nucleated primary magnesium grains. This was attributed to small lattice mismatch (4.36 %) between MgB_2 and Pure Mg. Therefore, it can be concluded that MgB_2 is capable of refining AZ91E grains.

4.5 Fading Analysis

This section summarizes the effect of holding time on the grain size of Pure Mg and AZ91E Mg alloy treated with MgB_2 micro and nano-powder. The results relating to Pure Mg are presented first followed by the results of the AZ91E castings.

4.5.1 Pure Mg + MgB_2

The fading behavior of MgB_2 added Pure Mg was examined by comparing the resultant microstructure at 5, 10 and 20 minutes after addition. The microstructural changes with increases in holding time are shown in Figure 4-19. The increased holding time resulted in an appreciable growth in average grain size such that considering the error bars, the average grain size for most addition levels at the 20-minute holding time level was very close to the base metal. It was also observed that the nano refined castings were more resistant to fading effects such that the increased holding time only resulted in a small increase in average grain size. The significance of the change in grain size based on holding time was examined with an analysis of variance (ANOVA) in Appendix D.

Figure 4-18 displays a summary of the average grain sizes at 5, 10 and 20 minutes of holding. The fading effects could be attributed to the difference in density of Pure Mg (1.74 g/cm^3 [10]) and MgB_2 (2.57 g/cm^3 [56]). As the holding time increased, the denser MgB_2 particles may settle to the bottom of the crucible, thereby reducing the number of potent nucleants within each casting [60]. Moreover, for each casting, liquid metal was ladled from the top of the crucible which could have further contributed to the fading effects.

The nano-sized particles indicated a higher resistance to fading compared to the micro-particles. This occurrence can be explained by Stokes', which states that the settling behavior of particles

is influenced by the particle size, characteristics, and density [61]. The size of the grain refiner particles can impact the settling rate, and Stokes' law predicts that larger grain refiner particles settle more quickly compared to smaller particles. Following this, the grain size of the nano refined casting remained quite stable throughout the 20 minutes of holding time.

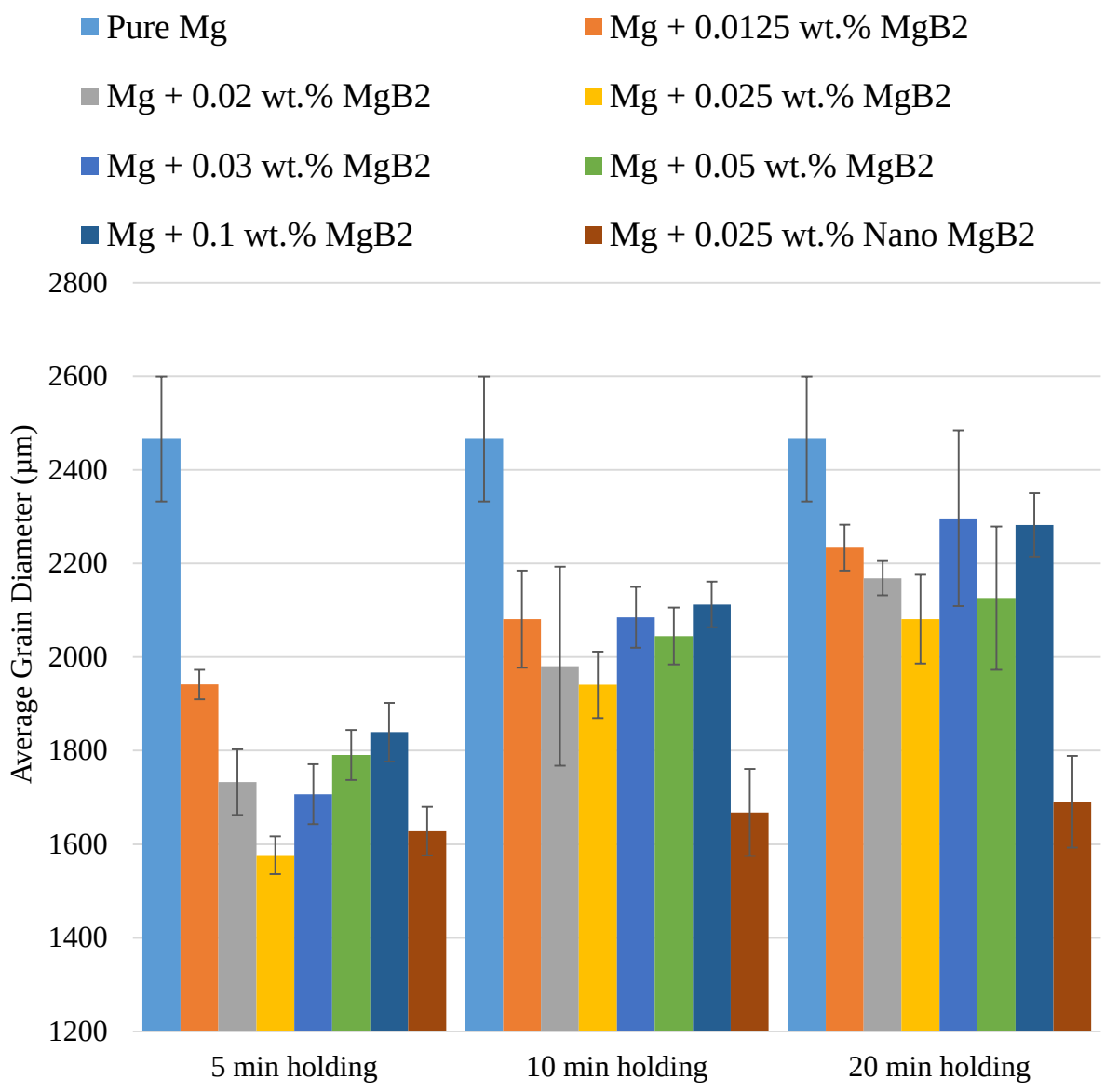

Figure 4-18: Influence of MgB_2 micro- and nano-powder addition levels and holding time on the grain size of Pure Mg

Figure 4-19: Optical macrographs of Pure Mg with various MgB_2 micro- and nano-powder additions and 5, 10 and 20 min holding times

The result of the fading analysis of Pure Mg with various MgB_2 additions indicated that the sensitivity of the used micro-refiner to inoculation-fading is relatively high, and the holding time should not exceed 5 min. Additionally, it was determined that the nano-refined castings were very resistant to fading compared to the micro-refined castings due to their fine particle size. It is well known that inoculation fading is a common phenomenon during grain-refining treatment [60]. As discussed above, the inoculation fading is thought to have resulted from settling of the nucleating particles. The longer the holding time, the less the number of the effective nucleation sites. Therefore, such inoculants can be used successfully only in the continuous casting or in-mould grain refinement.

4.5.2 AZ91E + MgB_2

Figure 4-20 displays the fading behavior of AZ91E + 0.025 wt.% MgB_2 micro- and nano-powder. Similar to the Pure Mg fading analysis, holding times of 5, 10 and 20 minutes were examined. It was observed that as holding time increased, the grain size of both the nano and micro refined castings increased as well. It was also observed that similar to the nano refined Pure Mg castings, the nano refined AZ91E castings also showed reduced signs of fading compared to the micro refined castings. The significance of the change in grain size based on holding time was examined with an analysis of variance (ANOVA) in Appendix D.

The variation in grain size with holding time of the AZ91E alloys treated with MgB_2 powder is shown in Figure 4-21. Not unlike the Pure Mg castings, the fading can be attributed to settling of the nucleating substrates with increased holding time since the density of MgB_2 is higher compared to AZ91E (2.57 g/cm^3 for MgB_2 [56] compared to 1.81 g/cm^3 for AZ91E [10]). Following this it can be expected that as the holding time increases a smaller number of effective nucleant substrates remain active in the melt, and thus the larger the resulting average grain size. The nano refined castings however, displayed a decreased rate of fading. As discussed in section 4.5.1 the increased resistance to fading may have been a result of the fine particle size of the nano MgB_2 powder.

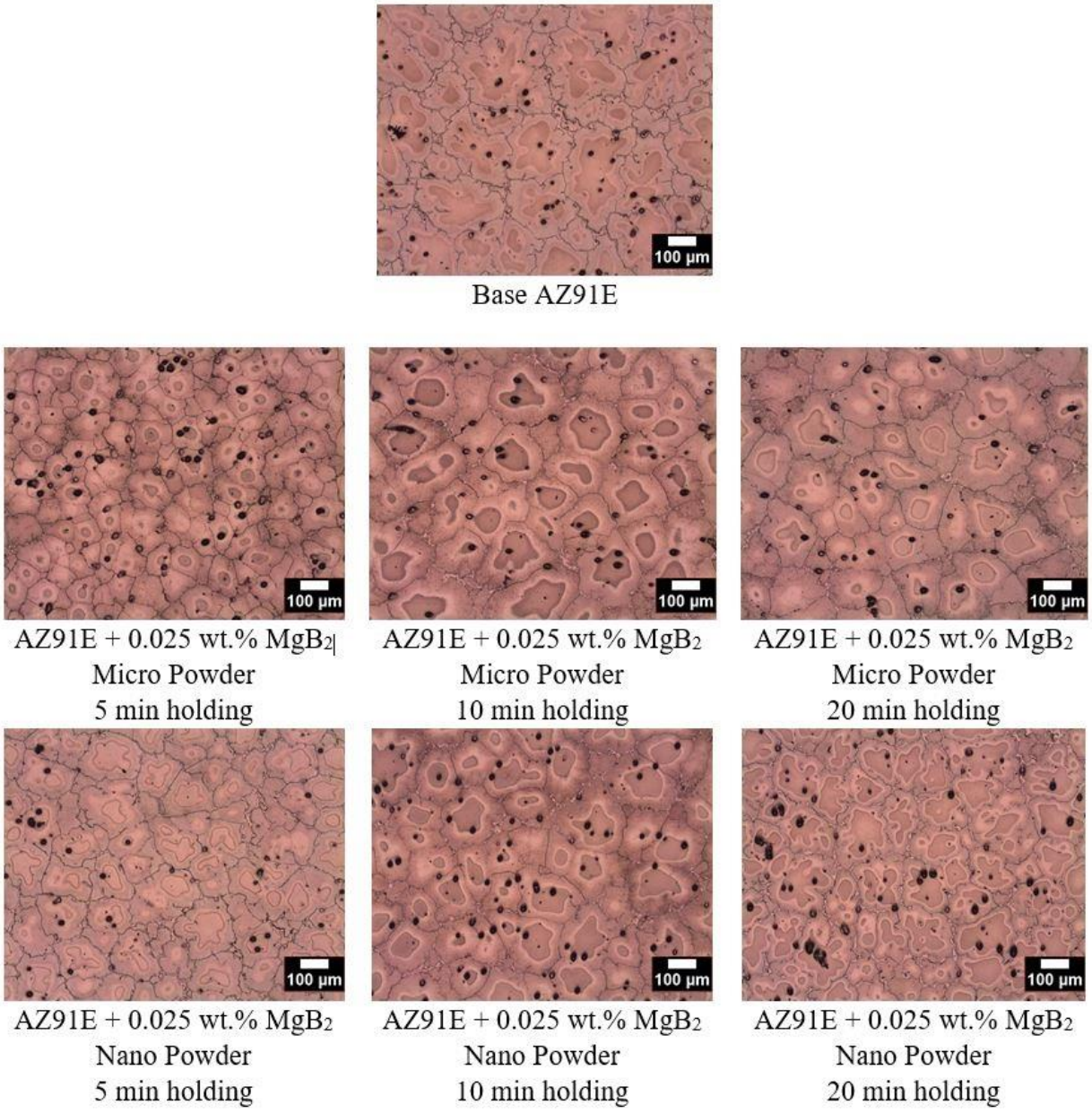

Figure 4-20: Optical micrographs of solution treated AZ91E + 0.025 wt.% MgB_2 micro- and nano-powder with 5, 10 and 20 min holding times

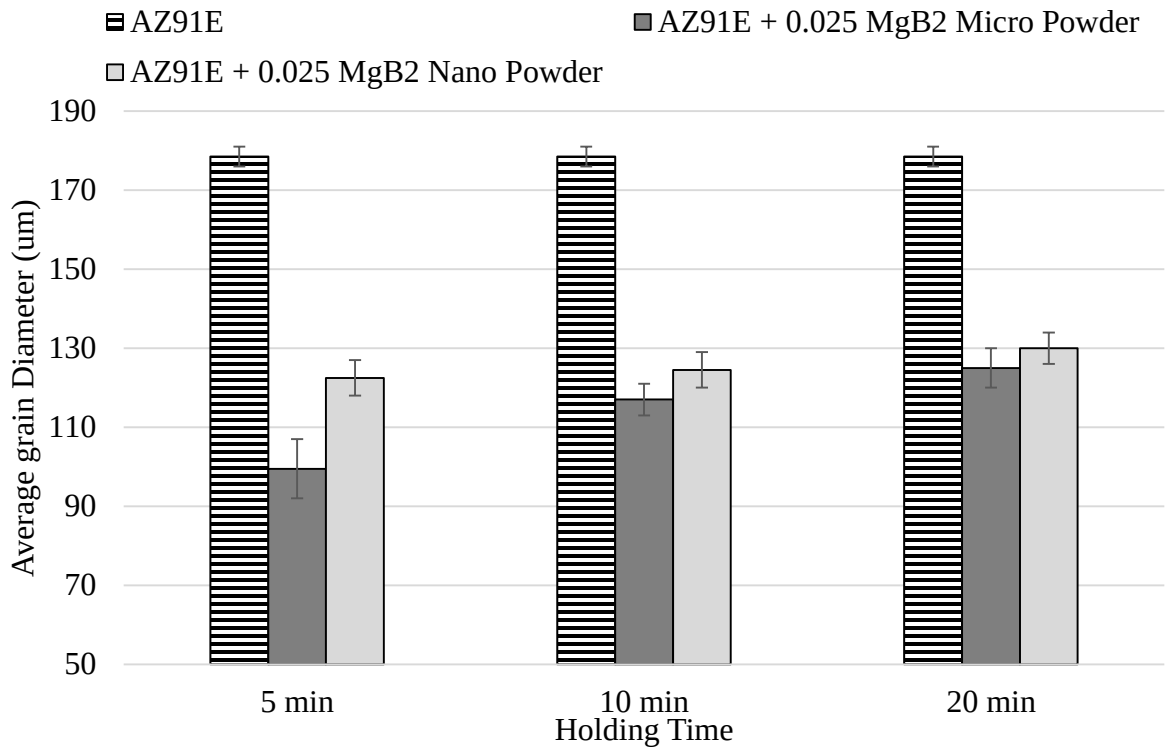

Figure 4-21: Influence of 0.025 wt.% MgB_2 micro and nano-powder addition and holding time on the grain size of AZ91E

The results of the AZ91E + 0.025 MgB_2 micro and nano-powder castings indicated that there is appreciable fading during the 20 minute holding time period. The fading of the micro refined castings was attributed to settling due to higher density compared to AZ91E. The nano refined castings displayed an increased resistance to fading due to their fine particle size. From the results presented above it is evident that the melt must be poured as soon as possible post inoculation in order to mitigate fading effects.

4.6 Mechanism of Refinement

Microstructure examination using SEM was performed on the grain refined castings produced in graphite moulds. Samples were examined in the same area that was used for the grain size measurements. The purpose of the microscopy was to identify the particles responsible for grain refinement and to observe whether any reactions occurred within the melt. The results related to castings with Pure Mg are presented first, followed by the AZ91E alloy castings.

4.6.1 Pure Mg + MgB_2

Using Scanning Electron Microscopy and EDS analysis, an attempt was made to determine whether the added particles were responsible for grain refinement in MgB_2 refined Pure Mg. Figure 4-22 displays an SEM micrograph of Pure Mg + 0.1 wt.% MgB_2 micro-powder. The figure shows a blocky type particle approximately 40 µm in size. Moreover, the particle lies within the center portion of a α-Mg grain. The results of the corresponding EDS analysis carried out on the particle are shown in Figure 4-22 as well. From the resultant EDS spectrum, one can see that the particle mainly contains Mg, O, and B. Hence, it can be suggested that the particle is indeed MgB_2. Similar to a study performed by Suresh et al. [54] (Section 2.10.10), this observation confirms the presence of MgB_2 in liquid Mg, and it follows that the particles aid in the refinement of α-Mg grains by increasing the nucleation sites.

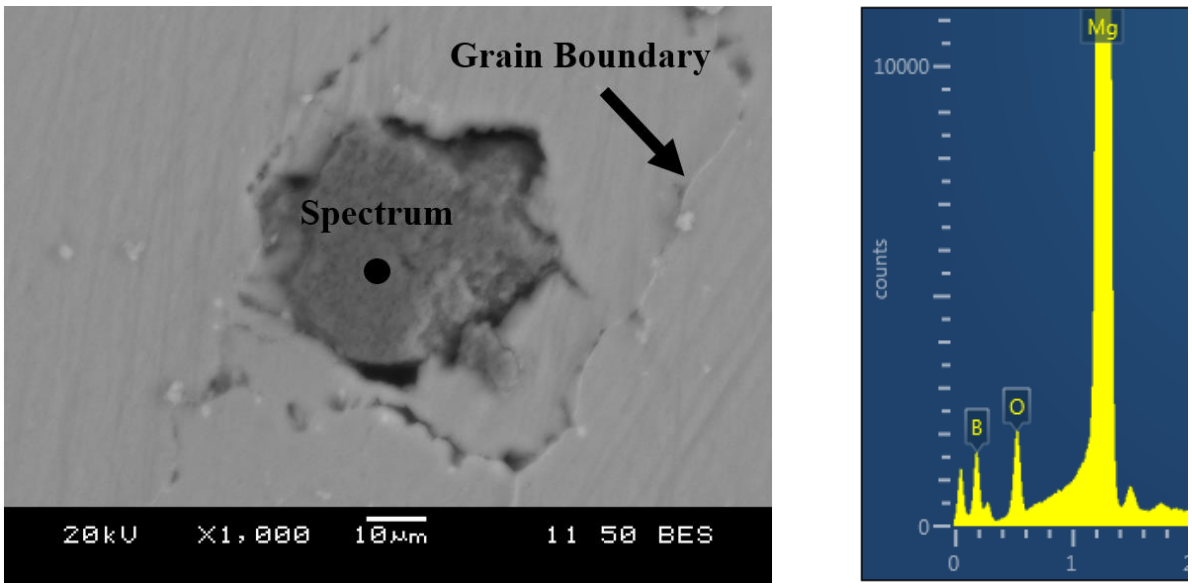

(a) (b)

Figure 4-22: (a) SEM image of Pure Mg + 0.1 wt.% MgB_2 and (b) EDS spectrum of MgB_2 particle within the center of a grain

Figure 4-23 displays an MgB_2 particle found along a grain boundary. It is believed that the smaller grain size in the MgB_2 refined Pure Mg samples might also be directly attributed to the particle/solidification front interaction, which is the subject of several investigations [62, 63]. When a moving solid-liquid interface (solidification front) approaches a suspended foreign particle, the particle can be either captured by the melt or pushed away by the solidification front. Both occurrences, i.e., particle capture and particle pushing, have been observed in the

microstructure and can be seen in Figure 4-22 and Figure 4-23 respectively. It can be assumed that this interaction resulted in a reduced growth rate for the primary Mg phase since the presence of MgB_2 particles around the growing Mg grains would create diffusion barriers to growth [64, 65, 66]. Moreover, it may be the reason for the serrated type grain boundaries observed in the microstructure at 5 minute holding times (Figure 4-19). This is further confirmed by the observation that as the grain refining effects of MgB_2 fade, i.e., the particles settle, the grain boundaries take on their normal smooth shape again.

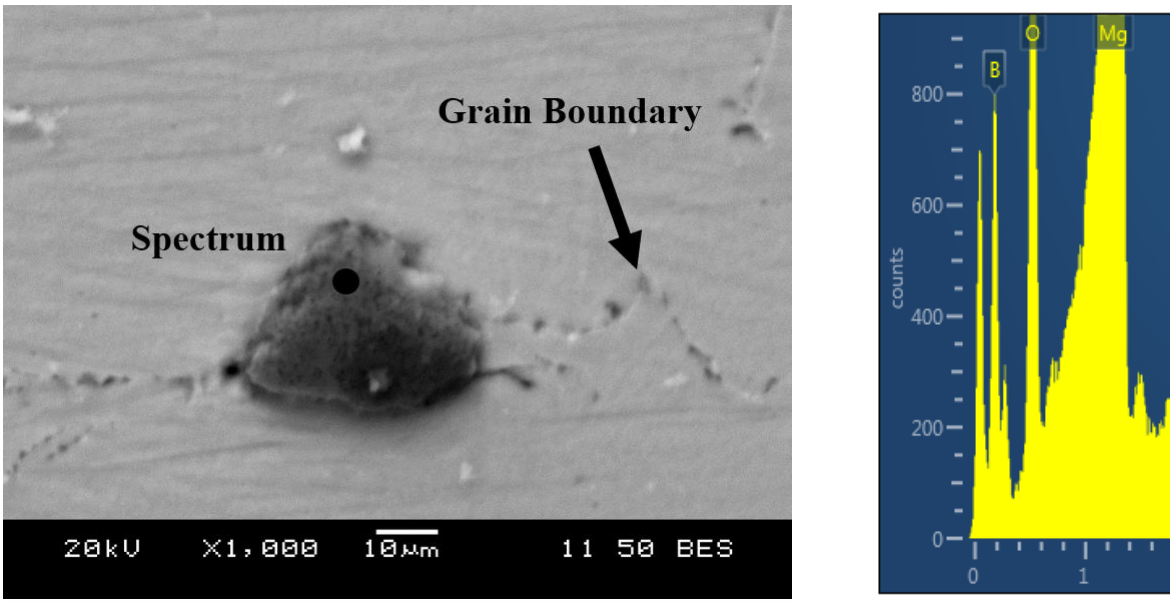

(a) (b)

Figure 4-23: (a) SEM image of Pure Mg + 0.1 wt.% MgB_2 and (b) EDX spectrum of MgB_2 particle along a grain boundary

It must be noted that the lattice disregistry between MgB_2 and Mg was calculated to 4.36 % for the $(1000)_{MgB_2}//(1000)_{Mg}$ orientation relationship. The disregistry value suggests good nucleation potency of MgB_2 in magnesium melts. Moreover, it also implies that effective heterogeneous nucleation only occurs when the (1000) basal planes of MgB_2 particles are exposed to the melt, and Mg nuclei come to form with a basal plane in contact with the particle surface. This is in agreement with the observation that only some of the MgB_2 particles are able to nucleate the primary Mg phase in the Pure Mg + MgB_2 castings.

From the results above it was determined that the significant grain refinement (36 %) was due to the effect of enhanced heterogeneous nucleation and restricted grain growth. It was observed that the MgB_2 particles were at the center of grains which indicated that they promoted heterogeneous nucleation. Particles were also observed on grain boundaries, which acted as diffusion barriers for grain growth.

4.6.2 AZ91E + MgB_2

Scanning electron microscopy (SEM) analysis of refined AZ91E samples revealed no direct observation of MgB_2 particles within the center of Mg grains at the 0.025 wt.% MgB_2 micro- and nano- particle addition level. This was in contrast to the results obtained in the previous section with Pure Mg castings. Since boron is a light element, its detection is challenging at small addition levels. Therefore, samples with high concentrations were produced (0.1 wt.% micro MgB_2) for the purpose of microscopy. The samples were prepared using the same experimental parameters as described in Section 3.3.1 with no holding time.

Figure 4-24 displays an SEM micrograph of AZ91E + 0.1 wt.% MgB_2. The figure depicts an MgB_2 particle situated in the center of Mg grains (indicated by the arrow) with the corresponding EDS spectrum. Similar to the Pure Mg castings, it is believed that the particles act as heterogeneous nucleation sites which promote a fine grain structure. These findings are in line with the observed higher nucleating temperature during solidification and also the resultant fine grain size (44 % reduction in grain size).

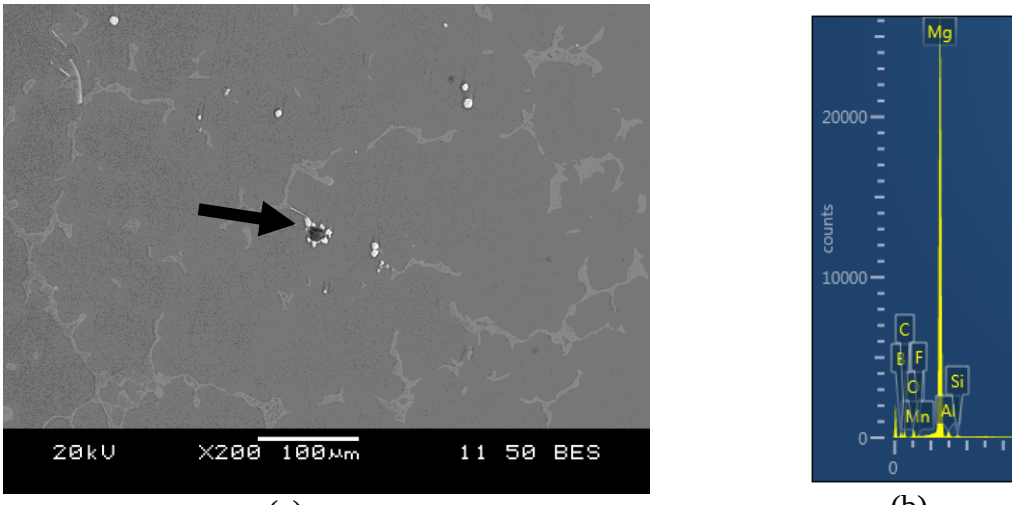

(a) (b)

Figure 4-24: SEM Image of AZ91E + 0.1 wt.% MgB_2 (a) MgB_2 particle at the center of grains (b) Corresponding EDS analysis

From the results above, it was determined that the significant grain refinement (44 %) was the due to the effect of enhanced heterogeneous nucleation. It was observed that the MgB_2 particles were at the center of grains which indicated that they promoted heterogeneous nucleation.

4.7 Mechanical Properties

The following section summarizes the effect of MgB_2 particle additions on the mechanical properties, in particular, UTS, YS and % Elongation of Pure Mg and AZ91E Mg alloy. The results relating to Pure Mg are presented first followed by the results of the AZ91E castings.

4.7.1 Pure Mg + MgB_2

Figure 4-25 presents the room temperature tensile properties of Pure Mg before and after 0.025 wt.% MgB_2 micro- and nano-powder addition. For the micro MgB_2 additions, making an allowance for the error bars, UTS remains relatively constant whereas, the YS decreases by 16 % from 23.7 MPa to 19.8 MPa. The % El, however, increases significantly from 3.3 to 5.0 % (52 % increase). It was observed that the nano refined castings produced similar results with the exception of UTS which improved marginally from 65 MPa in the base metal to 67 MPa for the refined castings. Furthermore, the YS decreased to 19.7 MPa (19 % reduction), and the % Elongation increased to 3.87 % (17 % increase).

The % Elongation of Pure Mg containing 0.025 wt.% MgB_2 micro and nano-particles significantly increased by 52 % and 17 %, respectively (Appendix E). The increased ductility with little or no improvement in YS and UTS can be attributed to weakening of the strong basal texture of Pure Mg by the presence of MgB_2 particles. Similar observations have been reported in literature for Mg and its alloys containing fine reinforcements in the form of particles [67, 68, 69, 70]. The studies suggest grain refinement is beneficial in improving the mechanical response by the activation of non-basal slip modes. It was also noticed that the increase in elongation of the nano refined castings was not as significant compared to the micro refined castings. The decreased elongation could be attributed to oxidation of the powders during the casting process which led to a relatively larger grain size.

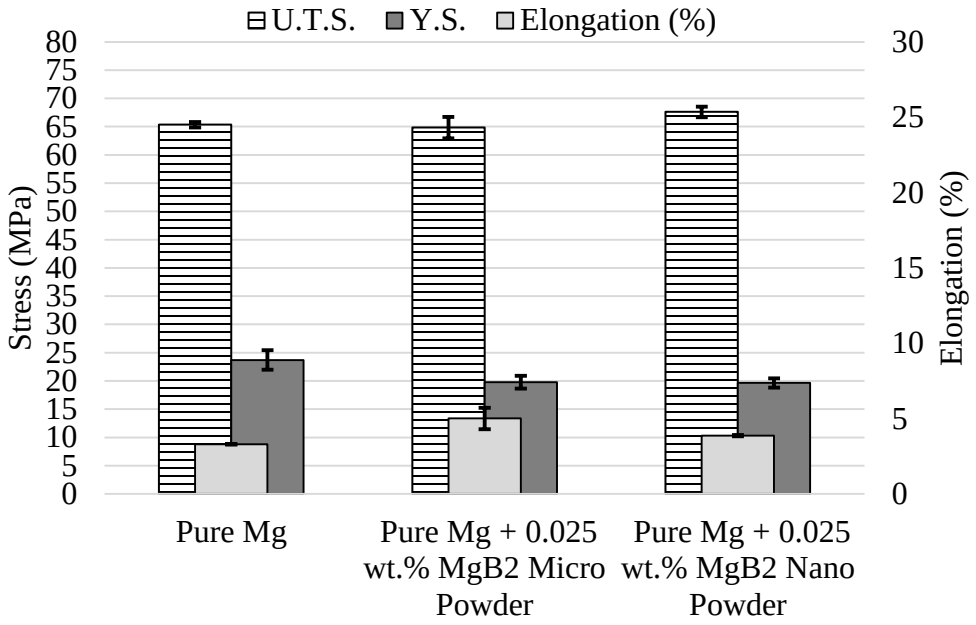

Figure 4-25: Room temperature tensile properties of Pure Mg with MgB_2 addition

The ductility improvements can also be attributed to the coefficient of thermal expansion (CTE) mismatch between the matrix (25-26x10^{-6} K^{-1} [10]) and the reinforcement particles (6.4-13.7x10^{-6} K^{-1} [71]). Coefficient of thermal expansion mismatch has been shown to produce geometrically necessary dislocations around the reinforcement particles to accommodate the CTE difference, thereby increasing overall dislocation density [72]. Furthermore, it has been reported that CTE mismatch strengthening is ineffective in the nano-particle range [73]. Hence, the nano refined castings did not benefit from this strengthening mechanism.

The tensile fracture surfaces of Pure Mg with MgB_2 additions are displayed in Figure 4-26. The Pure Mg samples display a typical cleavage type fracture mode which implied a brittle type fracture with minimal plastic deformation [74]. Upon adding 0.025 wt.% MgB_2, a change in fracture mode was observed (Figure 4-26 – c - f). The refined fracture surfaces displayed prominent ductile features and a decreased amount of cleavage steps which indicated increased plastic deformation relative to the base metal. Several cracks (indicated by arrows) were also observed in the refined fracture surfaces.

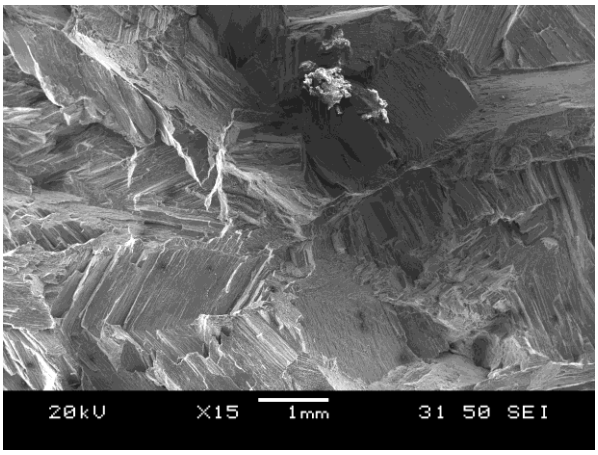

(a)

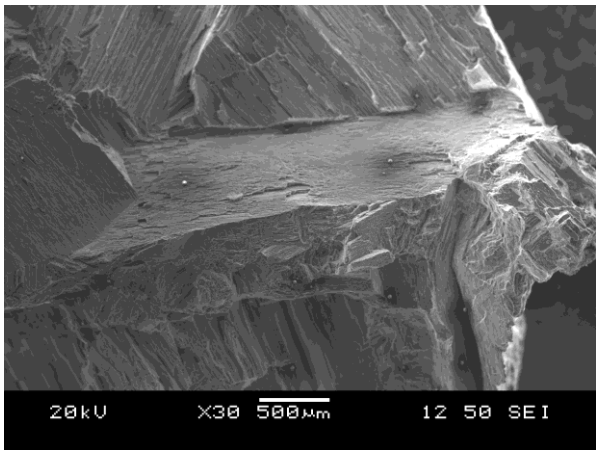

(b)

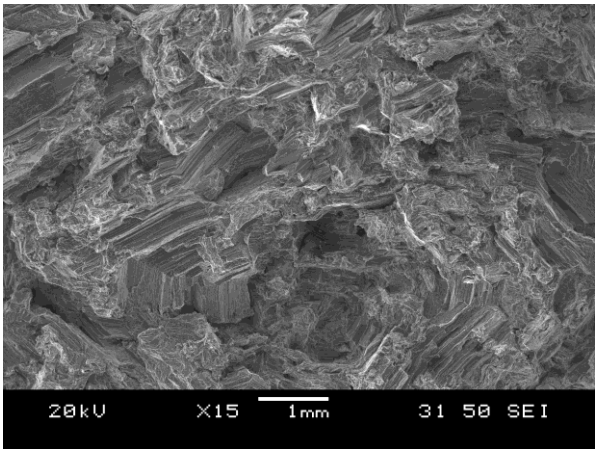

(c)

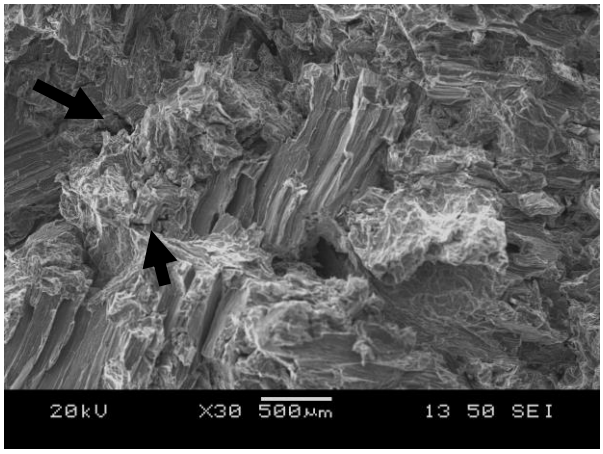

(d)

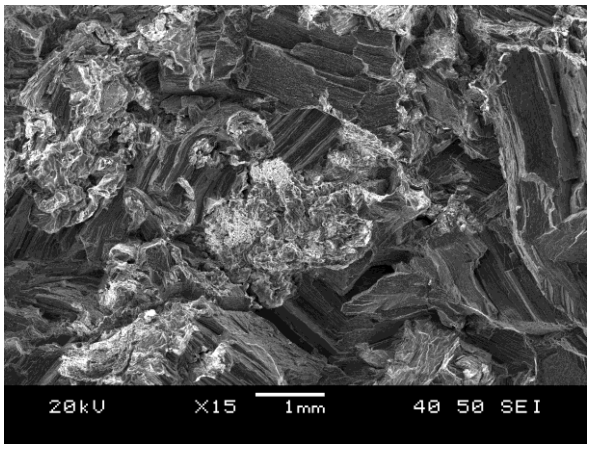

(e)

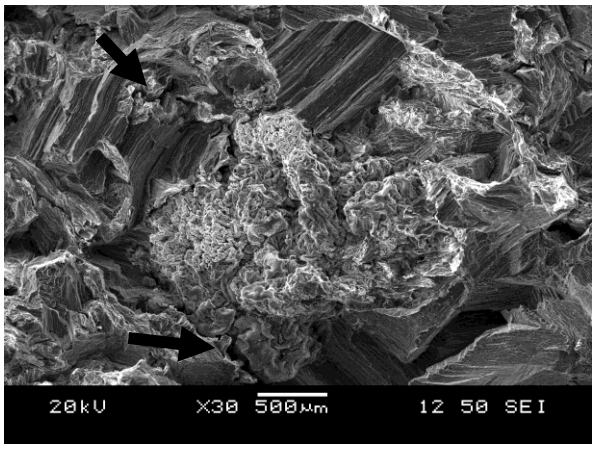

(f)

Figure 4-26: SEM fracture surface images for (a, b) Pure Mg, (c, d) Pure Mg + 0.025 wt.% micro-powder and (e, f) Pure Mg + 0.025 wt.% nano-powder

Hexagonal close-packed metals often exhibit transgranular type fracture modes owing to their limited number of slip systems and asymmetrical crystal structure. The presence of uniformly distributed phases has been known to act as ductility enhancers through grain boundary pinning [74, 75]. It follows that the MgB_2 particles in the matrix and along the grain boundaries would play a similar role. In addition, crack propagation for fracture is relatively easy in a brittle matrix because the mobility of dislocations are limited. In such cases, the presence of uniformly dispersed phases or particles would act as a ductility enhancer by providing sites for opening the cleavage cracks ahead of advancing crack front which dissipates the stress concentration at the crack tip [67, 68, 70, 74].

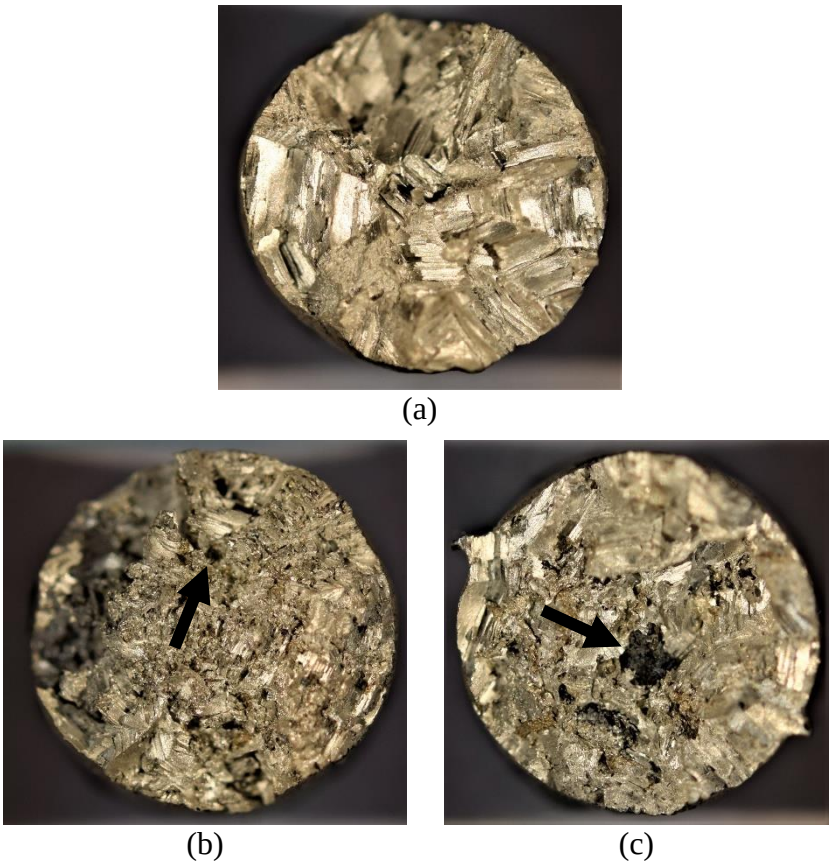

(a)

(b) (c)

Figure 4-27: Fracture surface optical macrographs of (a) Base Pure Mg, (b) Pure Mg + 0.025 wt. MgB_2 micro-powder and (c) Pure Mg + 0.025 wt.% MgB_2 nano-powder

Figure 4-27 displays optical macrographs of the tensile fracture surfaces. Similar to the SEM images, the fracture modes are easily identifiable. The Pure Mg samples indicate a cleavage type fracture with evident river patterns whereas the refined samples display a mix mode fracture with signs of plastic deformation along with cleavage planes. The figure also shows the inclusion content of the fracture surfaces. The Pure Mg samples appeared to be relatively inclusion free whereas the refined samples contained dark-colored inclusions (indicated). It was also observed that the nano refined castings exhibited a larger number of inclusions compared to the micro refined samples.

As mentioned in Section 3.3, the refined samples were prepared using mechanical stirring. The stirring process can agitate the melt surface, thereby introducing further oxides in the castings. Additionally, the nano-MgB_2 particles were observed to oxidize during addition which may have been an additional source for inclusions. Following this, the increased inclusion content of the nano-powder may have led to premature failure and therefore decreased elongation.

To conclude, the addition of MgB_2 particles to Pure Mg, significantly improved the ductility (52 %). The UTS and YS of the castings, however, showed negligible or no improvement. The improved ductility of the samples was believed to be due to the decrease in grain size and the CTE mismatch between the matrix and the reinforcement particles which activated non-basal slip modes. Furthermore, the increased inclusion content in the nano refined castings may have caused the samples to fail prematurely.

4.7.2 AZ91E + MgB_2

The mechanical properties for base AZ91E alloy and AZ91E + 0.025 wt.% MgB_2 micro and nano additions are shown in Figure 4-28. Compared with as-cast samples, the refined samples did not exhibit an increase in mechanical properties. The yield strength of both the micro and nano refined alloys remained constant. The UTS decreased from 158 MPa for the base alloy to 147 MPa 140 MPa for the micro and nano refined castings respectively. The % El of the castings also decreased from 3.3 % to 1.9 % for the micro refined and 1.3 % for the nano refined. Although the MgB_2 refined castings resulted in a significant decrease in grain size, the tensile properties revealed no sign of improvements. This is unusual considering that it is widely accepted in literature that decreases in grain size lead to improved strength and ductility with the exception of nano-sized grains which follow the inverse Hall-Petch relation [76].

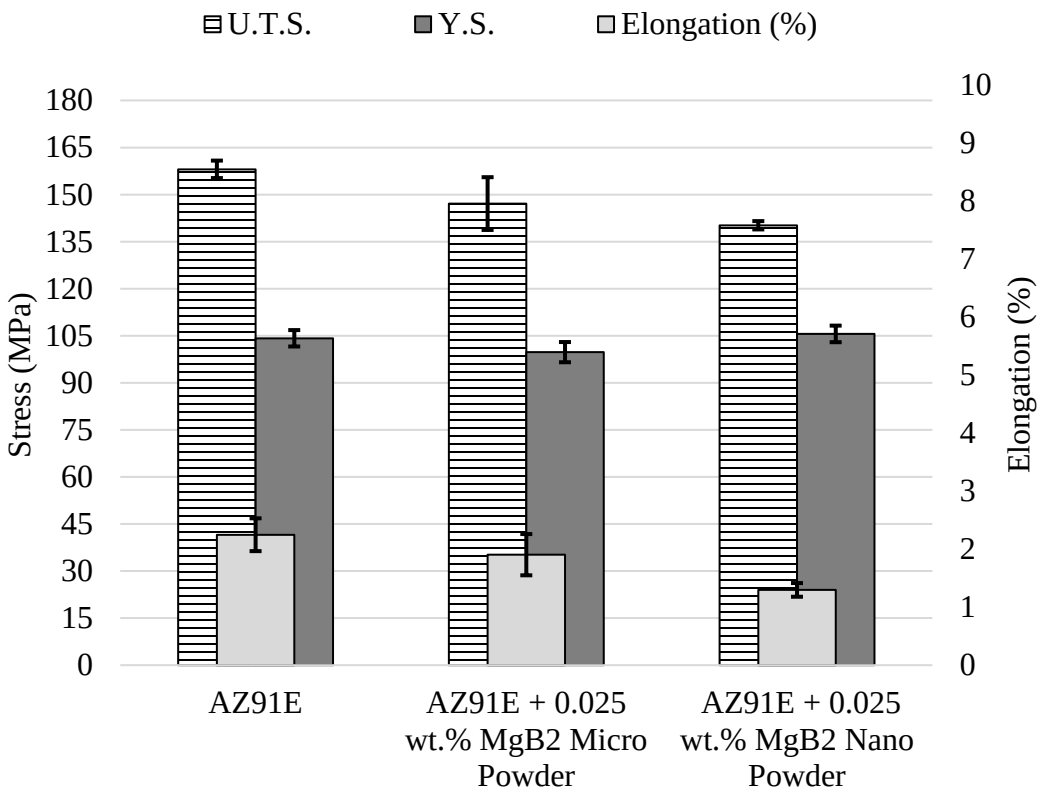

Figure 4-28: Room temperature tensile properties of AZ91E with MgB_2 addition

Upon examining the microstructure of the refined alloys (Figure 4-29), it was noticed that large clusters of Al-Mn intermetallics were found alongside the MgB_2 particles. Typically the Al-Mn particles play a major role in strengthening AZ91. It has been reported that their quasiperiodic nature enables them to resist dislocation shearing, therefore strengthening the alloy [77]. Moreover, $Mg_{17}Al_{12}$ precipitates preferentially on the Al-Mn particles, and thus more of such particles can result in a finer distribution of $Mg_{17}Al_{12}$ precipitates [78].

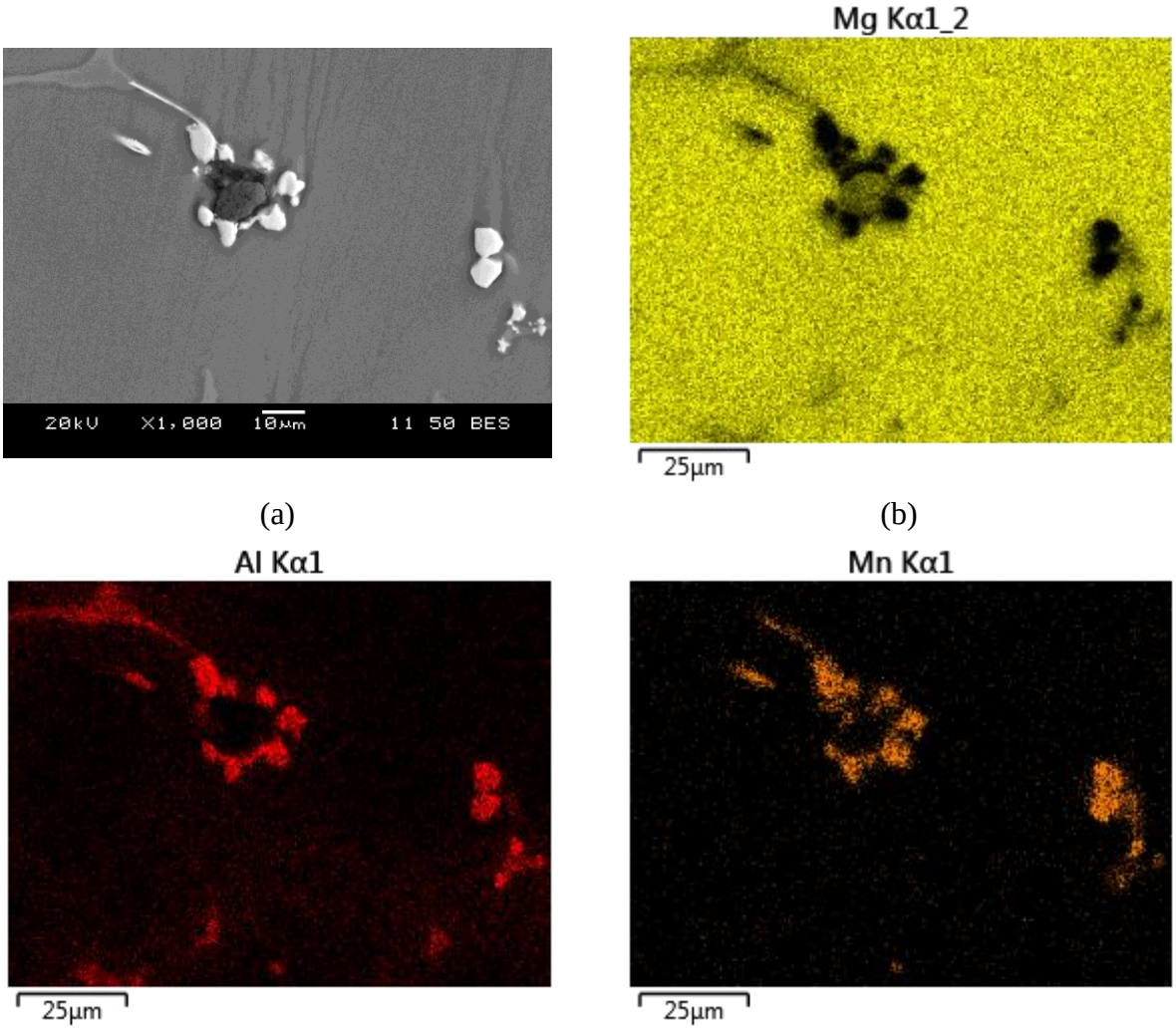

Figure 4-29: (a) SEM image of AZ91E + 0.10 wt.% MgB_2 Showing an MgB_2 particle surrounded by Al-Mn based intermetallics and (b, c, d) EDS element maps of phases

Table 4-5 and Table 4-6 summarize the planar disregistry calculations (Bramfitt model – Section 4.1) for the Al-Mn – Mg and the Al-Mn – MgB_2 systems. From a crystallographic point of view, the HCP structured Al-Mn phase (a = 0.2697 nm [79]) was found to be more likely to be nucleated by MgB_2 particles rather than magnesium grains (a = 0.321 nm [18]). Aluminum-Manganese intermetallics have a smaller lattice mismatch (12.05 % disregistry) against MgB_2 compared to Mg (15.89 % disregistry). It is therefore hypothesized that the MgB_2 particles acted as the nucleating sites for the Al-Mn intermetallics. As a result, the reduced mechanical properties of the refined castings may be attributed to the agglomeration and inhomogeneous distribution of Al-Mn

intermetallics within the Mg matrix due to their preferential nucleation from MgB_2 substrates. The agglomerated intermetallics could have promoted crack initiation and propagation. Moreover, heterogeneity may have caused severe stress concentrations and resulted in premature fracture.

Table 4-5: Calculated values of planar disregistry between Al-Mn and Mg at ambient temperature

	$[uvw]_s$	$[uvw]_n$	$d[uvw]_{Al\text{-}Mn}$ (nm)	$d[uvw]_{Mg}$ (nm)	θ (deg)	$d[uvw]_{Al\text{-}Mn}*\cos(\theta)$ (nm)	$\delta^{(hkl)_{Al-Mn}}_{(hkl)_{Mg}}$
$(0001)_{Al\text{-}Mn} \parallel (0001)_{Mg}$	$2\bar{1}\bar{1}0$	$2\bar{1}\bar{1}0$	0.270	0.321	0	0.270	15.89 %
	$11\bar{2}0$	$11\bar{2}0$	0.270	0.321	0	0.270	
	$\bar{1}2\bar{1}0$	$\bar{1}2\bar{1}0$	0.270	0.321	0	0.270	

Table 4-6: Calculated values of planar disregistry between Al-Mn and MgB_2 at ambient temperature

	$[uvw]_s$	$[uvw]_n$	$d[uvw]_{Al\text{-}Mn}$ (nm)	$d[uvw]_{MgB2}$ (nm)	θ (deg)	$d[uvw]_{Al\text{-}Mn}*\cos(\theta)$ (nm)	$\delta^{(hkl)_{Al-Mn}}_{(hkl)_{MgB2}}$
$(0001)_{Al\text{-}Mn} \parallel (0001)_{MgB2}$	$2\bar{1}\bar{1}0$	$2\bar{1}\bar{1}0$	0.270	0.307	0	0.270	12.05 %
	$11\bar{2}0$	$11\bar{2}0$	0.270	0.307	0	0.270	
	$\bar{1}2\bar{1}0$	$\bar{1}2\bar{1}0$	0.270	0.307	0	0.270	

In summary, the addition of MgB_2 particles to AZ91E, contrary to expectations due to fine grain size, did not improve the mechanical properties of the alloy. The decreased UTS and % El of the samples was believed to be caused by agglomeration of Al-Mn intermetallics near MgB_2 particles. It was suggested that Al-Mn intermetallics might have preferentially nucleated from MgB_2 particles due to the low planar disregistry compared to Mg (12.05 compared to 15.89 %) which resulted in a decrease in mechanical properties.

5 Conclusions

This study was conducted in order to examine the effectiveness of MgB_2 as a potential grain refiner for Pure Mg and AZ91E Mg alloys. The influence of MgB_2 on the grain size and tensile properties at ambient temperature were studied. The results obtained concluded that although MgB_2 was an effective grain refiner for both Pure Mg and AZ91E, its addition was detrimental to their overall mechanical properties. Concluding remarks from each of the relevant sections are presented below.

5.1.1 Theoretical Considerations and Particle Size Analysis

1) Magnesium Boride particles met the requirements to act as efficient nucleating sites due to their low crystallographic disregistry with a Mg matrix (4.36 %) at the (0001) matching planes.
2) Ball milling for 480 minutes with 300 RPM successfully decreased the average particle size for MgB_2. The results from the particle size distribution calculations indicated that the MgB_2 particles had been successfully reduced to an average diameter of 100 nm.

5.1.2 Grain Refinement and Mechanical Properties of Pure Mg

1) Additions of MgB_2 to Pure Mg decreased the average grain size. The ideal addition level was determined to be 0.025 wt.%. The micro powder additions decreased the grain size from 2256 to 1577 µm, and the nano-powder additions decreased the grain size to 1628 µm.
2) Thermal analysis indicated that MgB_2 could act as a potent nucleant for Pure Mg. With MgB_2 addition, the average undercooling of Pure Mg decreased significantly from 2.0 °C to 0.9 and 0.8 °C for Pure Mg + 0.025 wt.% micro and nano-powder respectively.
3) The fading analysis of Pure Mg with various MgB_2 additions indicated that the sensitivity of the used refiner to inoculation fading is relatively high and the longest holding time cannot exceed 5 minutes. The fading was attributed to the higher density of the grain refining particles compared to the Mg matrix. The nano refined castings were found to be more resistant to fading compared to the micro refined castings due to their fine particle size.
4) The grain refinement was determined to be the result of the combined effect of enhanced heterogeneous nucleation and restricted grain growth. It was observed that the MgB_2 particles were at the center of grains which indicated that they promoted heterogeneous

nucleation. In addition, some particles were observed at grain boundaries which impeded grain growth.

5) The addition of MgB_2 particles to Pure Mg significantly improved the ductility (52 %). The UTS and YS of the castings, however, showed negligible or no improvement. The improved ductility of the samples was believed to be due to the decrease in grain size and the CTE mismatch between the matrix and the reinforcement particles which activated non-basal slip modes.

5.1.3 Grain Refinement and Mechanical Properties of AZ91E

1) Magnesium Boride additions resulted in the grain refinement of AZ91E Mg alloy. The addition level for efficient refinement was chosen to be 0.025 wt.% which resulted from the Pure Mg trials. The unrefined grain size was 179 µm. It was also observed that the micro MgB_2 acted as a more efficient grain refiner (44 % decrease) compared to the nano-sized MgB_2 (35 % decrease).
2) The thermal analysis indicated that MgB_2 could act as a potent nucleant for AZ91E. It was observed that with MgB_2 addition, the average nucleating temperature of the alloy increased. The higher nucleating temperature suggested that MgB_2 particles have effectively nucleated a great number of primary magnesium grains.
3) The fading analysis determined that there was appreciable loss in grain refining efficiency during the 20 minute holding time period. The fading of the micro refined castings was attributed to settling due to higher density compared to AZ91E. The nano refined castings displayed an increased resistance to fading due to their fine particle size.
4) Significant refinement in grain size was due to the effect of heterogeneous nucleation. It was observed that the MgB_2 particles were at the center of grains which indicated that they promoted heterogeneous nucleation.
5) The addition of MgB_2 particles to AZ91E did not improve the mechanical properties of the alloy. The decreased UTS and % Elongation of the samples was believed to be caused by agglomeration of Al-Mn intermetallics near MgB_2 particles. It was suggested that Al-Mn intermetallics might have preferentially nucleated from MgB_2 particles due to the low planar disregistry compared to Mg (12.05 % compared to 15.89 %).

6 Future Work

The current study examined the effects of MgB_2 on the grain size and mechanical properties of Pure Mg and AZ91E Mg alloy. Further investigations are required to examine the influence of different addition methods, temperatures, stirring times and stirring techniques. The refining effects on other commercial alloy systems should be examined as well.

Addition of the MgB_2 refiner was carried out using a mechanical stirrer which may have introduced oxides within the melt. Future research work could examine the potential for stirring mechanisms that do not agitate the melt surface such as ultrasonic or electromagnetic stirring.

The refiner addition parameters such as addition temperature and stirring time could also be widened in order to gain a full understanding of the inoculating effects. The nano-size refiners were also observed to oxidize during addition. Future investigations could employ an alternate addition mechanism to prevent oxidation.

Appendices

A. Phase Diagrams

The equilibrium Mg-Al and Mg-B phase diagrams are shown in Figure A-1 and Figure A-2.

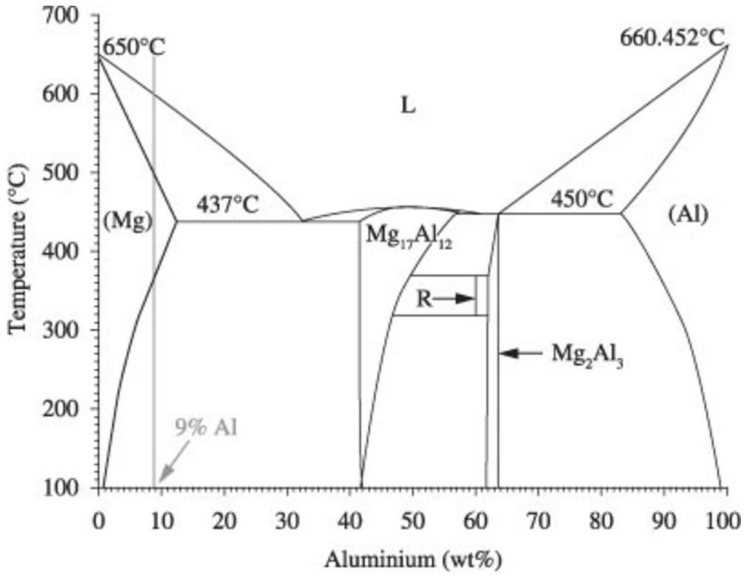

Figure A-1: Magnesium – Aluminum phase diagram [80]

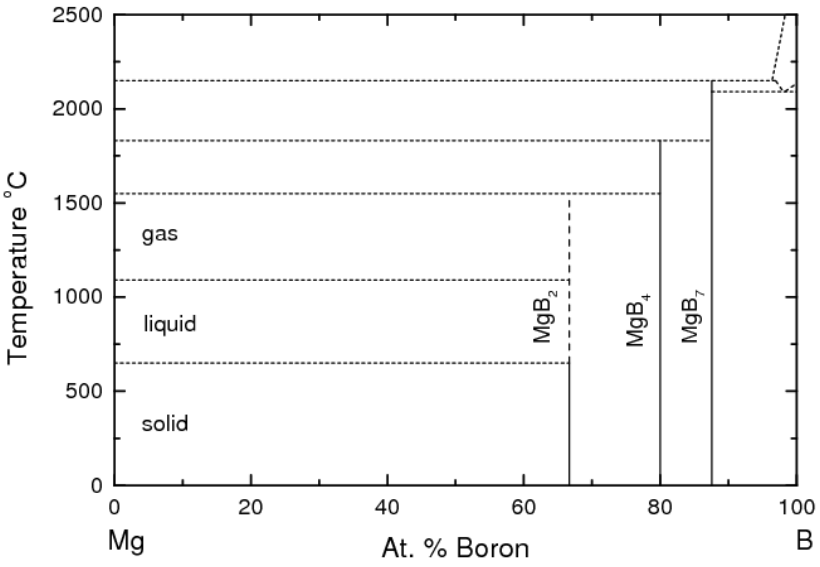

Figure A-2: Magnesium – Boron phase diagram [56]

B. Planar Disregistry Orientation Relationships

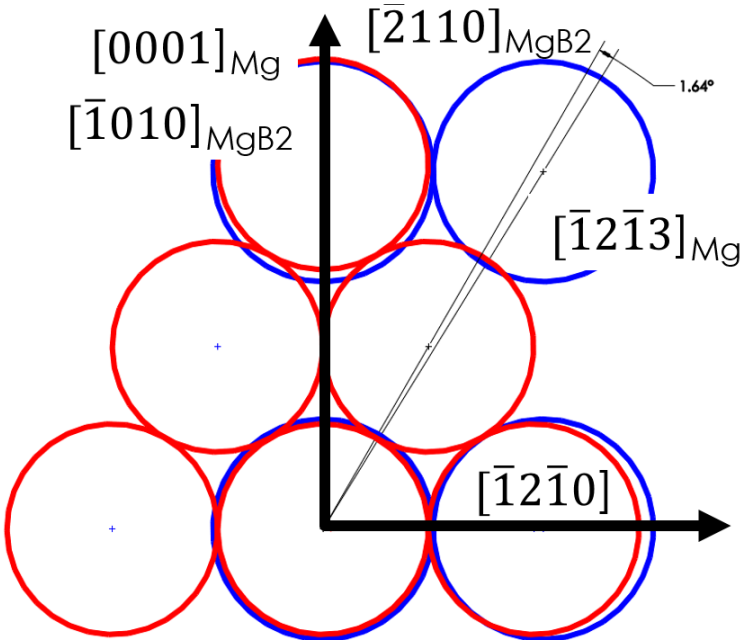

Figure B-1: Superimposed (0001) plane of Mg (blue) and (10$\bar{1}$0) plane of MgB_2 (red) with closed packed directions

Table B-1: Calculated values of planar disregistry between Mg and MgB_2 at ambient temperature for (0001) and (10$\bar{1}$0) planes

[uvw]s	$[\bar{1}010]$	$[\bar{2}110]$	$[\bar{1}2\bar{1}0]$
[uvw]n	[0001]	$[\bar{1}2\bar{1}3]$	$[\bar{1}2\bar{1}0]$
d[uvw]s [nm]	0.532	0.307	0.307
d[uvw]n [nm]	0.521	0.612	0.321
θ [Deg]	0	1.64	0
δ [%]	18.78		

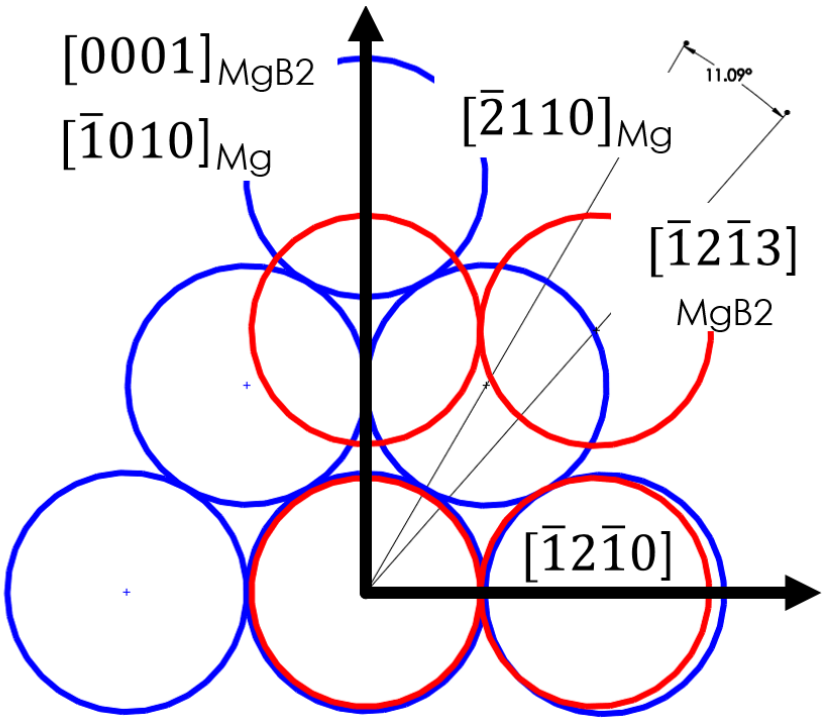

Figure B-2: Superimposed ($10\bar{1}0$) plane of Mg (blue) and (0001) plane of MgB_2 (red) with closed packed directions

Table B-2: Calculated values of planar disregistry between Mg and MgB_2 at ambient temperature for ($10\bar{1}0$) and (0001) planes

[uvw]s	[0001]	[$\bar{1}2\bar{1}3$]	[$\bar{1}2\bar{1}0$]
[uvw]n	[$\bar{1}010$]	[$\bar{2}110$]	[$\bar{1}2\bar{1}0$]
d[uvw]s [nm]	0.352	0.467	0.307
d[uvw]n [nm]	0.555	0.321	0.321
θ [Deg]	0	11.09	0
δ [%]	27.90		

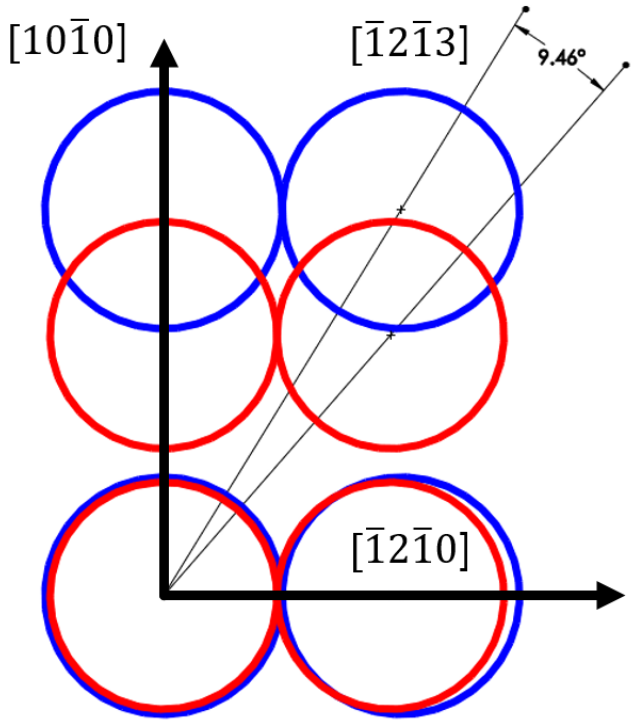

Figure B-3: Superimposed (10$\bar{1}$0) plane of Mg (blue) and (10$\bar{1}$0) plane of MgB_2 (red) with closed packed directions

Table B-3: Calculated values of planar disregistry between Mg and MgB_2 at ambient temperature for (10$\bar{1}$0) planes

[uvw]s	[**0001**]	[**$\bar{1}$2$\bar{1}$3**]	[**$\bar{1}$2$\bar{1}$0**]
[uvw]n	[**0001**]	[**$\bar{1}$2$\bar{1}$3**]	[**$\bar{1}$2$\bar{1}$0**]
d[uvw]s [nm]	0.352	0.467	0.307
d[uvw]n [nm]	0.521	0.612	0.321
θ [Deg]	0	9.46	0
δ [%]	20.51		

C. Cooling Curves

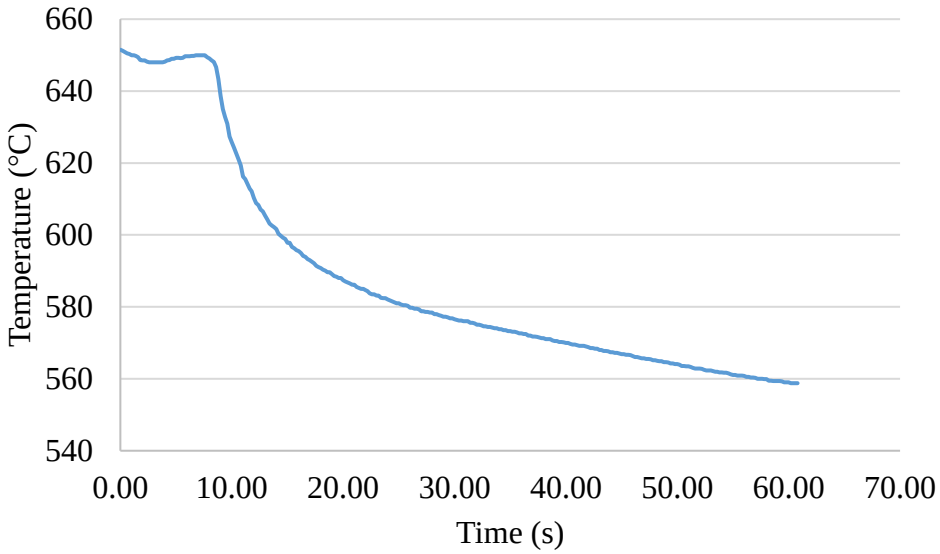

Figure C-1: Typical cooling curve of Pure Mg produced in a tensile mould

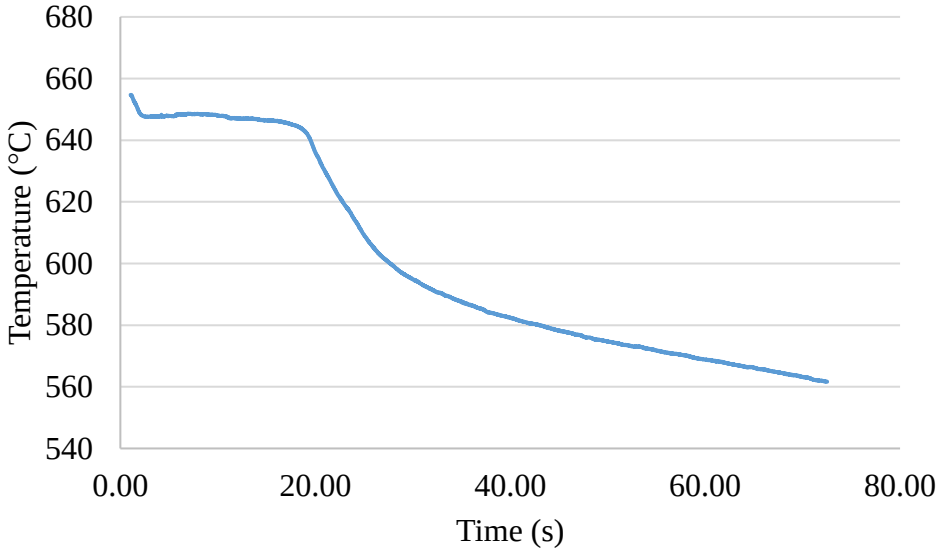

Figure C-2: Typical cooling curve of Pure Mg + 0.025 wt.% MgB_2 micro-particles produced in a tensile mould

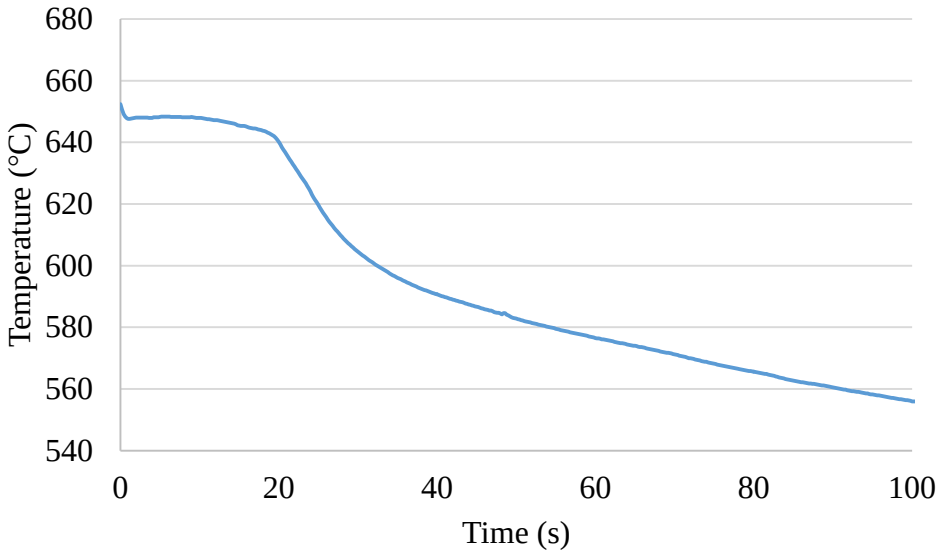

Figure C-3: Typical cooling curve of Pure Mg + 0.025 wt.% MgB_2 nano-particles produced in a tensile mould

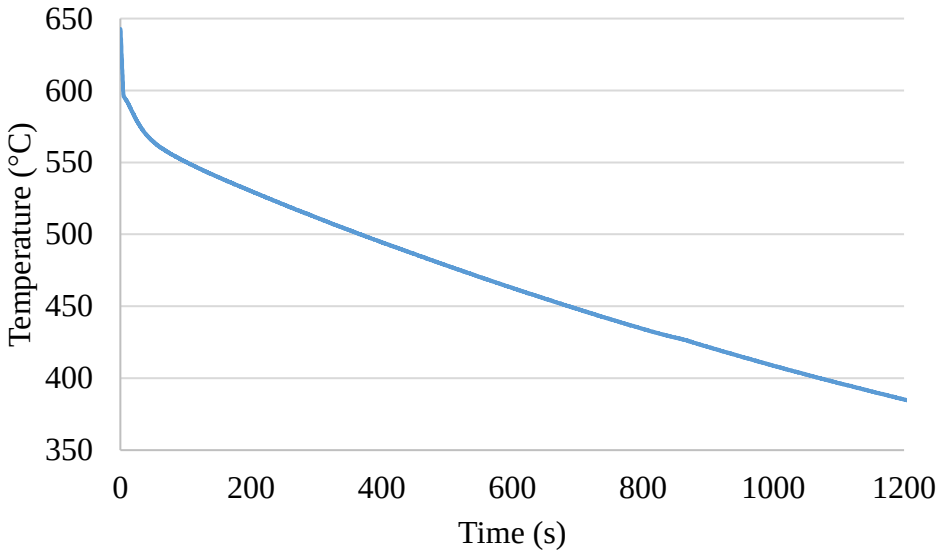

Figure C-4: Typical cooling curve of AZ91E produced in a tensile mould

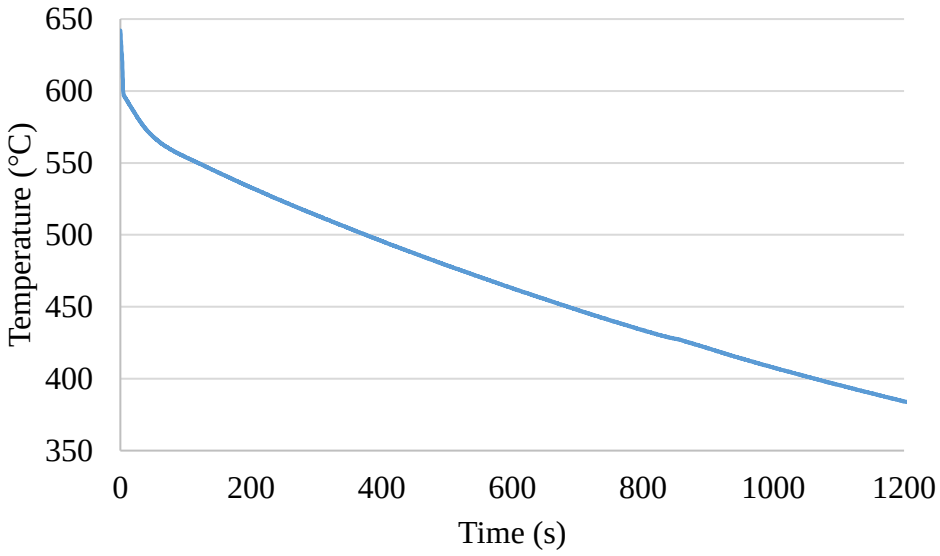

Figure C-5: Typical cooling curve of AZ91E + 0.025 wt.% MgB_2 micro-particles produced in a tensile mould

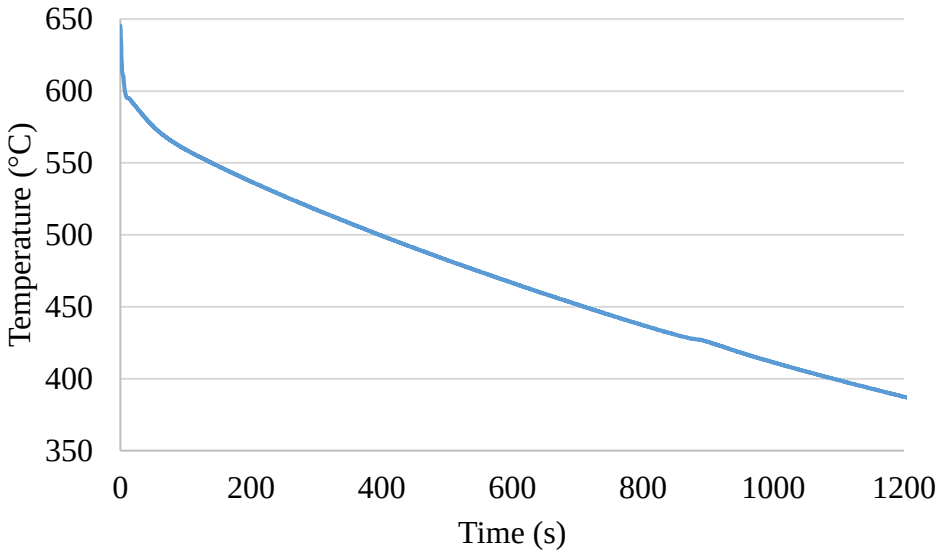

Figure C-6: Typical cooling curve of AZ91E + 0.025 wt.% MgB_2 nano-particles produced in a tensile mould

D. Analysis of Variance for Grain Size Measurements

An analysis of variance was performed for the grain size measurements to determine the maximum confidence level for which the following two null hypotheses could be tested:

1) The mean grain sizes with increasing MgB_2 addition level remain the same

2) The mean grain sizes with increasing holding time remain the same

D.1 Pure Mg + MgB_2

For the Pure Mg + MgB_2 castings, addition level and holding time were the two factors under consideration. The ANOVA for this case was performed as a two-factor experiment with two replications and a 95 % confidence interval. The raw data is presented in Table D-1 and the analysis in Table D-2.

Table D-1: Summary of Pure Mg grain sizes and addition levels for ANOVA

MgB_2 Addition Level		**Holding Time**		
		5 min	**10 min**	**20 min**
Pure Mg	**Grain Size (µm)**	2333	2333	2333
		2600	2600	2600
0.0125 wt.% MgB_2		1910	1977	2185
		1973	2185	2283
0.025 wt.% MgB_2		1536	2012	1986
		1617	1870	2176
0.05 wt.% MgB_2		1844	1984	1973
		1737	2106	2279
0.1 wt.% MgB_2		1777	2161	2350
		1902	2064	2215

Table D-2: Two factor analysis of variance for Pure Mg grain size and holding time

Source of Variation	Sum of Squares	Deg. of Freedom	Mean-Square	F	P-value	F_{crit}
Addition Level	1211967.20	4	302991.80	18.30	1.23E-5	3.06
Holding Time	512283.80	2	256141.90	15.47	0.00023	3.68
Interaction	167033.20	8	20879.15	1.26	0.33	2.64
Error	248378.50	15	16558.57	-	-	-
Total	2139662.70	29	-	-	-	-

For the null hypothesis, the mean grain size with increasing addition level remains the same:

F = 18.30 and F_{crit} = 3.06. Therefore, since F > F_{crit} the null hypothesis is rejected. It can be concluded that the MgB_2 addition level affects the grain size of Mg.

For the null hypothesis, the mean grain size with increasing holding time remains the same:

F = 15.47 and F_{crit} = 3.68. Therefore, since F > F_{crit} the null hypothesis is rejected. It can be concluded that the MgB_2 holding time affects the grain size of Mg.

D.2 AZ91E + MgB_2

For the AZ91E + MgB_2 castings, addition level and holding time were the two factors under consideration. The ANOVA for this case was performed as a two-factor experiment with two replications and a 95 % confidence interval. The raw data is presented in Table D-3 and the analysis in Table D-4.

Table D-3: Summary of AZ91E grain sizes and addition levels for ANOVA

MgB_2 Addition Level		Holding Time		
		5 min	10 min	20 min
AZ91E	**Grain Size (µm)**	181	181	181
		176	176	176
0.025 wt.% MgB_2		92	113	120
		107	121	130

Table D-4: Two factor analysis of variance for AZ91E grain size and holding time

Source of Variation	Sum of Squares	Deg. of Freedom	Mean-Square	F	P-value	F_{crit}
Addition Level	12545.33	1	12545.33	324.45	0.00	5.99
Holding Time	340.17	2	170.08	4.40	0.07	5.14
Interaction	340.17	2	170.08	4.40	0.07	5.14
Error	232.00	6	38.67	-	-	-
Total	13457.67	11	-	-	-	-

For the null hypothesis, the mean grain size with increasing addition level remains the same:

F = 324.45 and F_{crit} = 5.99. Therefore, since F > F_{crit} the null hypothesis is rejected. It can be concluded that the MgB_2 addition level affects the grain size of AZ91E.

For the null hypothesis, the mean grain size with increasing holding time remains the same:

F = 4.40 and F_{crit} = 5.14. Therefore, since F < F_{crit} we fail to reject the null hypothesis. It can be concluded that the MgB_2 holding time does not significantly affect the grain size of AZ91E.

E. Analysis of Variance for Ductility

An analysis of variance was performed for the mechanical properties to determine the maximum confidence level for which the following null hypothesis could be tested:

1) The mean % Elongation with micro-MgB_2 addition remained the same

The ANOVA for this case was performed as a single factor experiment and a 90 % confidence interval. The raw data is presented in Table E-1 and the analysis in Table E-2.

Table E-1: Summary of AZ91E % Elongation for ANOVA

MgB_2 Addition Level	**% Elongation**
AZ91E	3.28
	3.31
0.025 wt.% MgB_2	4.71
	5.99

Table E-2: Two factor analysis of variance for AZ91E grain size and holding time

Source of Variation	**Sum of Squares**	**Deg. of Freedom**	**Mean-Square**	**F**	**P-value**	**F_{crit}**
Between Groups	4.22	1	4.22	10.30	0.085	8.53
Within Groups	0.82	2	0.41	-	-	-
Total	5.04	3	-	-	-	-

For the null hypothesis, the mean % Elongation with micro-MgB_2 addition remained the same:

$F = 10.30$ and $F_{crit} = 8.53$. Therefore, since $F > F_{crit}$ the null hypothesis is rejected. It can be concluded that the MgB_2 addition level affects the % Elongation of AZ91E.

References

[1] A. Luo, "Recent magnesium alloy development for elevated temperature applications," *International Materials Reviews,* vol. 49, no. 1, pp. 13-30, 2013.

[2] S. Kollamthodi, D. Kay, I. Skinner, C. Dun and S. Hausberger, "The potential for mass reduction of passenger cars and light commercial vehicles in relation to future CO2 regulatory requirements," Ricardo-AEA, Harwell, U.K., 2015.

[3] U.S. Dept. of Energy, "2014 Annual Progress Report," Vehicle Technologies Office, 2014.

[4] B. Shia, R. Chena and W. Kea, "Influence of grain size on the tensile ductility and deformation modes of rolled Mg–1.02 wt.% Zn alloy," *Journal of Magnesium and Alloys,* vol. 1, no. 3, pp. 210-216, 2013.

[5] J. Davis, Aluminum and Aluminum Alloys, Materials Park, USA: ASM International, 1993.

[6] M. Kulekci, "Magnesium and its alloys applications in automotive industry," *The International Journal of Advanced Manufacturing Technology,* vol. 39, pp. 851-865, 2008.

[7] North American Die Casting Association, "Magnesium Die Casting Handbook," NADCA, Rosemont, IL, 1998.

[8] H. Hu, A. Yu, N. Li and J. Allison, "Potential magnesium alloys for high temperature die cast automotive applications: a review," *Materials and Manufacturing Processes,* vol. 18, no. 5, pp. 687-717, 2003.

[9] E. Emley, Principles of magnesium technology, Oxford, United Kingdom: Pergamon Press, 1966.

[10] M. Avedesian and H. Baker, Magnesium and Magnesium Alloys, Materials Park, USA: ASM International, 1999.

[11] A. Elsayed, "Inclusion Removal and Grain Refinement of Magnesium Alloy Castings, PhD dissertation," Ryerson University, Toronto, 2015.

[12] Y. Wang, X. Liao and Y. Zhu, "Grain refinement and growth induced by severe plastic deformation," *International Journal of Materials Research,* vol. 100, no. 12, pp. 1632-1637, 2009.

[13] A. Ramirez, M. Qian, B. Davis, T. Wilks and D. St.John, "Potency of high-intensity ultrasonic treatment for grain refinement of magnesium alloys," *scripta materialia,* vol. 59, no. 1, pp. 19-22, 2008.

[14] M. Qian and P. Cao, "Discussions on grain refinement of magnesium alloys by Carbon innoculation," *scripta materialia,* vol. 52, pp. 415-419, 2005.

[15] A. Chaturvedi, A. Sharma and U. Pandel, "Effect of mechanical vibrations on grain refinement of AZ91 Mg alloy," *Materials Research Express,* vol. 4, pp. 1-11, 2017.

[16] V. Chaturvedi, R. Sen, U. Pendel and A. Sharma, "An overview of improvement of properties of AZ91 Mg alloy by grain refinement through vibrations," in *International conference on advance trends in engineering and technology*, Jaipur, India , 2013.

[17] D. St.John, M. Qian, M. Easton, P. Cao and Z. Hildebrand, "Grain Refinement of Magnesium Alloys," *Metallurgical and Materials Transactions A,* vol. 36, no. 7, pp. 1669-1679, 2005.

[18] W. Callister and D. Rethwisch, Materials Science and Engineering: an Introduction, Hoboken, NJ: John Wiley, 2009.

[19] R. Schmid-Fetzer and A. Kozlov, "Thermodynamic aspects of grain growth restriction in multicomponent alloy solidification," *Acta Materialia,* vol. 59, no. 15, pp. 6133-6144, 2011.

[20] E. Castle, A. Mullis and R. Cochrane, "Mechanism selection for spontaneous grain refinement in undercooled melts," *Acta Materialia,* vol. 77, pp. 76-84, 2014.

[21] D. Turnbull and B. Vonnegut, "Nucleation catalysis," *Industrial and Engineering Chemistry*, vol. 44, no. 6, pp. 1292-1298, 1952.

[22] B. Bramfitt, "The effect of carbide and nitride additions on the heterogeneous nucleation behavior of liquid iron," *Metallurgical Transactions,* vol. 1, no. 7, pp. 1987-1995, 1970.

[23] P. Kelly and M. Zhang, "Edge-to-edge matching – A new approach to the morphology and crystallography of precipitates," *Materials Forum,* vol. 23, pp. 41-62, 1999.

[24] A. Greer, A. Bunn, A. Tronche, P. Evans and D. Bristow, "Modeling of inoculation of metallic melts: application to grain refinement of aluminium by Al–Ti–B," *Acta Materialia*, vol. 48, pp. 2823-2835, 2000.

[25] D. St.John, M. Qian, M. Easton and P. Cao, "The interdependence theory: the relationship between grain formation and nucleant selection," *Acta Materialia,* vol. 59, no. 12, pp. 4907-4921, 2011.

[26] M. Zhang, P. Kelly, M. Easton and J. Taylor, "Crystallographic study of grain refinement in aluminum alloys using the edge-to-edge matching model," *Acta Materialia,* vol. 53, no. 5, pp. 1427-1438, 2005.

[27] M.-X. Zhang and P. Kelly, "Edge-to-edge matching model for predicting orientation relationships and habit planes—the improvements," *Scripta Materialia,* vol. 52, pp. 963-968, 2005.

[28] M. Qian, D. St.John and M. Frost, Magnesium Technology 2003, San Diego, United States: Kaplan, 2003.

[29] H. Okamoto, "Mg-Zr (Magnesium - Zirconium)," *Journal of Phase Equilibria,* vol. 23, no. 2, pp. 198-199, 2002.

[30] Y. Tamura, N. Kono, T. Motegi and E. Sato, "Grain Refining Mechanism and Casting Structure of Mg-Zr Alloy," *Journal of Japan Institute of Light Metals,* vol. 48, pp. 185-189, 1998.

[31] M. Qian, L. Zheng, D. Graham, M. Frost and D. St.John, "Settling of undissolved zirconium particles in pure magnesium melts," *Journal of Light Metal,* vol. 1, pp. 157-165, 2001.

[32] M. Qian, D. St.John and M. Frost, "Zirconium alloying and grain refinement of magnesium alloys," in *Magnesium Technology 2003,* San Diego, CA, 2003.

[33] Z. Hildebrand, M. Qian, D. St.John and M. Frost, "Influence of zinc on the soluble zirconium content in magnesium and the subsequent grain refinement by zirconium," in *Magnesium Technology 2004,* Warrendale, PA, 2004.

[34] D. St.John, Q. Ma, M. Easton, P. Cao and Z. Hildebrand, "Grain Refinement of Magnesium Alloys," *Metallurgical and Materials Transactions,* vol. 36, pp. 1669-1679, 2005.

[35] F. Kabirian and R. Mahmudi, "Effects of Zirconium Additions on the Microstructure of As-cast and Aged AZ91 Magnesium Alloy," *Advanced Engineering Materials,* vol. 11, no. 3, pp. 189-193, 2009.

[36] Y. Lee, X. Liu and H. Yang, "The Role of Solute in Grain Refinement of Magnesium," *Metallurgical and Materials Transactions,* vol. 31, pp. 2895-2906, 2000.

[37] I. Polmear, "Magnesium alloys and applications," *Materials science and technology,* vol. 10, no. 1, pp. 1-16, 1994.

[38] V. Kondic, Metallurgical Principles of Founding, London, U.K.: Edward Arnold, 1968.

[39] C. Nelson, "Grain size behavior in magnesium casting alloys," *Transaction AFS,* vol. 56, pp. 1-23, 1948.

[40] N. Tiner, "Superheating of magnesium alloys," *AIME Tech Publications,* vol. 12, no. 7, pp. 1-19, 1945.

[41] K. Achenbach, H. Nipper and E. Piwowarsky, "Contribution to the question of melting practice for cast magnesium alloys," *Die Giesserei,* vol. 26, pp. 597-604, 1939.

[42] P. Cao, M. Qian and D. St.John, "Effect of iron on grain refinement of high-purity Mg–Al alloys," *Scripta Materialia,* vol. 51, no. 2, pp. 125-129, 2004.

[43] P. Cao, M. Qian, D. St.John and M. Frost, "Uptake of iron and its effect on grain refinement of pure magnesium by zirconium," *Materials Science And Technology,* vol. 20, no. 5, pp. 585-592, 2004.

[44] A. Nayed-Hashemi and J. Clark, "Phase diagrams of binary magnesium alloys, Monograph Series on Alloy Phase Diagrams," *ASM International,* 1988.

[45] Y. Lee, "Grain Refinement of Magnesium, Department of Mining, Minerals and Engineering," The University of Queensland, Queensland, 2002.

[46] Y. Wang, X. Z. Ding, A. Luo and A. Sachdev, "Grain refinement of AZ31 magnesium alloy by titanium and low-frequency electromagnetic casting," *Metallurgical and Materials Transactions A,* vol. 38, no. 6, pp. 1358-1366, 2007.

[47] X. Ai and G. Quan, "Effect of Ti on the Mechanical Properties and Corrosion of Cast AZ91 Magnesium Alloy," *The Open Materials Science Journal,* vol. 6, pp. 6-13, 2012.

[48] S. Li, B. Tang and D. Zeng, "Effects and mechanism of Ca on refinement of AZ91D alloy," *Journal of Alloys and Compounds,* vol. 437, no. 1-2, pp. 317-321, 2007.

[49] K. Hirai, H. Somekawa, Y. Takigawa and K. Higashi, "Effects of Ca and Sr addition on mechanical properties of a cast AZ91 magnesium alloy at room and elevated temperature," *Materials Science and Engineering: A,* Vols. 1-2, no. 403, pp. 276-280, 2005.

[50] A. Srinivasan, U. Pillai and B. Pai, "Microstructure and mechanical properties of Si and Sb added AZ91 magnesium alloy," *Metallurgical and Materials Transactions A,* vol. 36, no. 8, pp. 2235-2243, 2005.

[51] A. Srinivasan, U. Pillai, J. Swaminathan, S. Das and B. Pai, "Observations of microstructural refinement in Mg–Al–Si alloys containing strontium," *Journal of Materials Science,* vol. 41, no. 18, pp. 6087-6089, 2006.

[52] Y. Guangyin, "Microstructure and mechanical properties of Mg/Zn/Si-based alloys," *Materials Science and Engineering: A,* vol. 357, no. 1-2, pp. 314-320, 2003.

[53] Y. Turen, "Effect of Sn addition on microstructure, mechanical and casting properties," *Materials and Design,* vol. 49, pp. 1009-1015, 2013.

[54] M. Suresh, A. Srinivasan, K. Ravi, U. Pillai and B. Pai, "Influence of Boron Addition on the Grain Refinement and Mechanical Properties of AZ91 Mg Alloy," *Materials Science and Engineering A,* vol. 525, pp. 207-210, 2009.

[55] B. Murty, S. Kori and M. Chakraborty, "Grain Refinement of Aluminum and its Alloys by Heterogeneous Nucleation and Alloying," *International Materials Reviews,* vol. 47, no. 1, pp. 3-29, 2002.

[56] J. Jorgensen, D. Hinks and S. Short, "Lattice Properties of MgB2 versus Temperature and Pressure," Materials Science Division, Argonne National Laboratory, Argonne, IL, 2001.

[57] D. Porter, Phase Transformations in Metals and Alloys, London, U.K.: Chapman and Hall, 1992.

[58] A. Luo, "Heterogeneous nucleation and grain refinement in cast Mg(AZ91)/SiCp metal matrix composites," *Canadian Metallurgical Quarterly,* vol. 35, no. 4, pp. 375-383, 1996.

[59] P. Cao, M. Qian and D. St.John, "Grain refinement of commercial purity Mg-9%Al alloys by superheating," in *Magnesium Technology 2005*, Warrendale, TMS, 2005, p. 297−302.

[60] L. Lua and A. Dahle, "Effects of combined additions of Sr and AlTiB grain refiners in hypoeutectic Al–Si foundry alloys," *Materials Science and Engineering A,* vol. 435, pp. 288-296, 2006.

[61] P. Schaffer and K. Dahle, "Settling behaviour of different grain refiners in aluminium," *Materials Science and Engineering A,* vol. 413, p. 373–378, 2005).

[62] D. Stefanescu and B. Dhindaw, Metals handbook, Materials Park, OH: ASM Int, 1988.

[63] G. Lei, L. Song-mao, C. Rong-shi and H. En-hou, "Correlation of recalescence with grain refinement of magnesium alloys," *Transactions of Nonferrous Metals Society of China,* vol. 18, pp. 288-291, 2008.

[64] K. Nie, X. Wang, X. Hu, L. Xu, K. Wu and M. Zheng, "Microstructure and mechanical properties of SiC nanoparticles reinforced magnesium matrix composites fabricated by ultrasonic vibration," *Materials Science and Engineering A,* vol. 528, pp. 5278-5282, 2011.

[65] K. Deng, K. Wu, X. Wang, Y. Wu, X. Hu, M. Zheng, W. Gan and H. Brokmeier, "Microstructure evolution and mechanical properties of a particulate reinforced magnesium matrix composites forged at elevated temperatures," *Materials Science and Engineering: A,* vol. 527, no. 6, pp. 1630-1635, 2010.

[66] K. Deng, K. Wu, Y. Wu, K. Nie and M. Zheng, "Effect of submicron size SiC particulates on microstructure and mechanical properties of AZ91 magnesium matrix composites," *Journal of Alloys and Compounds,* vol. 504, no. 2, pp. 542-547, 2010.

[67] G. Meenashisundaram, M. Nai, A. Almajid, K. Khalil, H. Abdo and M. Gupta, "Effects of TiO2 powder morphology on the mechanical response of pure magnesium: 1D nanofibers versus 0D nanoparticulates," *Journal of Alloys and Compounds,* vol. 664, pp. 45-58, 2016.

[68] G. Meenashisundaram, S. Sankaranarayanan and M. Gupta, "Enhancing overall tensile and compressive response of pure Mg using nano-TiB2 particulates," *Materials Characterization,* vol. 94, pp. 178-188, 2014.

[69] G. Meenashisundaram and M. Gupta, "Synthesis and characterization of High performance low volume fraction TiC reinforced Mg nanocomposites targeting biocompatible/structural applications," *Materials Science and Engineering: A,* vol. 627, pp. 306-315, 2015.

[70] G. Meenashisundaram, M. Nai, A. Almajid and M. Gupta, "Development of high performance Mg–TiO2 nanocomposites targeting for biomedical/structural applications," *Materials & Design (1980-2015),* vol. 65, pp. 104-114, 2015.

[71] H. Birkedal, W. V. Beek, H. Emerich and P. Pattison, "Thermal expansion and phase purity of commercial MgB2," *Journal of Materials Science Letters,* vol. 22, no. 15, pp. 1069-1071, 2003.

[72] C. Kim, I. Sohn, M. Nezafati, J. Ferguson, B. Schultz, Z. Bajestani-Gohari, P. Rohatgi and K. Cho, "Prediction models for the yield strength of particle-reinforced unimodal pure magnesium (Mg) metal matrix nanocomposites (MMNCs)," *Journal of Materials Science,* vol. 48, no. 12, pp. 4191-4204, 2013.

[73] A. Redsten, E. Klier, A. Brown and D. Dunand, "Mechanical properties and microstructure of cast oxide-dispersion-strengthened aluminum," *Materials Science and Engineering: A,* vol. 201, no. 1-2, pp. 88-102, 1995.

[74] S. Sankaranarayanan, R. Sabat, S. Jayalakshmi, S. Suwas and M. Gupta, "Effect of nanoscale boron carbide particle addition on the microstructural evolution and mechanical response of pure magnesium," *Materials & Design (1980-2015),* vol. 56, p. 428–436, 2014.

[75] H. Dieringa, "Properties of magnesium alloys reinforced with nanoparticles and carbon nanotubes: a review," *Journal of Materials Science,* vol. 46, no. 2, p. 289–306, 2011.

[76] M. Basariya, V. Srivastava and N. Mukhopadhyay, "Inverse Hall–Petch like behaviour in a mechanically milled nanocrystalline Al5Fe2 intermetallic phase," *Philosophical Magazine* , vol. 96, no. 23, pp. 2445-2456, 2016.

[77] J. Zhang, L. Pei, H. Du, W. Liang, C. Xu and B. Lu, "Effect of Mg-based spherical quasicrystals on microstructure and mechanical properties of AZ91 alloys," *Journal of Alloys and Compounds,* vol. 453, no. 1-2, pp. 309-315, 2008.

[78] R. Zeng, Y. Chiu and I. Jones, "Characterisation of nano-sized Al–Mn–(Mg) particles in AZ91 and their effect on Mg17Al12 precipitation," *Journal of Alloys and Compounds,* vol. 579, pp. 34-38, 2013.

[79] P. Cao, M. Qian and D. St.John, "Effect of manganese on grain refinement of Mg–Al based alloys," *Scripta Materialia,* vol. 54, no. 11, p. 1853–1858, 2006.

[80] T. Massalski and H. Okamoto, Binary Alloys Phase Diagrams, Materials Park, Ohio: ASM, 1990.